

European Journal of Medicinal Chemistry

A further pocket or conformational plasticity by mapping COX-1 catalytic site through modified-mofezolac structure-inhibitory activity relationships and their antiplatelet behavior

--Manuscript Draft--

Manuscript Number:	
Article Type:	Full Paper
Keywords:	cyclooxygenase-1; inhibitors; diarylisoxazoles; catalytic site mapping; antiplatelet agent; hemolysis; QSAR; drug design
Corresponding Author:	Antonio Scilimati University of Bari Bari, Italy ITALY
First Author:	Antonio Scilimati, PhD
Order of Authors:	Antonio Scilimati, PhD Roberta Solidoro, PhD Student Morena Miciaccia, PhD Carmela Bonaccorso, PhD Cosimo Gianluca Fortuna, PhD Domenico Armenise, PhD Student Antonella Centonze, PhD Savina Ferorelli, PhD Paola Vitale, PhD Priscila Rodrigues, PhD Renilda Guimarães, PhD Alana de Oliveira, PhD Mariana da Paz, PhD Luciana Rangel, PhD Plínio Cunha Sathler, PhD Angela Altomare, PhD Maria Grazia Perrone, PhD
Abstract:	<p>Cyclooxygenase enzymes have distinct roles in cardiovascular, neurological, and neurodegenerative disease. They are differently expressed in different type of cancers. Specific and selective COXs inhibitors are needed to be used alone or in combination therapies. Fully understand the differences at the catalytic site of the two cyclooxygenase (COX) isoforms is still opened to investigation. Thus, two series of novel compounds were designed and synthesized in fair to good yields using the highly selective COX-1 inhibitor mofezolac as the lead compound to explore a COX-1 zone formed by the polar residues Q192, S353, H90 and Y355, as well as hydrophobic amino acids I523, F518 and L352. According to the structure of the COX-1:mofezolac complex, hydrophobic amino acids appear to have free volume eventually accessible to the more sterically hindering groups than the methoxy linked to the phenyl groups of mofezolac, in particular the methoxyphenyl at C4-mofezolac isoxazole. Mofezolac bears two methoxyphenyl groups linked to C3 and C4 of the isoxazole core ring. Thus, in the novel compounds, one or both methoxy groups were replaced by the higher homologous ethoxy, normal and isopropyl, normal and tertiary butyl, and phenyl and benzyl. Furthermore, a major difference between the two sets of compounds is the presence of either a methyl or acetic moiety at the C5 of the isoxazole. Among the C5-</p>

	<p>methyl series, 12 (direct precursor of mofezolac) (COX-1 IC₅₀ = 0.076 μM and COX-2 IC₅₀ = 0.35 μM) and 15a (ethoxy replacing the two methoxy groups in 12; COX-1 IC₅₀ = 0.23 μM and COX-2 IC₅₀ > 50 μM) were still active and with a Selectivity Index (SI = COX-2 IC₅₀/COX-1 IC₅₀) = 5 and 217, respectively. The other symmetrically substituted alkoxyphenyl moieties were inactive at 50 μM final concentration. Among the asymmetrically substituted, only the 16a (methoxyphenyl on C3-isoxazole and ethoxyphenyl on C4-isoxazole) and 16b (methoxyphenyl on C3-isoxazole and n-propoxyphenyl on C4-isoxazole) were active with SI = 1087 and 38, respectively. Among the set of compounds with the acetic moiety, structurally more similar to mofezolac (SI= 6329), SI ranged between 1.4 and 943. It is noteworthy that 17b (n-propoxyphenyl on both C3- and C4-isoxazole) were found to be a COX-2 slightly selective inhibitor with SI= 0.072 (COX-1 IC₅₀ > 50 μM and COX-2 IC₅₀ = 3.6 μM). Platelet aggregation induced by arachidonic acid (AA) can be in vitro suppressed by the synthesized compounds, without affecting of the secondary hemostasia, confirming the biological effect provided by the selective inhibition of COX-1. A positive profile of hemocompatibility in relation to erythrocyte and platelet toxicity was observed. Additionally, these compounds exhibited a positive profile of hemocompatibility and reduced cytotoxicity. Quantitative structure activity relationship (QSAR) models and molecular modeling (Ligand and Structure based virtual screening procedures) provide key information on the physicochemical and pharmacokinetic properties of the COX-1 inhibitors as well as new insights into the mechanisms of inhibition that will be used to guide the development of more effective and selective compounds. X-ray analysis was used to confirm the chemical structure of 14 (MSA17).</p>
<p>Suggested Reviewers:</p>	<p>José Carlos Menéndez Ramos, PhD Full Prof., Complutense University of Madrid josecm@farm.ucm.es Expert in the field.</p> <p>Md Jashim Uddin, PhD Associate Professor, Vanderbilt University jashim.uddin@vanderbilt.edu Expert in the Field.</p>



Department of Pharmacy – Pharmaceutical Sciences

15th September, 2023

Dear Prof.

we are submitting the manuscript "*A further pocket or conformational plasticity by mapping COX-1 catalytic site through modified-mofezolac structure-inhibitory activity relationships and their anti-platelet behavior*" to be evaluated for publication in *European Journal of Medicinal Chemistry* as part of the work made by as R. Solidoro, M. Miciaccia, C. Bonaccorso, C. G. Fortuna, D. Armenise, A. Centonze, S. Ferorelli, P. Rodrigues, R. Guimarães, A. de Oliveira, M. da Paz, L. Rangel, P. Cunha Sathler, A. Altomare, M. G. Perrone and A. Scilimati*.

The work described in this manuscript is a continuation of our efforts aimed at definitively mapping the differences of the catalytic site of the two known cyclooxygenases (COXs) isoforms, specifically focusing on COX-1 as being the less studied among COX-1 and COX-2.

During the years, we prepared a high number of compounds targeting the two enzymes and endowed with a different degree of selectivity.

From a chemical point of view, such compounds are diarylheterocycles. As core rings, we used the thiazole, imidazole, triazole and isoxazole.

Extensive structure modifications were accomplished on the diarylisoxazole. A lot of chemical groups were linked to the C5-position of the isoxazole leading to compounds with different chemical-physic and biological properties. Some molecules bear a fluorescent moiety to be used in fundamental drug discovery investigations, other to be used as fluorescent imaging probes for *in vivo* ovarian cancer targeted detection and intraoperative fluorescence image-guided surgery (FIGS) or bearing the positron emitting [18F]-fluorine used in pre-clinical ovarian cancer imaging. Other compounds were found cytotoxic in myeloma and ovarian cell lines or have a synergistic effect with already used cancer drugs in disease in which COX-1 is the main enzyme isoform expressed.

Our *in vitro* and *in vivo* model of neuroinflammation showed to benefit from treatment with our selective COX-1 inhibitors.

Furthermore, some of those compounds were deprived of gastrointestinal toxicity if compared to traditional NSAIDs included Aspirin.

Regarding this manuscript, X-ray analysis of 3D crystal of the human COX-1 (PDB: 6Y3C) and ovine COX-1 complexed with an almost apolar molecule (P6, PDB: 5U6X) or polar mofezolac (PDB: 5WBE) showed that COX-1 would have a further zone to be explored. Then, two sets of *ad hoc* designed novel compounds P6-equivalent and mofezolac derivatives were prepared and studied as COXs inhibitors and evaluated as possible antiplatelet active ingredient of drugs; aspirin was used

for comparison. *In silico* investigation is also reported to support the existence or not of a further pocket into the COX-1 active site or the inhibitory activity found was a result of the enzyme plasticity.

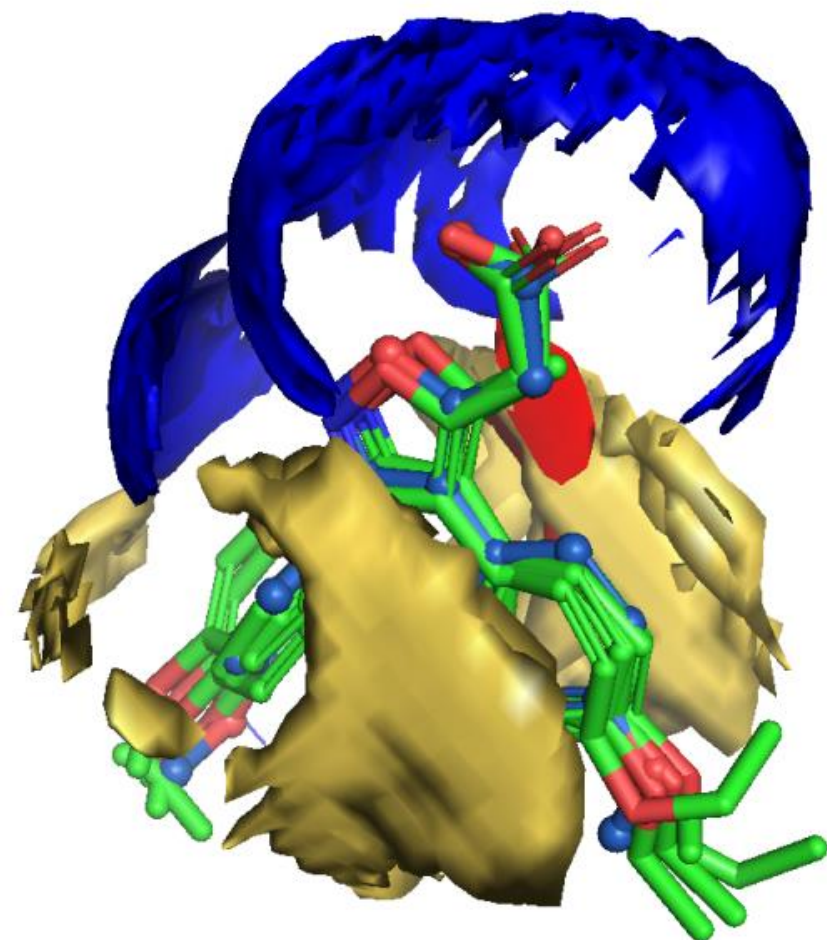
In the light of these considerations, we hope this manuscript will be sent to referees for comment. We also hope that this manuscript will find space in the *European Journal of Medicinal Chemistry* considering that most of the papers reporting the above-mentioned results have been published in this journal.

Best regards.

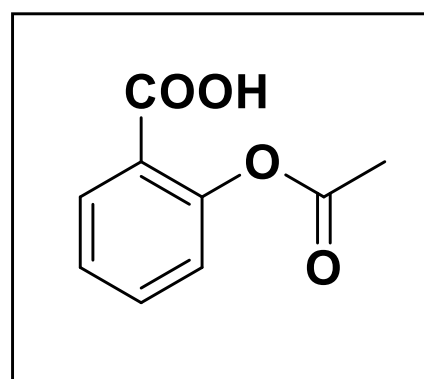
Prof. Antonio Scilimati

A handwritten signature in black ink, appearing to read "Antonio Scilimati". The signature is written in a cursive style with a large initial 'A' and 'S'.

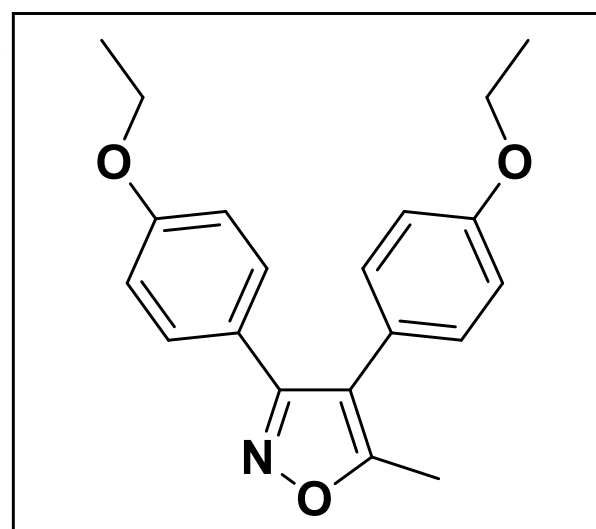
Target compounds
pose into the COX-1
catalytic site



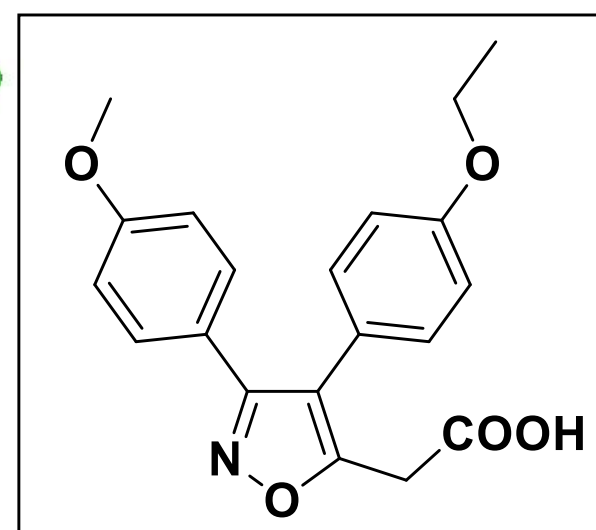
Acetylsalicylic acid (ASA)



15a

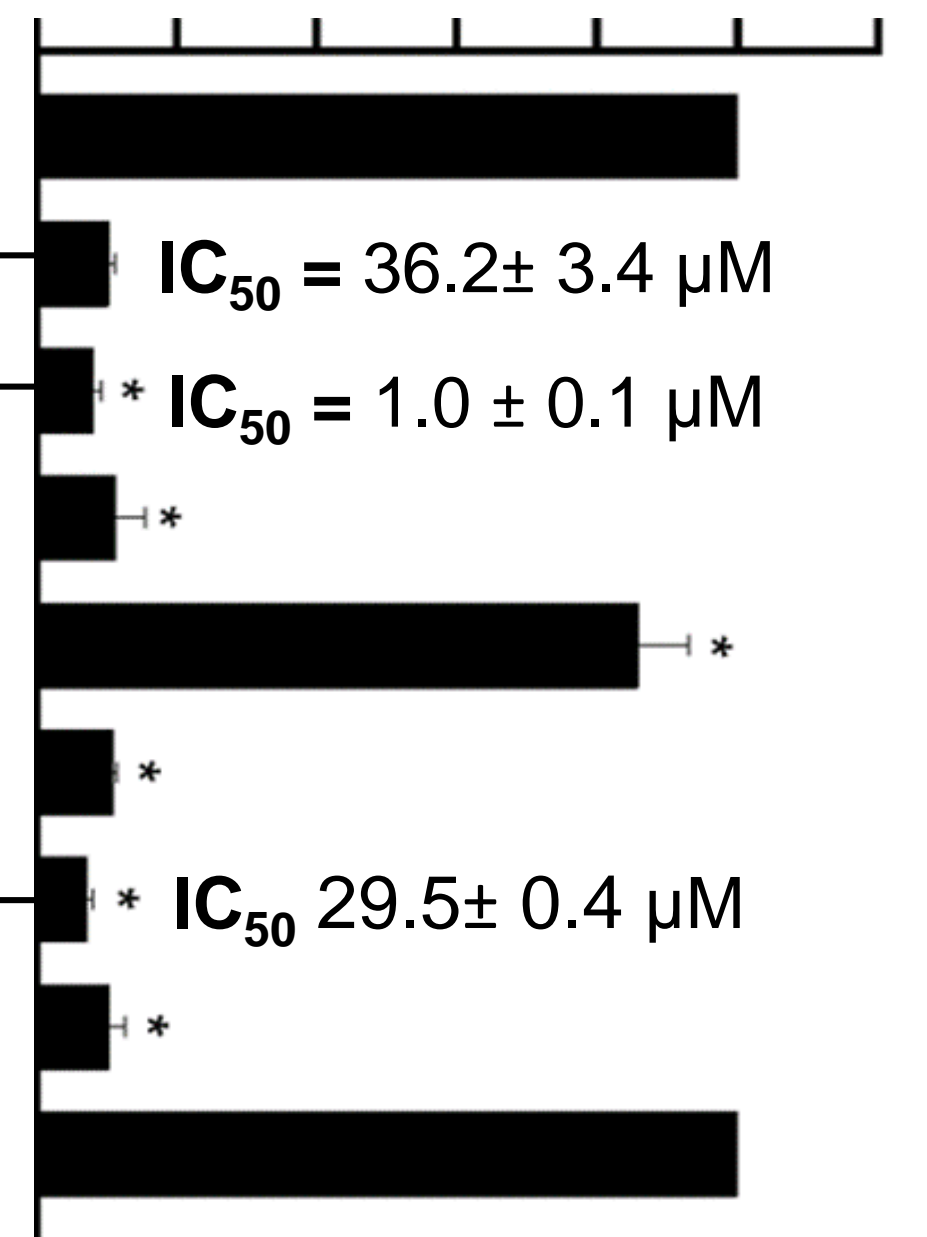


17g



% Max Platelet Aggregation

0 20 40 60 80 100 120



A further pocket or conformational plasticity by mapping COX-1 catalytic site through modified-mofezolac structure-inhibitory activity relationships and their antiplatelet behavior

Roberta Solidoro^{a§}, Morena Miciaccia^{a§}, Carmela Bonaccorso^{b§}, Cosimo Gianluca Fortuna^b, Domenico Armenise^a, Antonella Centonze^a, Savina Ferorelli^a, Paola Vitale^a, Priscila Rodrigues^c, Renilda Guimarães^c, Alana de Oliveira^c, Mariana da Paz^d, Luciana Rangel^d, Plínio Cunha Sathler^c, Angela Altomare^e, Maria Grazia Perrone^{a*}, Antonio Scilimati^{a*}

^a*Research Laboratory for Woman and Child Health, Department of Pharmacy - Pharmaceutical Sciences, University of Bari "Aldo Moro", Via E. Orabona 4, 70125, Bari, Italy*

^b*Laboratory of Molecular modelling and Heterocyclic compounds ModHet, Department of Chemical Sciences, University of Catania, Viale Andrea Doria 6, 95125 Catania, Italy*

^c*Laboratory of Experimental Hemostasis and* ^d*Laboratory of Tumoral Biochemistry, Faculty of Pharmacy, Federal University of Rio de Janeiro, Carlos Chagas Filho Avenue, 373, 21941599, Rio de Janeiro, Brazil*

^e*Institute of Crystallography-CNR Via Amendola 122/o 70126 Bari, Italy*

*Corresponding author.

Email address: antonio.scilimati@uniba.it (A. Scilimati) and mariagrazia.perrone@uniba.it (Maria Grazia Perrone).

Present address: Research Laboratory for Woman and Child Health, Department of Pharmacy - Pharmaceutical Sciences, University of Bari "Aldo Moro", Via E. Orabona 4, 70125, Bari, Italy.

§Co-first authors: RS, MM and CB contributed equally to the work.

KEYWORDS: cyclooxygenase-1, inhibitors, diarylisoxazoles, catalytic site mapping, antiplatelet agent, hemolysis, QSAR, drug design.

ABSTRACT

Cyclooxygenase enzymes have distinct roles in cardiovascular, neurological, and neurodegenerative disease. They are differently expressed in different type of cancers. Specific and selective COXs inhibitors are needed to be used alone or in combo-therapies. Fully understand the differences at the catalytic site of the two cyclooxygenase (COX) isoforms is still opened to investigation. Thus, two series of novel compounds were designed and synthesized in fair to good yields using the highly selective COX-1 inhibitor mofezolac as the lead compound to explore a COX-1 zone formed by the polar residues Q192, S353, H90 and Y355, as well as hydrophobic amino acids I523, F518 and L352. According to the structure of the COX-1:mofezolac complex, hydrophobic amino acids appear to have free volume eventually accessible to the more sterically hindering groups than the methoxy linked to the phenyl groups of mofezolac, in particular the methoxyphenyl at C4-mofezolac isoxazole. Mofezolac bears two methoxyphenyl groups linked to C3 and C4 of the isoxazole core ring. Thus, in the novel compounds, one or both methoxy groups were replaced by the higher homologous ethoxy, normal and isopropyl, normal and tertiary butyl, and phenyl and benzyl. Furthermore, a major difference between the two sets of compounds is the presence of either a methyl or acetic moiety at the C5 of the isoxazole. Among the C5-methyl series, **12** (direct precursor of mofezolac) (COX-1 $IC_{50} = 0.076 \mu M$ and COX-2 $IC_{50} = 0.35 \mu M$) and **15a** (ethoxy replacing the two methoxy groups in **12**; COX-1 $IC_{50} = 0.23 \mu M$ and COX-2 $IC_{50} > 50 \mu M$) were still active and with a Selectivity Index ($SI = COX-2 IC_{50}/COX-1 IC_{50}$) = 5 and 217, respectively. The other symmetrically substituted alkoxyphenyl moieties were inactive at 50 μM final concentration. Among the asymmetrically substituted, only the **16a** (methoxyphenyl on C3-isoxazole and ethoxyphenyl on C4-isoxazole) and **16b** (methoxyphenyl on C3-isoxazole and *n*-propoxyphenyl on C4-isoxazole) were active with $SI = 1087$ and 38, respectively. Among the set of compounds with the acetic moiety, structurally more similar to mofezolac ($SI = 6329$), SI ranged between 1.4 and 943. It is noteworthy that **17b** (*n*-propoxyphenyl on both C3- and C4-isoxazole) were found to be a COX-2 slightly selective inhibitor with $SI = 0.072$ (COX-1 $IC_{50} > 50 \mu M$ and COX-2 $IC_{50} = 3.6 \mu M$). Platelet aggregation induced by arachidonic acid (AA) can be *in vitro* suppressed by the synthesized compounds, without affecting of the secondary hemostasia, confirming the biological effect provided by the selective inhibition of COX-1. A positive profile of hemocompatibility in relation to erythrocyte and platelet toxicity was observed. Additionally, these compounds exhibited a positive profile of hemocompatibility and reduced cytotoxicity. Quantitative structure activity relationship (QSAR) models and molecular modeling (Ligand and Structure based virtual screening procedures) provide key information on the physicochemical and pharmacokinetic properties of the COX-1 inhibitors as well as new insights into the mechanisms of inhibition that will be used to guide the development of more effective and selective compounds. X-ray analysis was used to confirm the chemical structure of **14** (MSA17).

1. Introduction

The complete three-dimensional structures of the two isoforms of cyclooxygenase (COX) have long been sought [1–2]. Extensive single crystal X-ray analyses have been accomplished on the human, ovine and murine COX enzymes, as wild types and with a single amino acid replacement in their primary structure, to definitively identify residues determining the COX-mediated transformation of arachidonic acid into PGG₂/PGH₂ [2,3–5]. The latter is subsequently transformed into prostaglandins (PGs), prostacyclin (PGI₂) and thromboxane (TXA₂) by tissue-specific enzymes. The catalytic site of the COXs is a ~25 Å long hydrophobic L-shaped channel in which approximately fifty amino acids are involved in substrate/inhibitor recognition and catalysis [6]. The rationale behind the above-mentioned investigations of structural biology resides in the need to develop specific and selective inhibitors of COXs catalytic activity in diseases in which such enzymes distinctly play a pivotal role in onset and/or progression of such pathologies [7–9]. The selectivity of COXs inhibition is crucial, being related to inhibitor pharmacodynamic properties, including their toxicity. Non-selective inhibitors such as traditional Non-Steroidal Anti-inflammatory Drugs (tNSAIDs) produce gastrointestinal (GI) and renal severe adverse events, conversely highly selective COX-1 or COX-2 in *in vivo* testing showed to preserve the GI mucosa integrity [10]. Furthermore, platelet COX-1 selective inhibitors block the production of TAX₂ without modifying the biosynthesis of the atheroprotective PGI₂, whereas the selective inhibition of monocyte COX-2 activity by COXIBs completely blocks PGI₂ formation but not COX-1 derived TAX₂ production, a pro-aggregatory and vasoconstrictor mediator, which might predispose patients to heart attack and stroke [11–12].

Antiplatelet therapies reduce the risk of developing atherothrombotic disease and are a mainstay in the treatment of patients who have established cardiovascular, cerebrovascular, and peripheral artery disease. Antiplatelet drugs serve as a first-line antithrombotic therapy for the management of the prevention of secondary complications in vascular diseases. Numerous antiplatelet therapies have been developed; however, currently available agents are still associated with inadequate efficacy, risk of bleeding, and variability in individual response. Oral antiplatelet therapies for secondary prevention of ischemic recurrences in patients with atherosclerotic disease manifestations include aspirin (**1**, Figure 1) and P2Y₁₂ receptor antagonists. [13–15] Platelet COX-1 is the target of low-dose aspirin (75-100 mg/die for primary prophylaxis, 75 up to 300 mg/die for secondary prophylaxis). It irreversibly inhibits COX-1 by acetylating S530 as one of the residues of the enzyme catalytic site. Mature platelets predominantly express COX-1. Enhanced platelet activation and de novo TAX₂ biosynthesis by endothelial cells and monocytes are COX-1-mediated processes [16]. COX-2 expression is primarily induced upon mitogen and mechanical stimuli. Aspirin despite its use on a large scale, it has some limitations. Specifically, there are a lot of aspirin “not responders” mainly in

the secondary cardiovascular prevention (approximately 70% of patients), or patients allergic to the acetyl salicylic acid, active principle of aspirin. In addition, as aspirin is not a COX-1 selective inhibitor, it also inhibits COX-2 blocking the overall production of the GI protective prostaglandin E₂ (PGE₂) producing GI mucosa erosion and then bleeding [10,17].

Attempts to develop compounds (**2** with COX-1 IC₅₀ = 5 μM and COX-2 IC₅₀ > 100 μM [18]; **3** with COX-1 IC₅₀ = 0.16 μM and COX-2 IC₅₀ > 100 μM and **4** with COX-1 IC₅₀ > 100 μM and COX-2 IC₅₀ > 100 μM [5], Figure 1) eventually behaving as irreversible COX-1 inhibitors have been performed. *In silico* and X-Ray investigations showed that the acetoxy or methoxyacetoxy group linked to the C5-isoxazole core ring points far from S530 and towards the exit of the long hydrophobic catalytic site of the enzyme [3].

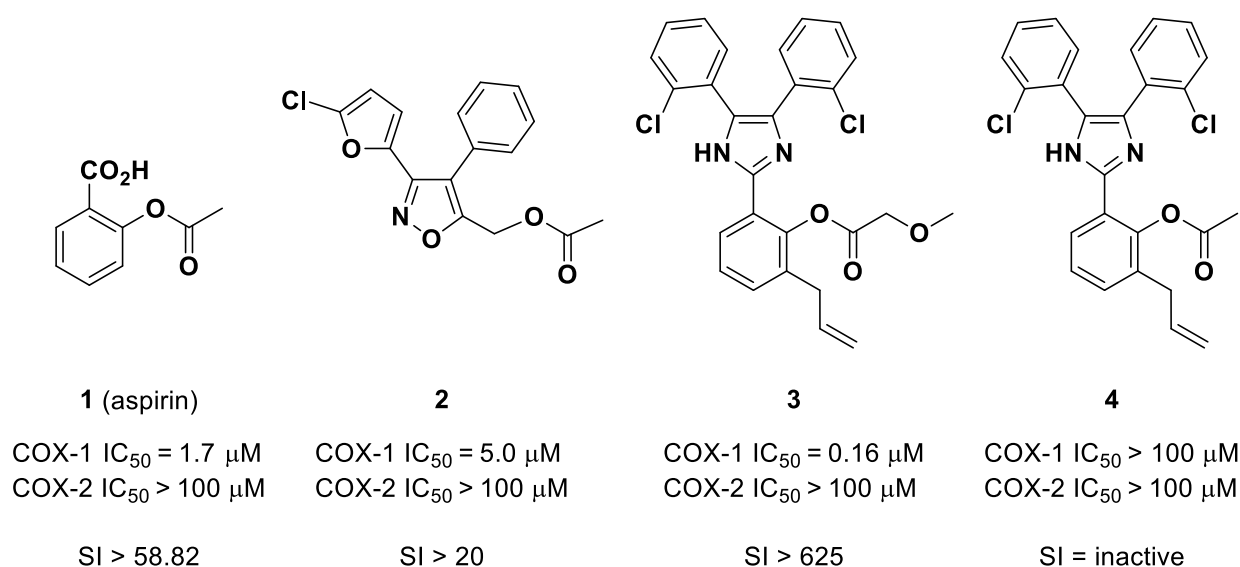


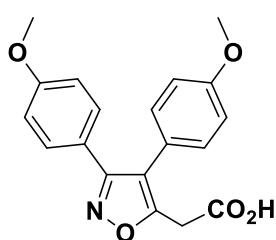
Figure 1. Comparison between **1** (aspirin), **2**, **3** and **4** chemical structure and their COXs IC₅₀ values and Selective Index (SI) = COX-2 IC₅₀/ COX-1 IC₅₀. Aspirin and **2** were determined by Human Whole Blood Assay (HWBA). **3** and **4** values were determined by a colorimetric assay (Cayman kit).

Based on the above considerations and in continuation of our previous work aimed at identifying determinants for a COX-1 selective inhibition [19–21], a further zone of this enzyme was mapped by designing structurally modified mofezolac (**5**, Figure 2), the most potent selective inhibitor of COX-1. Mofezolac was chosen not only for its high COX-1 selectivity but also because among the known selective COX-1 inhibitors (P6 (**6**), P9 (**7**), P10 (**8**), SC560 (**9**), FR122047 (**10**), ABEX-3TF(**11**), Figure 2) it is already used in humans to treat rheumatoid arthritis. The crystal structure of COX-1 bound to mofezolac reveals its binding to the enzyme active site in a planar conformation, with one methoxyphenyl group inserted deep inside the active site channel facing Y385 and the other methoxyphenyl group sandwiched between Y355 and F518 [3]. The carboxyl moiety at position 5 of the isoxazole group faces the active site channel entry point (R120, E524 and Y355). The

methoxyphenyl at C3-isoxazole is surrounded by almost exclusively hydrophobic residues (Y385, W387, F381, L384 and G526), including the catalytic Y385, while the methoxyphenyl group at C4 makes van der Waals interactions with more polar residues such as Q192, S353, H90 and Y355, as well as hydrophobic contacts with I523, F518 and L352.

In our crystal structure of COX-1:mofezolac complex [3], it seems that the space available for methoxyphenyl in C4-isoxazole would be higher and that it is assumed that increasing the size of the methoxy, by replacing it with more hindered alkoxy moieties, would result in tighter binding to the enzyme and consequently the inhibitory potency and possibly the selectivity of the novel compounds would be higher to those of mofezolac. Overall, this could mean that an additional unexplored pocket is present in the COX-1 catalytic site.

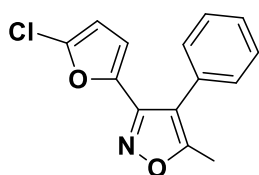
Then, to prove the latter two hypotheses two sets of novel compounds were prepared and evaluated as COXs inhibitors. Some selective COX-1 inhibitors were also tested as antiplatelet agents in platelet-rich plasma samples. *In silico* investigation were also carried out as a support to explain the observed COXs structure-inhibitory activity of the novel compounds.



5 (mofezolac)

COX-1 IC_{50} = 0.0079 μ M
COX-2 IC_{50} > 100 μ M

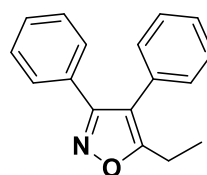
SI > 12,658



6 (P6)

COX-1 IC_{50} = 0.5 μ M
COX-2 IC_{50} > 100 μ M

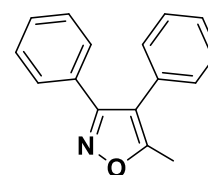
SI > 200



7 (P9)

COX-1 IC_{50} = 0.05 μ M
COX-2 IC_{50} > 1.49 μ M

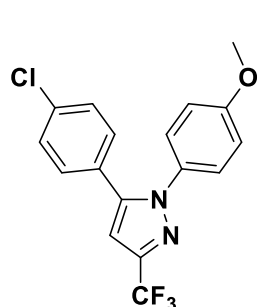
SI = 2.98



8 (P10)

COX-1 IC_{50} = 0.09 μ M
COX-2 IC_{50} = 2.49 μ M

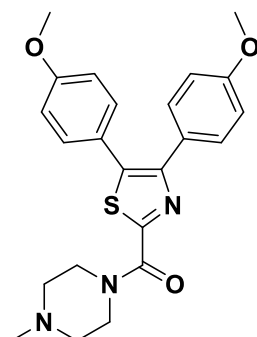
SI = 27.67



9 (SC560)

COX-1 IC_{50} = 0.07 μ M
COX-2 IC_{50} = 74.9 μ M

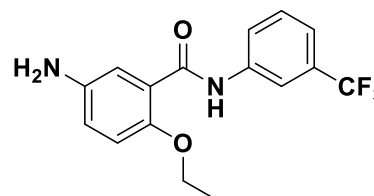
SI = 1,070



10 (FR122047)

COX-1 IC_{50} = 0.028 μ M
COX-2 IC_{50} = 65 μ M

SI = 2,321



11 (ABEX-3TF)

COX-1 IC_{50} = 3.2 μ M
COX-2 IC_{50} > 100 μ M

SI > 31.25

Figure 2. Chemical structure of some COX-1 selective inhibitors and, their COXs IC₅₀ values and Selective Index (SI) = COX-2 IC₅₀/COX-1 IC₅₀. **6** (P6), **7** (P9) and **8** (P10) were determined by Human Whole Blood Assay (HWBA). The other values were determined by a colorimetric assay (Cayman kit).

2. Results and discussion

2.1 Rational behind the design of the novel compounds

A plenty of compounds, belonging to at least five chemical classes, has been proved to be COXs inhibitors with a different extent of selectivity towards both COX isoforms. COX-1 catalytic site remains not fully mapped by their inhibitors. Using as a scaffold the chemical structure of mofezolac, several modifications of the group linked to the isoxazole ring-C5 have been made, bringing to compounds endowed with different inhibitory activity in terms of potency and selectivity [22]. The methoxyphenyl at isoxazole-C3 is surrounded by almost exclusively hydrophobic residues (Y385, W387, F381, L384 and G526), including the catalytic Y385 responsible to be transformed into its tyrosyl radical as first step of the bis-addition of two O₂ molecules to arachidonic acid catalyzed by COXs [23–24], while the methoxyphenyl group at C4 makes van der Waals interactions with more polar residues such as Q192, S353, H90 and Y355, as well as hydrophobic contacts with I523, F518 and L352. Then, the two methoxys linked to the phenyls linked to the C3- and C4-isoxazol were symmetrically and asymmetrically replaced (only at C4-phenylisoxazole) by linear and branched alkoxy chains, phenoxy, and benzyloxy as unexplored mofezolac structure modification. The replacing groups of the methoxy were carefully chosen (Scheme 1 and 2).

2.2 Chemistry

The synthesis of target compounds **15a-f** and **16a-f** were prepared in yields ranging between 28 and 95% (Scheme 1). 3,4-Bis(hydroxyphenyl)-4-methylisoxazole (**13**) and 4-(4-hydroxyphenyl)-3-(4-methoxyphenyl)-4-methylisoxazole (**14**) were prepared by reacting 3,4-bis(methoxyphenyl)-4-methylisoxazole (**12**) with 1M BBr₃ at -78 °C for 3 h and 16 h, respectively [25]. The chemical structure of **14** (MSA17) was also confirmed by X-ray diffractometric analysis of its single crystal (Figure 3) [26] (Figure S1 and Figure S2 for full XR data). Compounds **15a-d** and **16a-d** were prepared by reacting **13** and **14**, respectively, with the alkyl bromide in the presence of Cs₂CO₃. Compounds **15e** and **16e** were prepared from **13** and **14** in the presence of 2-bromine-2-methylpropane, lead(II)

carbonate basic $[(\text{PbCO}_3)_2\text{Pb}(\text{OH})_2]$ and solvent free [27]. The synthesis of **15f** and **16f** were carried out by reacting the compound **13** and **14** with silyl phenyl triflate in the presence of CsF [28].

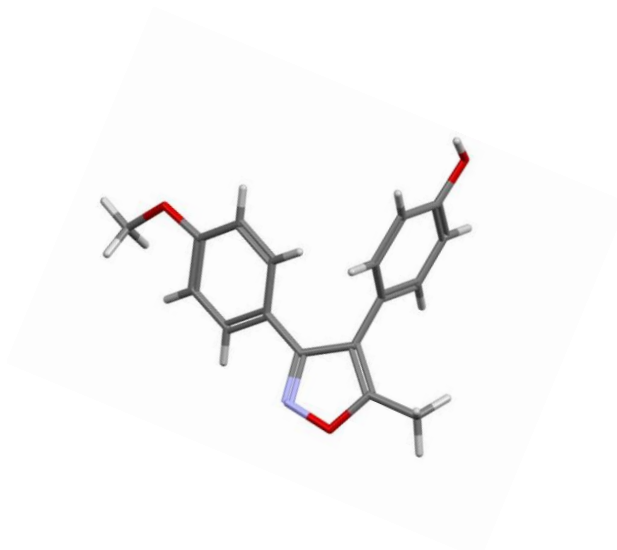
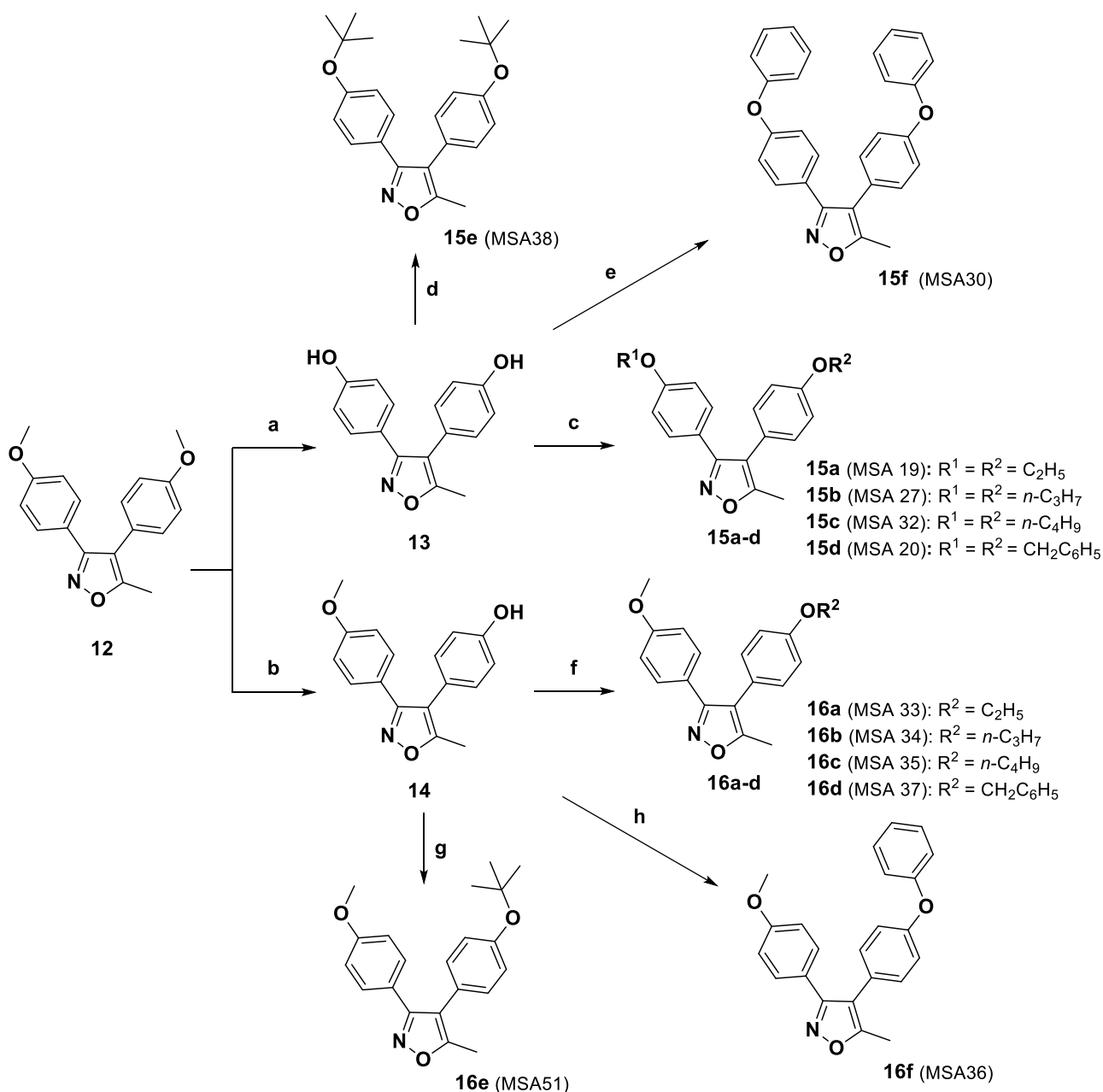
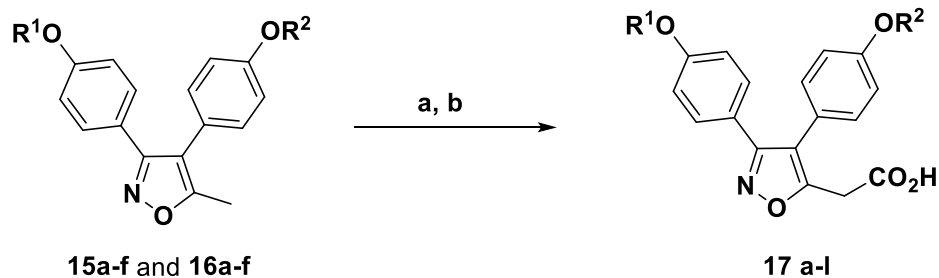


Figure 3. X-ray molecular structure of 4-[3-(4-methoxyphenyl)-5-methylisoxazol-4-yl]phenol (**14**, MSA 17).



Scheme 1. Reagents and conditions: a) anhydrous CH_2Cl_2 , BBr_3 (1M in CH_2Cl_2), $-78 \div +20^\circ C$, 16 h; b) anhydrous CH_2Cl_2 , BBr_3 (1M in CH_2Cl_2), $-78^\circ C \div +20^\circ C$, 3 h; c) anhydrous CH_3CN , Cs_2CO_3 , r.t., 30 min., alkyl or aryl bromide, $90^\circ C$, 15 min; d) solvent free, lead (II) carbonate basic $[(PbCO_3)_2Pb(OH)_2]$, 2-bromo-2-methylpropane, $0^\circ C$ for 60 min.; reflux, 15 min.; e) anhydrous CH_3CN , CsF_2 , silyl phenyl triflate, r.t., 24 h; f) anhydrous CH_3CN , Cs_2CO_3 , r.t., 30 min., alkyl or aryl bromide, $90^\circ C$, 15 min; g) solvent free, lead (II) carbonate basic, 2-bromo-2-methylpropane, $0^\circ C$ for 60 min.; reflux, 15 min; h) anhydrous CH_3CN , CsF , silyl phenyl triflate, r.t., 24 h.

The carbonation reaction was used to prepare the acetic acids **17a-i**. Compounds **15a-f** and **16a-f** were first converted into their corresponding anions with *n*-butyllithium. Then, all the corresponding diarylisoxazolyl acids were obtained by bubbling gaseous CO_2 into lithiated intermediates in anhydrous conditions. (Scheme 2) [25].



15a (MSA 19): $\text{R}^1 = \text{R}^2 = \text{C}_2\text{H}_5$

15b (MSA 27): $\text{R}^1 = \text{R}^2 = n\text{-C}_3\text{H}_7$

15c (MSA 32): $\text{R}^1 = \text{R}^2 = n\text{-C}_4\text{H}_9$

15d (MSA 20): $\text{R}^1 = \text{R}^2 = \text{CH}_2\text{C}_6\text{H}_5$

15e (MSA 38): $\text{R}^1 = \text{R}^2 = \text{C}(\text{CH}_3)_3$

15f (MSA 30): $\text{R}^1 = \text{R}^2 = \text{C}_6\text{H}_5$

16a (MSA 33): $\text{R}^1 = \text{CH}_3, \text{R}^2 = \text{C}_2\text{H}_5$

16b (MSA 34): $\text{R}^1 = \text{CH}_3, \text{R}^2 = n\text{-C}_3\text{H}_7$

16c (MSA 35): $\text{R}^1 = \text{CH}_3, \text{R}^2 = n\text{-C}_4\text{H}_9$

16d (MSA 37): $\text{R}^1 = \text{CH}_3, \text{R}^2 = \text{CH}_2\text{C}_6\text{H}_5$

16e (MSA 51): $\text{R}^1 = \text{CH}_3, \text{R}^2 = \text{C}(\text{CH}_3)_3$

16f (MSA 36): $\text{R}^1 = \text{CH}_3, \text{R}^2 = \text{C}_6\text{H}_5$

17a (MSA 42): $\text{R}^1 = \text{R}^2 = \text{C}_2\text{H}_5$

17b (MSA 55): $\text{R}^1 = \text{R}^2 = n\text{-C}_3\text{H}_7$

17c (MSA 39): $\text{R}^1 = \text{R}^2 = n\text{-C}_4\text{H}_9$

17d (MSA 57): $\text{R}^1 = \text{R}^2 = \text{CH}_2\text{C}_6\text{H}_5$

17e (MSA 60): $\text{R}^1 = \text{R}^2 = \text{C}(\text{CH}_3)_3$

17f (MSA 56): $\text{R}^1 = \text{R}^2 = \text{C}_6\text{H}_5$

17g (MSA 45): $\text{R}^1 = \text{CH}_3, \text{R}^2 = \text{C}_2\text{H}_5$

17h (MSA 53): $\text{R}^1 = \text{CH}_3, \text{R}^2 = n\text{-C}_3\text{H}_7$

17i (MSA 54): $\text{R}^1 = \text{CH}_3, \text{R}^2 = n\text{-C}_4\text{H}_9$

17j (MSA 59): $\text{R}^1 = \text{CH}_3, \text{R}^2 = \text{CH}_2\text{C}_6\text{H}_5$

17k (MSA 61): $\text{R}^1 = \text{CH}_3, \text{R}^2 = \text{C}(\text{CH}_3)_3$

17l (MSA 58): $\text{R}^1 = \text{CH}_3, \text{R}^2 = \text{C}_6\text{H}_5$

Scheme 2. Reagents and conditions: a) 1.6N *n*-BuLi (hexane solution), dry THF, -78°C , b) gaseous CO_2 .

2.3 Cyclooxygenase catalytic activity inhibition evaluation

Two sets of novel compounds were designed and synthesized in fair to good yields. Mofezolac (**5**) or its precursor 3,4-bis(4-methoxyphenyl)-5-methylisoxazole (**12**) were used as “lead compounds”, and their interactions established with the amino acid residues forming the catalytic site of the COX-1 were considered to design the new compounds to be synthesized. Human COX-1 (*h*COX-1) has a homology with ovine COX-1 (*o*COX-1) equal to 93%, whereas *h*COX-1 has a homology with *h*COX-2 equal to 63%, and in both cases the main differences did not reside in the active sites. As a consequence, at least the human or ovine COX-1 three-dimensional structure can be used to furthermap the enzyme three-dimensional structure and to develop selective inhibitors as active ingredient of drugs [29], fluorescent probes necessary for both drug discovery investigations and fluorescent-imaged guided surgery (i.e., ovarian cancer resection) [9, 21] and imaging agents for positron emission tomography (PET) [30].

The first set of molecules are 3,4-bis(4-methoxyphenyl)-5-methylisoxazole derivatives **15a-d**, in which both the phenyl-linked methoxy groups at the isoxazol-C3 and C4, were replaced by more sterically hindered alkoxy, phenoxy and benzyloxy (Scheme 1, Table 1).

Comparing with the lead compound **12** ($\text{IC}_{50} = 0.076 \mu\text{M}$ and COX-2 $\text{IC}_{50} = 0.35 \mu\text{M}$), steric hindrance determines an increase in selectivity in favor of COX-1 but only with the replacement with ethyl groups, **15a** (3,4-bis(4-ethoxyphenyl)-5-methylisoxazole) COX-1 IC_{50} is $0.23 \mu\text{M}$ and COX-2

IC₅₀ is higher than 50 μM; the COX-1 selectivity is greater than 217 with respect to 5 for compound **12**. In all other cases of increased steric hindrance, *n*-propyl (**15b**) and *n*-butyl (**15c**) or the branched *t*-butyl (**15e**) replacing methyl groups, there is a loss of potency and selectivity.

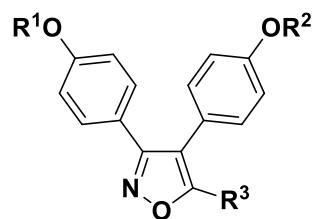
Another set of derivatives of the lead compound **12** was prepared obtaining **13** (3,4-bis(4-methoxyphenyl)-5-methylisoxazole), in which both methoxy groups were removed or derivatives (**16a-d**) in which only 4-methoxyphenyl at isoxazole-C4 was replaced by 4-ethoxy- (**16a**), 4-*n*-propoxy- (**16b**), 4-*n*-butoxy- (**16c**), 4-*t*-butoxy- (**16e**), 4-phenoxy- (**16f**) and 4-benzyloxy-phenyl (**16d**). The compounds with 4-ethoxyphenyl (**16a**) on isoxazole-C4 has COX-1 IC₅₀ = 0.046 μM and COX-2 IC₅₀ > 50 μM and 4-*n*-propoxyphenyl (**16b**) on isoxazole-C4 has COX-1 IC₅₀ = 1.3 μM and COX-2 IC₅₀ > 50 μM, showing SI > 1087 and > 38 for **16a** and **16b**, respectively. The more hindered substituents 4-*n*-butoxy (**16c**), 4-*t*-butoxy (**16e**), 4-phenoxy (**16f**) and 4-benzyloxy (**16d**) on the phenyl-C4 were completely inactive at the final concentration of 50 μM.

It is clear that, in the new molecules resembling mofezolac (**5**) the presence of the carboxyl group, thanks to its interaction with R122, E 524 and Y355 at the gate of the active site, allows to predict and thus confirm COXs inhibitory selectivity.

In particular, the 3,4-bis(4-methoxyphenyl)-5-methylisoxazole derivatives (**15a-f** and **16a-f**) were converted into their corresponding 5-acetic acids [symmetric **17a-f** and asymmetric substituted **17g-l** (Scheme 2)]. Mofezolac (**5**) has COX-1 IC₅₀ = 0.0079 μM and COX-2 IC₅₀ > 50 μM, whereas its ethyl derivative **17a** has COX-1 IC₅₀ = 0.12 μM and COX-2 IC₅₀ > 50 μM and the SI value dropped from 6329 (mofezolac) to 417 for **17a**, that remains a compound with high COX-1 selectivity. The introduction of the *n*-PrO (**17b**) in the place of the two mofezolac-MeO determines a reduction of the inhibitory activity and unexpected selectivity reversion in favor of COX-2. In fact, COX-1 IC₅₀ > 50 μM and COX-2 IC₅₀ = 3.6 μM (SI > 0.072, its inhibitory potency is 14 times greater for COX-2). On the other hand, *n*-BuO in the place of the two MeO afforded **17c** with COX-1 IC₅₀ = 0.053 μM and COX-2 IC₅₀ > 50 μM (SI > 943 in favor of COX-1). All the other substitution brought to compounds with no COXs inhibitory activity. Then, also the unsymmetrically substituted 3,4-bis(4-methoxyphenyl)-5-methylisoxazole derivatives (**16a-f**) were transformed into the mofezolac analogues **17g-l**. The compound with 4-methoxyphenyl on isoxazole-C3 and 4-ethoxyphenyl (**17g**) on isoxazole-C4 has COX-1 IC₅₀ = 0.12 μM and COX-2 IC₅₀ > 50 μM (COX-1 SI > 417). **17h** with 4-methoxyphenyl on isoxazole-C3 and 4-*n*-propoxyphenyl on isoxazole-C4 shows COX-1 IC₅₀ = 0.079 μM and COX-2 IC₅₀ = 6.9 μM (SI = 87 in favor of COX-1). **17i** with 4-methoxyphenyl on isoxazole-C3 and 4-*n*-butoxyphenyl on isoxazole-C4 has COX-1 IC₅₀ = 0.32 μM and COX-2 IC₅₀ = 0.45 μM (SI = 1.4 in favor of COX-1). The compounds with 4-methoxyphenyl on isoxazole-C3 and

4-*t*-butoxyphenyl (**17k**) or 4-phenoxyphenyl (**17l**) on isoxazole-C4 were found to be deprived of any COXs inhibitory activity. A recovered inhibitory activity was observed with **17j** having the 4-methoxyphenyl on isoxazole-C3 and benzyloxyphenyl on isoxazole-C4 [COX-1 IC₅₀ = 0.45 μM and COX-2 IC₅₀ > 50 μM (COX-1 SI > 111)].

Table 1. COX inhibitory activity of **12**, **15a-f** and **16a-f** and of the corresponding acetic acids **5**, **17a-l** and their Selectivity Index (SI).



Compound	R ¹	R ²	R ³	oCOX-1 IC ₅₀ (μM) ^a (percentage inhibition, %) ^b	hCOX-2 IC ₅₀ (μM) ^a (percentage inhibition, %) ^b	SI ^c
12	Me	Me	Me	0.076 (100)	0.35 (71)	5
15a (MSA19)	Et	Et	Me	0.23 (79)	>50	>217
15b (MSA27)	n-Pro	n-Pro	Me	>50 (40)	>50 (27)	na ^d
15c (MSA32)	n-Bu	n-Bu	Me	>50 (18)	>50 (7)	na
15d (MSA20)	Benzyl	Benzyl	Me	>50 (37)	>50 (13)	na
15e (MSA38)	<i>t</i> -Bu	<i>t</i> -Bu	Me	>50 (32)	>50 (31)	na
15f (MSA30)	Phenyl	Phenyl	Me	>50 (6)	>50 (8)	na
16a (MSA33)	Me	Et	Me	0.046 (76)	>50 (18)	>1087
16b (MSA34)	Me	n-Pro	Me	1.3 (61)	>50 (18)	>38
16c (MSA35)	Me	n-Bu	Me	>50 (42)	>50 (26)	na
16d (MSA37)	Me	Benzyl	Me	>50 (47)	>50 (12)	na
16e (MSA51)	Me	<i>t</i> -Bu	Me	>50 (0)	>50 (0)	na
16f (MSA36)	Me	Phenyl	Me	>50 (29)	>50 (8)	na

5 (mofezolac)	Me	Me	CH ₂ COOH	0.0079 (100)	>50 (45)	>6329
17a (MSA42)	Et	Et	CH ₂ COOH	0.12 (85)	>50 (12)	>417
17b (MSA55)	n-Pro	n-Pro	CH ₂ COOH	>50 (0)	3.6 (57)	<0.072
17c (MSA39)	n-Bu	n-Bu	CH ₂ COOH	0.053 (61)	>50 (16)	>943
17d (MSA57)	Benzyl	Benzyl	CH ₂ COOH	>50 (15)	>50 (4)	na
17e (MSA60)	Phenyl	Phenyl	CH ₂ COOH	>50 (0)	>50 /24)	na
17f (MSA56)	t-Bu	t-Bu	CH ₂ COOH	>50 (0)	>50 (16)	na
17g (MSA45)	Me	Et	CH ₂ COOH	0.12 (87)	>50 (7)	>417
17h (MSA53)	Me	n-Pro	CH ₂ COOH	0.079 (72)	6.9 (79)	87
17i (MSA54)	Me	n-Bu	CH ₂ COOH	0.32 (64)	0.45 (76)	1.4
17j (MSA59)	Me	Benzyl	CH ₂ COOH	0.45 (60)	>50 (35)	>111
17k (MSA61)	Me	Phenyl	CH ₂ COOH	>50 (0)	>50 (23)	na
17l (MSA58)	Me	t-Bu	CH ₂ COOH	>50 (0)	>50 (24)	na

^aIC₅₀ values are the means of at least three independent measurements. ^bInhibition percentage (%) determined at the highest final inhibitor concentration used (50 μM). ^cSelectivity Index (SI) = COX-2 IC₅₀/COX-1 IC₅₀. ^dnot applicable.

2.4 Inhibition of AA-induced platelet aggregation

Among all the synthesized compounds, a small set (**15a**, **16a**, **17c**, **17a**, **17g**, **17h**, and **17j**) was chosen to *in vitro* evaluate their antiplatelet profile. The pair **15a** and **17a** were chosen because the latter is the corresponding acid of the former and both carry two ethoxy groups. Same selection criterion for **16a** and **17g**, which carry a methoxy on the phenyl linked to the isoxazole-C3 and an ethoxy on the phenyl linked to the isoxazole-C4. **17c**, **17h** and **17j** were selected since their COX-1 SI is high ranging between 87 (**17h**) and 943 (**17c**): **17h** bearing a methoxy on the phenyl linked to the isoxazole-C3 and a *n*-propoxy on the phenyl linked to the isoxazole-C4, **17c** has a *n*-BuO on both the phenyl linked to the isoxazole-C3 and isoxazole-C4. **17j** bears the 4-methoxyphenyl on isoxazole-C3 and benzyloxyphenyl on isoxazole-C4.

The results of the platelet aggregation assays induced by arachidonic acid indicate that compounds **15a**, **16a**, **17a**, **17g**, and **17h**, in single concentration, promoted expressive inhibition of maximum

platelet aggregation ($p \leq 0.05$) (Figure 4). They also showed pharmacological activity equivalent or superior to acetylsalicylic acid (ASA) ($10.2\% \pm 0.7$), the clinically used drug that acts as cyclooxygenase-1 (COX-1) irreversible inhibitor. The compound **17c**, despite showing statistical significance, expressed inhibitory action below 50%. Then, the compounds were evaluated for their concentration required to inhibit 50% of platelet aggregation induced by the AA agonist (IC_{50}). The IC_{50} assay identified compound **17a** ($0.7 \pm 0.3 \mu\text{M}$) as the most potent, followed by **15a** ($1.0 \pm 0.1 \mu\text{M}$) and **16a** ($2.5 \pm 0.8 \mu\text{M}$). These compounds exhibited mean IC_{50} values lower than ASA ($36.36 \pm 5.32 \mu\text{M}$), indicating biological and statistical significance ($p \leq 0.05$). **17c** and **17j** showed the lowest inhibitory potency ($IC_{50} > 100 \mu\text{M}$) (Table 2). These data reveal the potency of these antiplatelet compounds to inhibit the arachidonic acid pathway of platelet aggregation, confirming a possible mechanism that enables the reduction of thromboxane A2 (TXA2) via COX-1 inhibition [6]

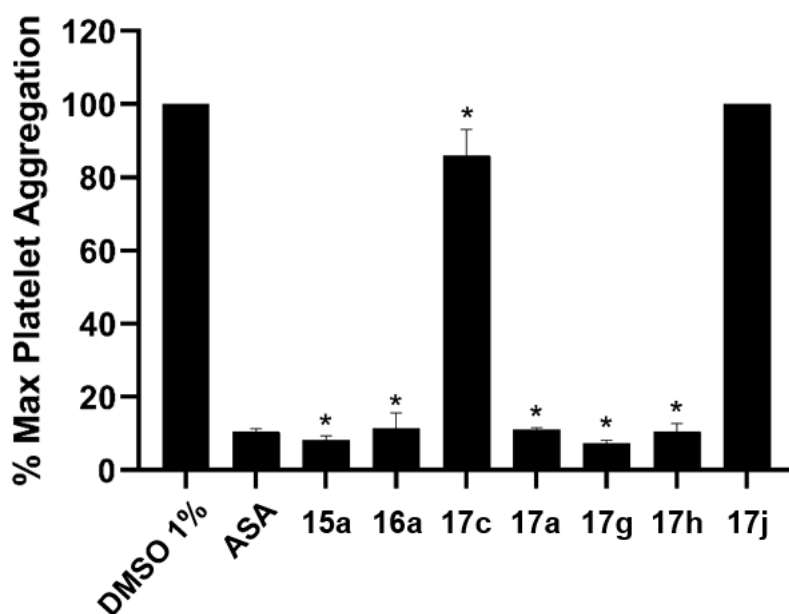


Figure 4. Antiplatelet profile of compounds (100 μM) compared to acetylsalicylic acid (ASA) tested at the same concentration on platelet aggregation induced by arachidonic acid (AA) (500 μM). * $p \leq 0.05$ (one-way ANOVA, Tukey test).

Table 2. Concentration required to inhibit 50% of arachidonic acid (AA)-induced platelet aggregation (IC_{50}) for the compounds. Results are expressed as mean \pm standard deviation (SD).

Compound	IC ₅₀ (μM)
ASA	36.2± 3.4
15a	1.0 ± 0.1
16a	2.5 ± 0.8
17c	>100
17a	0.7 ± 0.3
17g	29.5± 0.4
17h	72.1± 3.4
17j	>100

2.5 *In vitro* anticoagulant assay

The prothrombin time (PT) and activated partial thromboplastin time (APTT) assays revealed no anticoagulant activity for derivatives was observed. In this perspective, neither the extrinsic nor intrinsic pathways of the coagulation cascade were affected by the presence of the compounds, suggesting that the anti-hemostatic profile of the compounds described herein relies on the direct impairment of platelet aggregation, thus differing from dual action molecules (Figure 5). Although some compounds showed statistical significance, they were not able to increase the “ratio between test and control time” (T/Tc) by two times, not showing an anticoagulant activity. This result reveals lower risk compared to dual acting molecules whose mechanism often led to severe bleeding disorders [31].

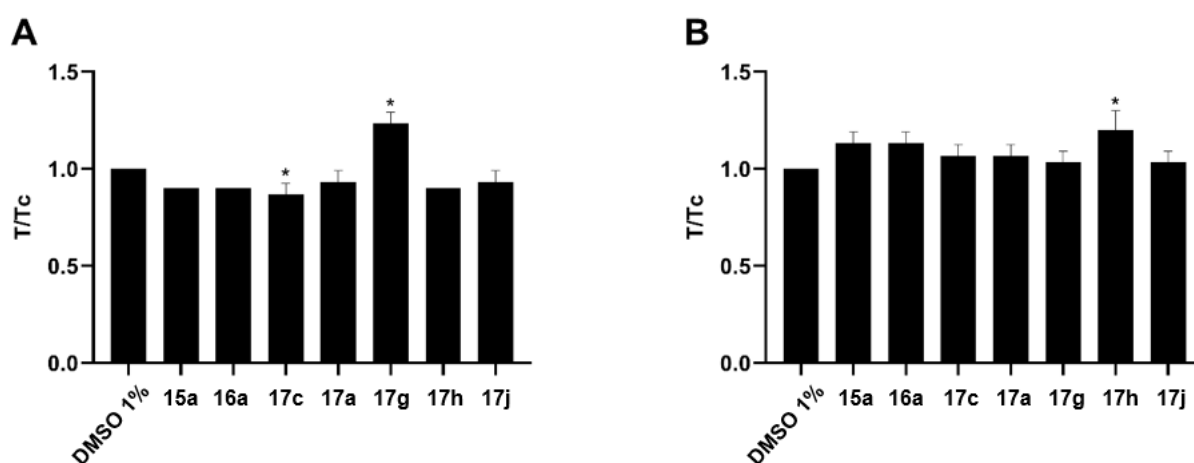


Figure 5. Evaluation of compounds on in vitro blood clotting by (A) prothrombin time (PT) and (B) activated partial thromboplastin time (APTT). All compounds were tested at 100 μM and DMSO (1%) was used as negative control. T/Tc is the ratio between test and control time in seconds. *p ≤ 0.05 (one-way ANOVA, Tukey test).

2.6 Hemocompatibility and cytotoxicity profiles

The erythrocyte hemocompatibility profile of the compounds was determined based on their degree of red blood cells lysis observed in the 3h incubation period at 37°C. The results obtained reveal that the derivatives promoted a reduced hemolytic profile (0 - 5.4%). According to Fisher et al. [32] hemolysis values below 10% are considered non-hemolytic, confirming the acceptable toxicity profile of the compounds tested (Figure 6A). For the analyses of the derivatives platelet hemocompatibility profile, the thrombocyte viability was evaluated by measuring lactate dehydrogenase (LDH) *in vitro*. The results show that all compounds, at the tested concentrations (100 µM), do not promote significant platelet lysis, since the observed LDH release is not significant ($p \geq 0.05$) (Figure 6B). In this perspective, it is possible to infer that the reduction of platelets aggregating character promoted by the compounds occurs by specific inhibition of the hemostatic mechanisms and not by cell destruction [33].

The cytotoxicity assay of the compounds in the Vero cell line was carried out using the MTT method. Although almost all compounds showed a significant difference ($p \leq 0.05$) in relation to the control, after 24 hours, except for **16a**, which displayed cell viability of $64 \pm 4\%$, all compounds demonstrated to be non-cytotoxic, with cell viability above 70% (Figure 6C). This result is according with ISO 10993:5 (2009) [34], which establishes that cell viability reductions above 30% indicate cytotoxicity.

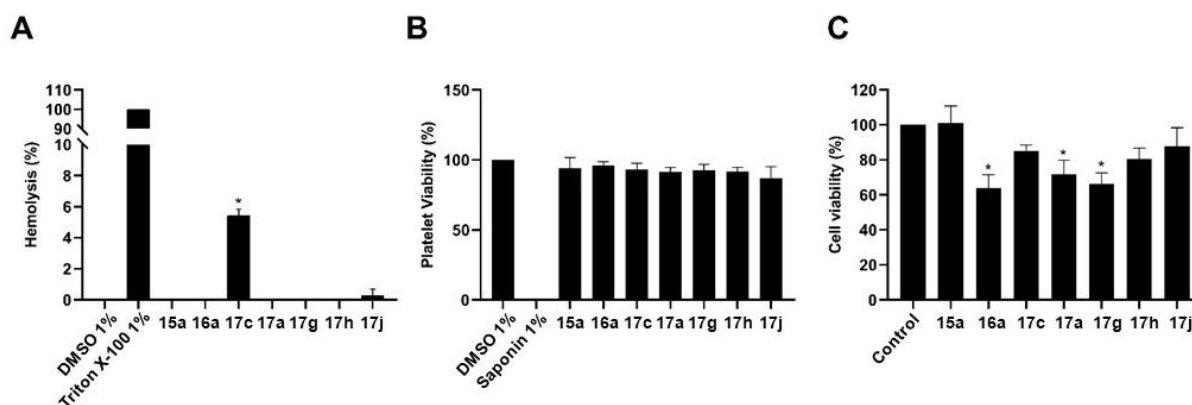


Figure 6. Erythrocyte hemocompatibility assessment of the compounds (100 µM) after 3 h of incubation. Values below 10% are considered non-hemolytic. Negative control: DMSO 1%, Positive control: Triton X-100 1% (A). Evaluation of *in vitro* platelet viability of compounds by LDH determination. Negative control: DMSO 1%, positive control: Saponin 10% (B). The low cytotoxicity profile displayed by compounds at 100 µM on Vero cells. Cells were treated for 24 hours, and cell viability was performed with MTT assay (C). * $p \leq 0.05$ (one-way ANOVA, Tukey test).

3. *In silico* investigation

The interactions established by mofezolac inside the catalytic site of the cyclooxygenase-1 have definitively been identified by studying X-ray of the *o*COX-1:mofezolac crystal [3]. The inhibition

of COX-1 is achieved by sterically hindering the entrance of arachidonic acid by the synergy of two sets of interactions with the active channel amino acid residues: i) a strong salt bridge with R120 and three hydrogen bonds with Y355 and R120 at the entry of the active site channel; ii) a dense network of Van der Waals and hydrophobic contacts with 17 amino acid residues within the COX-1 long L-shaped active site channel.

Data reported in Table 1 highlight how subtle structural variations [i.e., substitution of one or both methoxyphenyl moiety with ethoxyphenyl (mofezolac vs. **17a** and **17g**; SI = 6329 vs 417 for both compounds)], cause significant variation of the compound inhibition activity and selectivity. These data allowed us to propose a combined *in silico* approach based on i) the derivation of a Quantitative Structure Activity Relationship (QSAR) model and ii) two Virtual Screening procedure (LBVS) to infer the correlation between the chemical features of the proposed COX-1 inhibitors and the inhibitory activities (Ligand Based Virtual Screening, LBVS), and to analyze the pose of selected ligands on the COX-1 catalytic pocket (Structure Based Virtual Screening, SBVS). The QSAR model and the Virtual Screening studies were performed through the Volsurf+ (VS+) [35–37] and FLAP [38-40] software, respectively, developed by Molecular Discovery (www.moldiscovery.com/software/vsplus, www.moldiscovery.com/software/flap).

3.1 QSAR Model

The 26 compounds listed in Table 1 defined the dataset for the development of our QSAR model: among them, 11 compounds showed a percentage (%) inhibition, measured at 50 μ M compound final concentration, higher than 60% and an IC_{50} lower than 2 μ M. The structures were imported in the VS+ software which converts the structural information embedded in GRID MIFs into 128 descriptors, related to physicochemical and pharmacokinetic properties, such as size and shape, hydrophobicity and hydrophilicity, amphiphilic moment, flexibility, solubility, permeability and ADME properties. These descriptors for the mofezolac-like compounds were used as variables, whereas the COX-1 inhibition activities (IC_{50} values) were converted to a molar basis (mol/L) and then the logarithmically transformed data ($\log IC_{50}$) were used as response variables in the Partial Least Squares (PLS) analysis.

The PLS analysis resulted in a five latent-variable (LV) model with an overall $R^2 = 0.79$; the model was internally validated by Leave One Out (LOO) procedure yielding a Q^2 value = 0.47 at the second LV (Figure S3 for R^2 and Q^2 plot); further LVs in the model did not provide a significant improvement in Q^2 value. The first two LVs discriminate between molecules with high (red circle) and low (blue circle) inhibition potency while the two series of synthesized molecules (functionalized with methyl

or acetic moiety at the C5 of the isoxazole ring) can be clearly identified in the t/t scores plot (Figure 7).

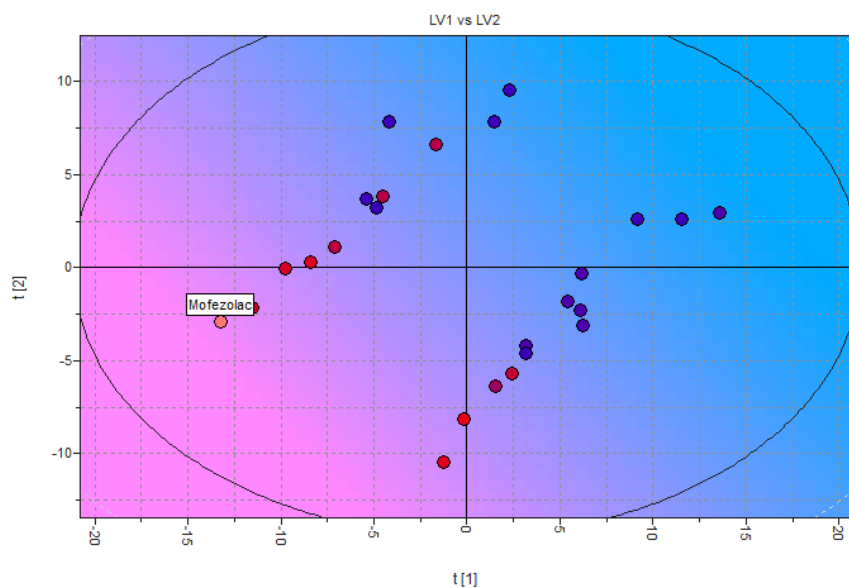


Figure 7. Scoring plot generated by the PLS activity model at the second latent variable (LV1 vs LV2). Compounds with no inhibitory capability are indicated in blue, and the inhibitors as red circles (according to the exp LogIC₅₀ behavior).

Relevant molecular descriptors were identified through the plot of PLS coefficients (Figure S4): variables contributing positively toward inhibition activity are depicted in the PLS coefficient profile with negative bars and those contributing negatively with positive bars. Relevant positive contribution was observed for the descriptors Hydrophilic Integy moment (IW4), Diffusivity (DIFF) and Intrinsic solubility (SOLY). A negative contribution emerged for the descriptor related to Volume (V), Rugosity (R), Polarizability (POL), Hydrophobic surface areas (HSA), mixed Dry-Dry-Acceptor 3D triplets pharmacophoric areas (DRDRAC), LogP octanol/water (LOGP *n*-Oct).

The distribution plots corresponding to these descriptors (Figure 8): in all cases compounds with no inhibitory capability are in blue, and the inhibitors in red (according to the experimental LogIC₅₀ values). When compounds with mixed inhibition behavior (low selectivity) are present for a certain descriptor range of values, the color produced for the bar is purple or violet. In the distribution plots, most histograms are clear red or blue, and this means a clear clustering of the compounds. This, further support that the selected descriptors are highly significant in predicting COX-1 inhibition effect.

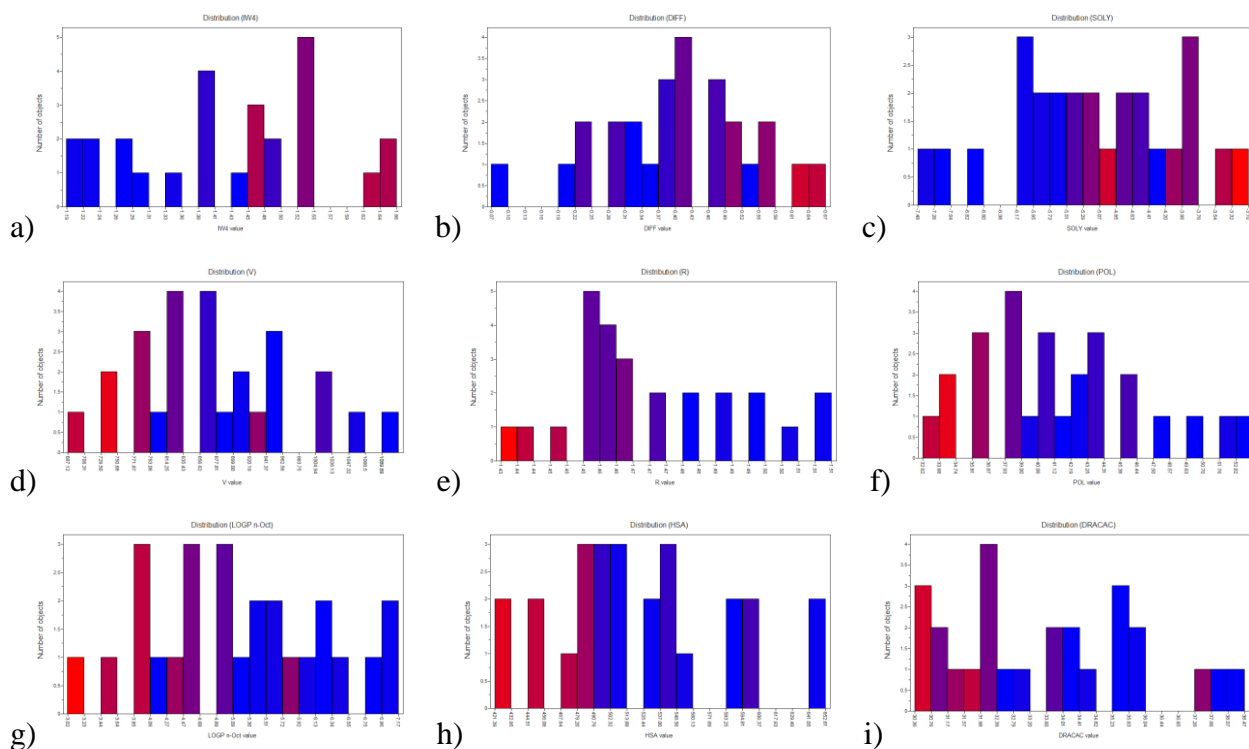


Figure 8. Distribution of selected VolSurf+ descriptors for the proposed COX-1inhibitors: compounds with no inhibitory capability are in blue, and the inhibitors in red (according to the experimental LogIC_{50} values). The descriptors are: a) Hydrophilic INTEGY moment (IW4), b) Diffusivity (DIFF), c) Solubility (SOLY), d) Volume (V), e) Rugosity (R), f) Polarizability (POL), g) LogP octanol/water (LOGP *n*-Oct), h) Hydrophobic surface areas (HSA) and i) mixed Dry-Dry-Acceptor 3D triplets pharmacophoric areas (DRDRAC).

A close inspection of the Distribution plots provides useful insight on the physicochemical and pharmacokinetic properties of the COX-1 inhibitors. Compounds with a Volume (water-excluded volume) below 790 \AA^3 and highest values for Diffusivity (Diff) and Rugosity (ratio of volume/surface) displayed relevant inhibition activity. Thus, it is simply to realize that smaller compounds show the highest activity (**15a**, **16a**, **17a**, **17g**, **17c**, **17i** and **12**), but also why, among the compounds with different alkoxy moieties, only the two possessing the smaller and wrinkled *n*-butyl (namely **17c** and **17i**) are effective COX-1 inhibitors, while no significant inhibitory activity was observed for **17f** and **17k**, endowed of the bulkier and almost spheric *t*-butyl groups. Descriptors related to hydrophobicity/hydrophilicity allowed to define further details of the inhibitor structures as they possess low values for: i) Molecular polarizability (POL), ii) Hydrophobic Surface Area (HAS: sum of hydrophobic region contributions), iii) partition coefficient between 1-octanol and water (LOGP *n*-Oct), iv) area (over all possible conformers) of the triangles derived from the Dry-Dry-Acceptor triplet (DRDRAC) but improved solubility (SOLY).

When referring to amphiphilic moment, some VS+ descriptors (namely Interaction Energy moments or INTEGY moments) can measure the unbalance between the center of mass of a molecule and the barycenter of the hydrophilic regions; our PLS model indicates that a clear concentration of hydrated

regions in only one part of the molecular surface (high IW4 values) due to the presence of polar/charged moieties (i.e. carboxylate group) improved the inhibitory activity.

3.2 Ligand and Structure Based Virtual Screening

In the last decade X-ray crystallography has played a pivotal role to unveil COX active site and understand the binding mode of COX inhibitors. Few COX-1 selective inhibitors have been developed (mofezolac (**5**), P6 (**6**), SC-560 (**9**), or FR122047 (**10**), Figure 1) [3,41,42] and among those only the X-ray structures of COX-1 co-crystallized with mofezolac and P6 have been reported so far (PDB IDs 5WBE and 5U6X) [3]. Ligand and Structure based Virtual screening employing the FLAP software was performed; these screening have to be considered as “local”, since they were built by using focused templates and datasets.

First, the mofezolac structure co-crystallized in the catalytic cavity (PDB IDs 5WBE) was chosen as a template to investigate the set of inhibitors (Table 1) in the Ligand Based procedure; then, to evaluate the performance of the screening the Enrichment Plots was analyzed (Figure 9). The enrichment curves (True positive rate vs. False positive rate, Receiver Operating Characteristic (ROC) plot) and the final Area Under the Curve (AUC) for the best performing similarity score, H*Dry*H (Shape combined with Hydrophobicity) were reported. The AUC and True positive rate, which are measures of the successful discrimination between known actives and not actives by the template, reached the values of 0.88 and 50%, respectively, indicating in general very good results in terms of retrieval and ranking of actives.

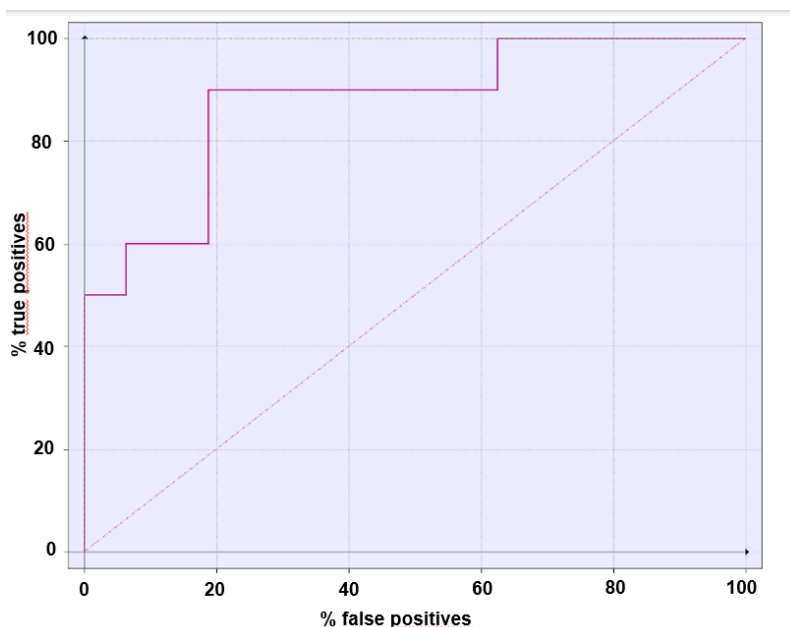


Figure 9. ROC plots for ligand-based modelling: False positive rate (x-axis) versus True positive rate (y-axis). Enrichment curves for FLAP LBVS model is given in blue for the H*Dry*H similarity score.

Finally, to determine the pharmacophoric features important for COX-1 inhibition activity, which similarity scores gave the best enrichments plots were examined. Most of the similarity scores provided good AUC values, however scores containing the "O" probe (Hydrogen-bond acceptor) did not perform well; the reason for this is clear as the mofezolac template possess no hydrogen-bond donors to generate the corresponding hydrogen-bond acceptor field as at physiological pH, the carboxylate form is the prevalent species.

The H*Dry*H scores (Shape combined with Hydrophobicity) provided the best AUC value, namely 0.89. This result is in good agreement with the QSAR study that highlighted how descriptors related to shape (V, Diff and R) or hydrophobicity (IW4, POL, HAS, LOGP n-Oct, DRDRAC and SOLY) correlate with COX-1 inhibition activity. Compounds **17h**, **12**, **17g**, **16a** and **17a** displayed the highest H*Dry*H similarity score.

To identify the most relevant Molecular Interaction Fields (MIFs) shared by this sub-set of inhibitors, we applied cumulative MIF analysis in the ligand-based FLAP mode and aligned these structures on the mofezolac template (Figure 10). Overall, their FLAP-derived orientation closely resembles the crystallographic structure of the template, with most variation around the phenoxy moieties linked at C4 position of the isoxazole ring. The isoxazole and the phenoxy rings gave reasons for the region of the Dry (hydrophobic) probe with overlap between the MIFs ranging from 46% (for compounds **12**) and 34% (for compound **17a**). The largest volume for the N1 (H-bond donor) probe is around the carboxylate and the isoxazole moieties and the overlap between the N1 MIFs range from 63% (for compounds **17h**) and 26% (for compound **12**). No relevant volume can be identified for the O (H-bond acceptor) probe both for the templates and the selected inhibitors.

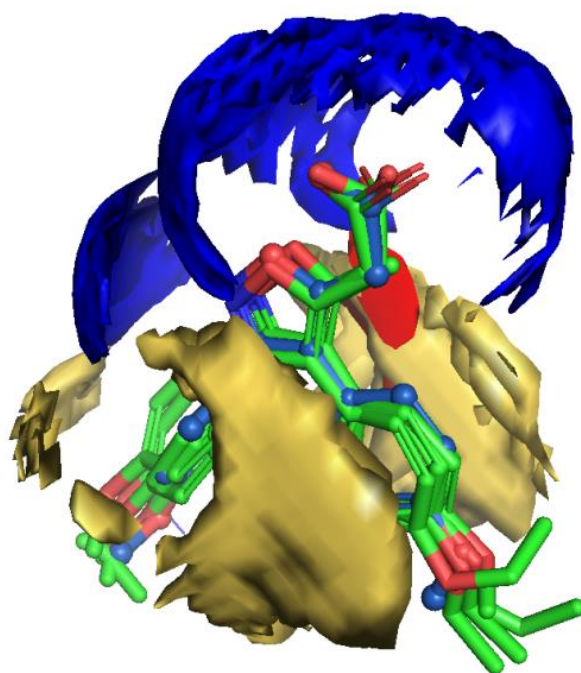


Figure 10. Cumulative MIF analysis for the 5 top ranked inhibitors (**17h**, **12**, **17g**, **16a** and **17a**, green) on the co-crystallized mofezolac (**5**, cyan) template. Yellow, blue and red fields respectively represent hydrophobic, H-bond donor and acceptor most relevant GRID interaction regions at -0.5, -4.0 and -2.0 kcal/mol energy level, respectively.

These structures were subsequently employed in the structure-based virtual screening (SBVS) using the catalytic sites of COX-1 (PDB IDs 5WBE) as templates. The aim is also the same: to validate the ligand based virtual screening performance, to increase confidence in the results if a future prospective screen is performed. This approach allowed also to generate binding poses of our database into the COX catalytic cavities based on the similarity between their GRID fields.

For the SBVS procedure, the best enrichment is found using the H (shape) score, with an AUC value of 0.82 and a true positive rate of 64 % (Figure 11).

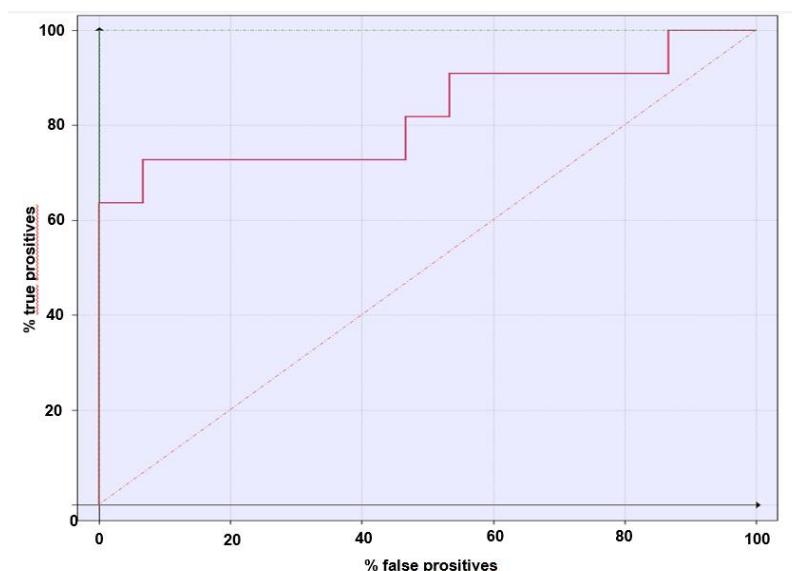


Figure 11. ROC plots for structure-based modelling: False positive rate (x-axis) versus True positive rate (y-axis). Enrichment curves for FLAP SBVS model is given in red for the H similarity score.

Similarity scores H (shape) and GlobProd were used to rank the most reliable poses for compounds **12**, **17g**, **16a**, **17h** and **17a**; the X-ray crystallographic pose previously defined for mofezolac[1] was also reported as a reference in Figure 12a. The interaction of compounds **17h** and **12** (Figure 12b and 12c), **17g** and **17a** (Figure S5a and S5b) with the catalytic pocket closely resembles that of mofezolac; they interacted with three key regions of the pockets: the first defined by R120 and Y355 at the entry of the catalytic channel, the second defined at the bottom of the cavity by a series of aromatic residues, as the fundamental Y385, and a central hydrophobic region mainly generated by the aliphatic chain and the protein backbone.

The key interactions at the entrance of the channel, namely the electrostatic interaction with R120 and the hydrogen bond with Y355, occurred for all acetic acid derivatives, even though the position of compound **17a** is slightly shifted toward the front end of the catalytic channel. The hydrogen bonding interaction with Y385 with the methoxyphenyl group, in the isoxazole-C3 position, was the second recurring binding motif for the interaction of the selected inhibitors and also compound **12**, lacking the charged group, retained the ‘mofezolac-like’ pose.

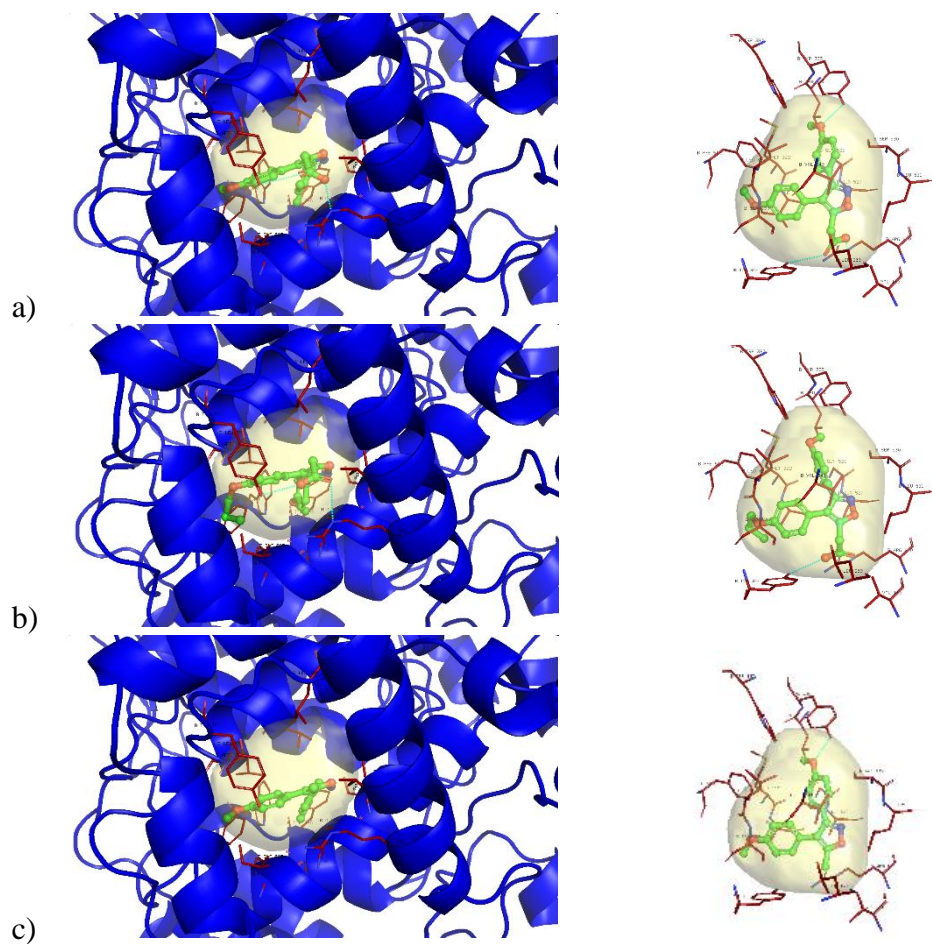


Figure 12. Prediction of the binding poses in the COX-1 catalytic site (from PDB ID: 5WBE). The binding poses (front view of the catalytic channel in the left column, top view in the right column) for the mofezolac (Mof) and for the new synthesized derivatives are shown according to the most representative FLAP poses by H (shape) and Glob-Prod descriptors. (a) mofezolac; (b) compound **17h**; (c) compound **12**. Amino acidic residues more involved in the protein ligand interactions and discussed in the text are highlighted.

Compound **16a**, instead, showed a twofold pose (Figure 13a and 13b): in both cases one of the methoxyphenyl group in the isoxazole-C3 position realized strong π - π interaction with F518 and multiple CH- π interactions with L352 and I523. The former pose (Figure 13b, right column) resembled what was previously seen for compounds **12**, **17g**, **16a**, **17h** and **17a**; in the latter ‘inverted’ pose (Figure 13b, left column), the isoxazole ring pointed towards the bottom of the cavity and

realized an effective hydrogen bond with Y385 and S530 while the methoxyphenyl group, caught between I523 and L531 by multiple CH- π interactions, allowed for hydrogen bonds between the oxygen atom and both Y355 and R120 and effectively reduced the steric hindrance of the ethoxy moiety. This dense network of Hydrophobic and H-bond interactions gave reason for alternative but still favourable binding modes for the effective inhibitor **16a**.

Compounds **17c** is an outlier in all the approaches described, but SBVS procedure indicated that it still adopted a ‘mofezolac like’ pose inside the catalytic cavity.

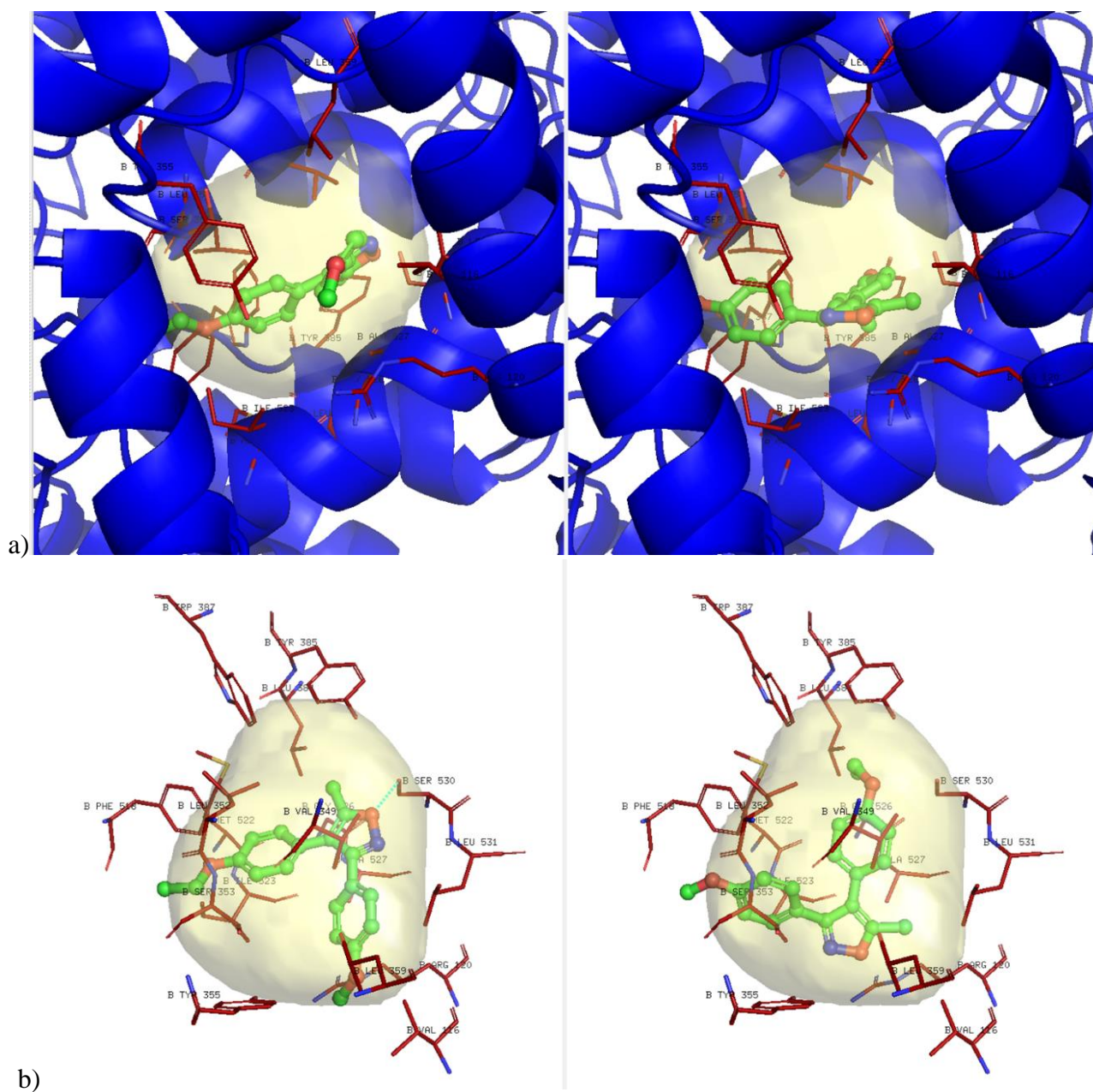


Figure 13. Prediction of the binding poses of compounds **16a** in the COX-1 catalytic site (from PDB ID: 5WBE). The binding poses front view (a) and top view (b) of the catalytic channel are shown according to the most representative FLAP poses by H (shape) and Glob-Prod descriptors. Amino acidic residues more involved in the protein ligand interactions and discussed in the text are highlighted.

4. Conclusion

Based on our previously acquired knowledge, mofezolac (**5**) and its precursor (**12**) herein choose as the lead compounds, could establish additional interactions with polar residues such as Q112, S353, H90 and Y355; less investigated is the position occupied by mofezolac methoxy bound to the phenyl linked to the isoxazole-C4.

Compounds **15a** and **17g**, although showing a reduced COX-1 inhibitory activity compared to their lead compounds mofezolac (**5**) and its precursor (**12**), give important indications about the small space present in the cavity of the catalytic site of the subject COX-1 object of this exploration. Very bulky groups significantly reduce the ability to inhibit COX-1 indicating that the methoxy group present on mofezolac and its precursor are the right compromise of chemical, physical, and steric characteristics for a potent inhibition of the cyclooxygenase-1. In addition, **15a** and **17g** also present a very interesting antiplatelet profile since they inhibit platelet aggregation with a greater potency ($IC_{50} = 1.0 \pm 0.1 \mu M$ and $29.5 \pm 0.4 \mu M$) than the largely used aspirin ($IC_{50} = 36.2 \pm 3.4 \mu M$). The combined *in silico* studies herein proposed shed light on key structural properties of effective and selective COX-1 inhibitors. The QSAR study indicated that descriptors related to shape (V, Diff and R) or hydrophobicity (IW4, POL, HAS, LOGP n-Oct, DRDRAC and SOLY) are strictly related with COX-1 inhibition activity. The Ligand Based Virtual Screening allowed successful discrimination between known active and inactive compounds Overall, the results of the *in silico* study indicated the pivotal role of the alkoxyphenyl group at C4 of the isoxazole ring for the mofezolac-like inhibitors; the dataset of the novel compounds, herein reported, allowed us not only to highlight the hydrophobic interactions with the unexplored region present in the COX-1 catalytic pocket but also to point out how the molecular size/shape as well as the subtle interplay between the hydrogen-bond donors and acceptors affected the inhibitory potency and the selectivity. In addition, for the mofezolac analogues set, the observed inhibition potency and selectivity seem to be due to the conformational plasticity of the enzymes capable to arrange some space to accommodate the more hindered groups linked tho the phnyl at C4 position of the isoxazole.

5. EXPERIMENTAL SECTION

Chemistry. 1H NMR and ^{13}C NMR spectra were recorded on a Bruker 600 MHz or AGILENT 500 MHz spectrometer and chemical shifts are reported in parts per million (δ), and the following abbreviations were used to explain the multiplicities: s = singlet, d = doublet, t = triplet, q = quartet, m = multiplet, quin = quintuplet, sext = sextet, sep = septet, b = broad. FT-IR spectra were recorded on a Perkin-Elmer 681 spectrophotometer. GC analyses were performed on a HP 6890 model, Series II by

using a HP1 column (methyl siloxane; 30 m x 0.32 mm x 0.25 μ m film thickness). Analytical thin-layer chromatography (TLC) was carried out on pre-coated 0.25 mm thick plates of Kieselgel 60 F254; visualization was accomplished by UV light (254 nm). Column chromatography was accomplished by using silica gel 60 with a particle size distribution 40–63 μ m and 230–400 ASTM. GC-MS analyses were performed on HP 5995C model. High-resolution mass spectrometry (HRMS) analyses were performed using a Bruker microTOF QII mass spectrometer equipped with an electrospray ion source (ESI). Reagents and solvents were purchased from Sigma-Aldrich (Sigma-Aldrich, St. Louis, MO, USA) and used without any further purification. Full characterization data have been reported for both the newly synthesized compounds and the known compounds. All spectral data are consistent with the reported values.

Synthesis of 13 and 14

3,4-Bis(4-methoxyphenyl)-5-methylisoxazole (13). To a solution of 3,4-bis(4-methoxyphenyl)-5-methylisoxazole (**12**, 3.4 mmol) in dry CH_2Cl_2 (40 mL) at -78°C , was added a solution of 1 M BBr_3 in dry CH_2Cl_2 (13.6 mL, 13.6 mmol) dropwise. The reaction mixture was stirred at r.t. overnight. The reaction progress was monitored by TLC (hexane/EtOAc = 6:4 as phase mobile). The aqueous phase is extracted with CH_2Cl_2 , and the organic layer was dried on anhydrous Na_2SO_4 . The solvent was evaporated under reduced pressure giving the product (**13**) as a light-yellow solid (0.864 g). 86.4% yield; M.p. $252\text{--}255^\circ\text{C}$. ^1H NMR (500 MHz, CDCl_3 , δ): 9.79 (br s, 1H, OH, exchanges with D_2O), 9.64 (br s, 1H, OH, exchanges with D_2O), 7.21 (d, 2H, $J = 8.8$ MHz), 7.01 (d, 2H, $J = 8.8$ MHz), 6.79 (d, 2H, $J = 8.8$ MHz), 6.75 (d, 2H, $J = 8.8$ MHz), 2.40 (3H, s). GC-MS: (70 eV): m/z (%) = 267 (M^+ , 100), 252, 225, 120, 105.

4-(4-Idroxyphenyl)-3-(4-methoxyphenyl)-5-methylisoxazole (14). To a solution of 3,4-bis(4-methoxyphenyl)-5-methylisoxazole (**12**, 1.64 g, 2.10 mmol) in dry CH_2Cl_2 (40 mL), at -78°C , was added a solution of 1 M BBr_3 in dry CH_2Cl_2 (11.67 mL, 11.67 mmol) dropwise. The reaction progress was monitored by TLC (hexane/EtOAc = 6:4 as phase mobile). After 2 h, is observed the presence of the starting compound, the two mono-demethylated regioisomers and the 3,4-bis(4-hydroxyphenyl)-5-methylisoxazole. The reaction blank is drained, slowly, into 50 mL of a saturated aqueous solution of NaHCO_3 . The aqueous phase is extracted with CH_2Cl_2 and the organic solution, was dried on anhydrous Na_2SO_4 and the solvent was evaporated under reduced pressure. The raw product is purified by column chromatography (silica gel; hexane/EtOAc = 6:4 as phase mobile). The desired product is then obtained by fractional crystallization of hot/cold absolute EtOH providing a white solid (0.254 g). 15.5% yield; M.p. $180\text{--}182^\circ\text{C}$. ^1H NMR (500 MHz, CDCl_3 , δ): 8.58 (brs, 1H, phenyl-OH, exchanges with D_2O), 7.37 (d, 2H $J = 9.0$ Hz, aromatic protons); 7.06 (d, 2H, $J = 8.4$, aromatic

protons), 6.93 – 6.86 (m, 4H, aromatic protons), 3.81 (s, 3H, O-CH₃), 2.38 (s, 3H, CH₃). GC-MS: (70 eV): *m/z* (%) = 281 (M⁺, 100), 266 (8), 239 (63), 224 (30), 120 (12), 105 (34), 91 (10), 77 (11), 63 (8), 51 (9), 43 (17). HPLC: Rt = 2.941 min (mobile phase: CH₃CN/H₂O 70:30; stationary phase: ZORBAX ECLIPSE Plus C18, analytical 4.6x250mm, 5 μm); rate = 1mL/min.

General synthesis of 15a-d.

To a solution of 3,4-bis(hydroxyphenyl)-5-methylisoxazole (**13**) (0.56 mmol) in CH₃CN (25 mL), was added Cs₂CO₃ (1.12 mmol) and, the reaction mixture was stirred at r.t. for 30 minutes. After this time, the alkyl or aryl bromide (1.12 mmol) was added to the reaction mixture and the reaction was heated to 90 °C, for 15 minutes. The reaction progress was monitored by TLC (EtOAc/hexane = 3:7 as phase mobile). The reaction mixture was cooled to room temperature, and it was filtered under reduced pressure. AcOEt was added and the solution was washed with brine. The organic layer was dried on anhydrous Na₂SO₄, and the solvent was evaporated under reduced pressure giving a brown yellow solid (0.138 g). Column chromatography (silica gel; EtOAc/hexane = 3:7 as mobile phase for **15a**, **15b**, **15c** and EtOAc/hexane = 2:8 as mobile phase for **15d**) is performed to isolate the expected products.

3,4-Bis(4-ethoxyphenyl)-5-methylisoxazole (15a) 76% Yield, white solid. M.p. 101-102 °C. ¹H NMR (500 MHz, CDCl₃, δ): 7.37 (d, 2H, J = 8.8 Hz, aromatic protons); 7.08 (d, 2H, J = 8.7 Hz, aromatic protons); 6.89 (d, 2H, J = 8.9 Hz, aromatic protons); 6.82 (d, 2H, J = 8.8 Hz, aromatic protons); 4.07-4.00 (m, 4H, 2CH₃CH₂O); 2.40 (s, 3H, CH₃); 1.44 (t, 3H, J = 7.0 Hz, CH₃CH₂O); 1.40 (t, 3H, J = 7.0 Hz, CH₃CH₂O). ¹³C NMR (125 MHz, CDCl₃, δ): 165.97, 160.00, 159.63, 158.27, 130.86, 129.56, 122.39, 121.30, 115.04, 114.49, 114.21, 63.31, 63.27, 14.74, 14.66, 11.42. GC-MS (70 eV): *m/z* (%) = 323 (M⁺, 100), 294 (48), 281 (24), 252 (40), 224 (18), 120 (18), 105 (20), 91 (9), 77 (6), 43 (13). HPLC Rt = 13.583 min (mobile phase: CH₃CN/H₂O 70:30; stationary phase: ZORBAX ECLIPSE Plus C18, analytical 4.6x250mm, 5 μm); rate = 1mL/min.

3,4-Bis(4-propoxyphenyl)-5-methylisoxazole (15b) The chromatographed compound is also crystallized (ethyl acetate/hexane) for obtain a white solid. 41% Yield. M.p. 90-92 °C. ¹H NMR (300 MHz, CDCl₃, δ): 7.26 (d, 2H, J = 8.8 Hz, aromatic protons); 6.97 (d, 2H, J = 8.7 Hz, aromatic protons); 6.78 (d, 2H, J = 8.7 Hz, aromatic protons); 6.71 (d, 2H, J = 8.8 Hz, aromatic protons); 3.85-3.77 (m, 4H, 2CH₃CH₂CH₂O); 2.29 (s, 3H, CH₃); 1.77-1.65 (m, 4H, 2CH₃CH₂CH₂O); 0.97-0.89 (m, 6H, 2CH₃CH₂CH₂O). ¹³C NMR (300 MHz, CDCl₃, δ): 166.63, 161.37, 160.58, 159.23, 131.56, 130.25, 123.13, 122.05, 115.78, 115.28, 114.99, 70.11, 70.06, 23.20, 23.11, 12.07, 11.11, 11.05. GC-MS (70 eV): *m/z* (%) = 351 (M⁺, 100), 308 (35), 266 (18), 224 (26), 119 (13), 105 (18), 91 (7), 43 (19). HPLC

Rt = 28.997 min (mobile phase: CH₃CN/H₂O 70:30; stationary phase: ZORBAX ECLIPSE Plus C18, analytical 4.6x250mm, 5 μm); rate = 1mL/min.

3,4-Bis(4-butoxyphenyl)-5-methylisoxazole (15c) 64% yield, yellow oil. ¹H NMR (500 MHz, CDCl₃, δ): 7.38 (d, 2H, J = 8.9 Hz, aromatic protons); 7.09 (d, 2H, J = 8.8 Hz, aromatic protons); 6.90 (d, 2H, J = 8.7 Hz, aromatic protons); 6.82 (d, 2H, J = 8.9 Hz, aromatic protons); 4.00-3.94 (m, 4H, 2CH₃CH₂CH₂CH₂O); 2.41 (s, 3H, CH₃); 1.82-1.73 (m, 4H, 2CH₃CH₂CH₂CH₂O); 1.55-1.45 (m, 4H, 2CH₃CH₂CH₂CH₂O); 1.01-0.96 (m, 6H, 2CH₃CH₂CH₂CH₂O). ¹³C NMR (500 MHz, CDCl₃, δ): 166.21, 160.93, 160.13, 158.77, 131.11, 129.80, 122.64, 121.55, 115.33, 114.80, 114.52, 67.84, 67.79, 31.49, 31.40, 19.42, 19.37, 14.01, 13.98, 11.66. GC-MS (70 eV): *m/z* (%) = 379 (M⁺, 100), 337 (5), 322 (29), 280 (12), 267 (9), 224 (26), 120 (12), 105 (13), 91 (5), 57 (4), 41 (10). HPLC Rt = 9.872 min (mobile phase: CH₃CN/H₂O 70:30; stationary phase: ZORBAX ECLIPSE Plus C18, analytical 4.6x250mm, 5 μm); rate = 1mL/min.

3,4-Bis(4-(benzyloxy)phenyl)-5-methylisoxazole (15d) 58% yield, yellow oil. ¹H NMR (500 MHz, CDCl₃, δ): 7.42-7.27 (m, 12H, aromatic protons); 7.06 (d, 2H, J = 8.7 Hz, aromatic protons); 6.95 (d, 2H, J = 8.6 Hz, aromatic protons); 6.87 (d, 2H, J = 8.6 Hz, aromatic protons); 5.04 (s, 2H, C₆H₅CH₂O); 5.01 (s, 2H, C₆H₅CH₂O); 2.37 (s, 3H, CH₃). ¹³C NMR (500 MHz, CDCl₃, δ): 165.10, 159.60, 158.54, 157.22, 135.66, 135.56, 129.95, 128.65, 127.54, 127.51, 127.00, 126.96, 126.40, 121.88, 120.79, 113.99, 113.69, 68.99, 68.89, 10.46. GC-MS (70 eV): *m/z* (%) = 447 (M⁺, 8), 356 (24), 91 (100), 65 (7). HPLC Rt = 34.703 min (mobile phase: CH₃CN/H₂O 70:30; stationary phase: ZORBAX ECLIPSE Plus C18, analytical 4.6x250mm, 5 μm); rate = 1mL/min.

Synthesis of 15f and 16f

Synthesis of: **3,4-bis(4-phenoxyphenyl)-5-methylisoxazole (15f)**. To a solution of 3,4-bis(4-hydroxyphenyl)-5-methylisoxazole (**13**, 0.150 g, 0.56 mmol) and 2-(trimethylsilyl)phenyl trifluoromethanesulfonate (0.4 mL, 1.69 mmol) in dry acetonitrile (15 mL) was added CsF (0.510 g, 3.37 mmol). The reaction mixture was stirred at r.t. for 24 h. Diethyl ether was added, and the solution was washed with brine. The organic layer was dried on Na₂SO₄ anhydrous, and the solvent was evaporated under reduced pressure. The residual orange oil was purified through column chromatography (silica gel, hexane/ethyl acetate = 8:2). The obtained solid was crystallized (ethyl acetate/hexane) giving 0.159 g of white crystals. 68% yield. M.p. 103 – 104 °C. ¹H NMR (500 MHz, CDCl₃, δ): 7.43 (d, 2H, J = 8.8 Hz, aromatic protons); 7.39-7.33 (m, 4 H, aromatic protons); 7.16-7.12 (m, 4H, aromatic protons); 7.08-7.02 (m, 4H, aromatic protons); 7.02 (d, 2H, J = 9.3 Hz, aromatic protons); 6.94 (d, 2H, J = 8.8 Hz, aromatic protons); 2.44 (s, 3H, CH₃). ¹³C NMR (500 MHz, CDCl₃, δ): 166.33, 160.69, 158.78, 157.31, 156.64, 156.43, 131.34, 130.05, 130.0, 125.07, 124.03, 123.94,

123.87, 119.74, 119.56, 118.72, 118.29, 115.18, 11.73. GC-MS (70 eV): m/z (%): 419 (M^+ , 100), 377 (39), 181 (22), 167 (6), 152 (11), 105 (8), 77 (41), 51 (11), 43 (10). HPLC R_t = 18.470 min (mobile phase: CH₃CN/H₂O 70:30; stationary phase: ZORBAX ECLIPSE Plus C18, analytical 4.6x250mm, 5 μ m); rate = 1mL/min.

4-(4-Phenoxyphenyl)-3-(4-methoxyphenyl)-5-methylisoxazole (16f). To a solution of 4-(4-iodoxyphenyl)-3-(4-methoxyphenyl)-5-methylisoxazole (**14**, 0.165 g, 0.59 mmol) and 2-(trimethylsilyl)phenyl trifluoromethanesulfonate (0.21 mL, 0.88 mmol) in acetonitrile (15 mL) was added CsF (0.269 g, 1.77 mmol). The reaction mixture was stirred at r.t. for 24. Diethyl ether was added and the solution was washed with brine. The organic layer was dried on Na₂SO₄ anhydrous, and the solvent was evaporated under reduced pressure. The residual orange oil was purified through column chromatography (silica gel, hexane/ethyl acetate = 8:2). The obtained solid was crystallized (ethyl acetate/hexane) giving 0.059 g of white crystals. 28% yield. M.p. 129-131 °C. ¹H NMR (500 MHz, CDCl₃, δ): 7.38 (m, 4H, aromatic protons); 7.14 (m, 3H, aromatic protons); 7.07 (d, 2H, J = 7.7 Hz, aromatic protons); 6.70 (d, 2H, J = 8.6 Hz, aromatic protons); 6.85 (d, 2H, J = 8.8 Hz, aromatic protons); 3.81 (s, 3H, CH₃O); 2.43 (s, 3H, CH₃). ¹³C NMR (500 MHz, CDCl₃, δ): 166.18, 160.64, 160.32, 156.91, 156.42, 131.09, 129.74, 129.62, 129.62, 125.02, 123.63, 121.35, 119.24, 118.46, 114.84, 113.80, 55.13, 11.49. GC-MS (70 eV): m/z (%): 357 (M^+ , 100), 315 (42), 300 (10), 196 (5), 181 (23), 165 (4), 152 (13), 133 (6), 105 (7), 89 (9), 77 (33), 64 (6), 51 (13), 43 (15). HPLC R_t = 16.199 min (mobile phase: CH₃CN/H₂O 70:30; stationary phase: ZORBAX ECLIPSE Plus C18, analytical 4.6x250mm, 5 μ m); rate = 1mL/min.

General synthesis of 16a-d

To a solution of 4-(4-iodoxyphenyl)-3-(4-methoxyphenyl)-5-methylisoxazole (**14**, 0.288 mmol) in acetonitrile (25 mL) was added cesium carbonate (0.56 mmol) and, the mixture was stirred at r.t. for 30 minutes. After this time, the alkyl or aryl bromide (0.56 mmol) was added to the reaction mixture, and the reaction was heated to 90 °C for 15 minutes. The reaction progress was monitored by TLC (EtOAc/hexane = 3:7 as phase mobile). The reaction mixture was cooled to room temperature, and it was filtered under reduced pressure. AcOEt was added and the solution was washed with brine. The organic layer was dried on anhydrous Na₂SO₄, and the solvent was evaporated under reduced pressure. The crude reaction products (**16a-c**) were used without purification while **16d** was purified by column chromatography (silica gel; EtOAc/hexane = 3:7 as mobile phase).

4-(4-Ethoxyphenyl)-3-(4-methoxyphenyl)-5-methylisoxazole (16a) 91% yield, white solid. M.p. 99-100 °C. ¹H NMR (500 MHz, CDCl₃, δ): 7.28 (d, 2H, J = 8.9 Hz, aromatic protons); 6.98 (d, 2H, J = 8.7 Hz, aromatic protons); 6.79 (d, 2H, J = 8.7 Hz, aromatic protons); 6.73 (d, 2H, J = 8.9 Hz, aromatic protons); 3.95 (q, 2H, J = 7.0 Hz, CH₃CH₂O); 3.69 (s, 3H, CH₃O); 2.30 (s, 3H, CH₃); 1.33

(t, 3H, $J = 7.0$ Hz $\text{CH}_3\text{CH}_2\text{O}$). ^{13}C NMR (500 MHz, CDCl_3 , δ): 166.42, 161.03, 160.67, 158.74, 131.29, 129.99, 122.83, 121.97, 115.49, 114.96, 144.16, 63.75, 55.52, 15.15, 11.81. GC-MS (70 eV): m/z (%) = 309 (M^+ , 100), 280 (42), 267 (23), 238 (46), 120 (20), 105 (19), 91 (9), 77 (12), 63 (6), 43 (13). HPLC $R_t = 18.181$ min (mobile phase: $\text{CH}_3\text{CN}/\text{H}_2\text{O}$ 70:30; stationary phase: ZORBAX ECLIPSE Plus C18, analytical 4.6x250mm, 5 μm); rate = 1 mL/min. M.p. 99 – 100 °C.

4-(4-Propoxyphenyl)-3-(4-methoxyphenyl)-5-methylisoxazole (16b) 86% yield, light yellow oil. ^1H NMR (300 MHz, CDCl_3 , δ): 7.39 (d, 2H, $J = 8.9$ Hz, aromatic protons); 7.08 (d, 2H, $J = 8.6$ Hz, aromatic protons); 6.90 (d, 2H, $J = 8.6$ Hz, aromatic protons); 6.83 (d, 2H, $J = 8.8$ Hz, aromatic protons); 3.94 (t, 2H, $J = 6.5$ Hz, $\text{CH}_3\text{CH}_2\text{CH}_2\text{O}$); 3.80 (s, 3H, CH_3O); 2.40 (s, 3H, CH_3); 1.89-1.76 (m, 2H, $\text{CH}_3\text{CH}_2\text{CH}_2\text{O}$); 1.06 (t, 3H, $J = 7.4$ Hz, $\text{CH}_3\text{CH}_2\text{CH}_2\text{O}$). ^{13}C NMR (300 MHz, CDCl_3 , δ): 166.51, 161.13, 160.78, 159.04, 131.37, 130.10, 122.88, 122.09, 115.61, 115.09, 114.27, 55.62, 23.01, 11.91, 10.96. GC-MS (70 eV): m/z (%) = 323 (M^+ , 100), 280 (49), 238 (50), 224 (9), 120 (23), 105 (24), 91 (11), 77 (15), 63 (7), 43 (26). HPLC $R_t = 14.725$ min (mobile phase: $\text{CH}_3\text{CN}/\text{H}_2\text{O}$ 70:30; stationary phase: ZORBAX ECLIPSE Plus C18, analytical 4.6x250 mm, 5 μm); rate = 1 mL/min.

4-(4-Butoxyphenyl)-3-(4-methoxyphenyl)-5-methylisoxazole (16c) 95% yield, light yellow oil. ^1H NMR (300 MHz, CDCl_3 , δ): 7.39 (d, 2H, $J = 8.9$ Hz, aromatic protons); 7.08 (d, 2H, $J = 8.7$ Hz, aromatic protons); 6.89 (d, 2H, $J = 6.9$ Hz, aromatic protons); 6.83 (d, 2H, $J = 8.9$ Hz, aromatic protons); 3.98 (t, 2H, $J = 6.5$ Hz, $\text{CH}_3\text{CH}_2\text{CH}_2\text{CH}_2\text{O}$); 3.80 (s, 3H, CH_3O), 2.40 (s, 3H, CH_3); 1.82-1.75 (m, 2H, $\text{CH}_3\text{CH}_2\text{CH}_2\text{CH}_2\text{O}$); 1.53-1.48 (m, 2H, $\text{CH}_3\text{CH}_2\text{CH}_2\text{CH}_2\text{O}$); 0.99 (t, 3H, $J = 7.4$ Hz, $\text{CH}_3\text{CH}_2\text{CH}_2\text{CH}_2\text{O}$). ^{13}C NMR (300 MHz, CDCl_3 , δ): 166.26, 160.89, 160.75, 160.56, 158.84, 131.13, 129.86, 122.65, 121.87, 114.87, 114.04, 67.89, 55.37, 31.51, 19.43, 14.00, 11.64. GC-MS (70 eV): m/z (%): 337 (M^+ , 100), 295 (9), 280 (41), 266 (6), 238 (44), 224 (9), 120 (15), 105 (14), 91 (6), 77 (8), 43 (9). HPLC $R_t = 20.990$ min (mobile phase: $\text{CH}_3\text{CN}/\text{H}_2\text{O}$ 70:30; stationary phase: ZORBAX ECLIPSE Plus C18, analytical 4.6x250mm, 5 μm); rate = 1 mL/min.

4-(4-Benzyloxyphenyl)-3-(4-methoxyphenyl)-5-methylisoxazole (16d) 72% yield, light yellow oil. ^1H NMR (500 MHz, CDCl_3 , δ): 7.36-7.23 (m, 7H, aromatic protons); 6.70 (d, 2H, $J = 8.6$ Hz, aromatic protons); 6.88 (d, 2H, $J = 8.7$ Hz, aromatic protons); 6.73 (d, 2H, $J = 8.8$ Hz, aromatic protons); 4.98 (s, 2H, $\text{C}_6\text{H}_5\text{CH}_2\text{O}$); 3.70 (s, 3H, CH_3O); 2.30 (s, 3H, CH_3). ^{13}C NMR (500 MHz, CDCl_3 , δ): 166.05, 160.62, 160.26, 158.16, 136.62, 130.91, 129.59, 128.52, 127.98, 127.45, 122.86, 121.49, 114.93, 113.76, 69.45, 55.12, 11.43. GC-MS (70 eV): m/z (%): 371 (M^+ , 20), 280 (89), 238 (23), 133 (10), 105 (6), 91 (100), 77 (8), 65 (10), 43 (12). HPLC $R_t = 15.172$ min (mobile phase: $\text{CH}_3\text{CN}/\text{H}_2\text{O}$ 70:30; stationary phase: ZORBAX ECLIPSE Plus C18, analytical 4.6x250mm, 5 μm); rate = 1 mL/min.

Synthesis of 15e and 16e

3,4-Bis(4-t-butyloxyphenyl)-5-methylisoxazole (15e). To a solid mixture of 3,4-bis(4-hydroxyphenyl)-5-methylisoxazole (**13**, 0.150 g, 0.56 mmol) and basic lead (II) carbonate (3.48 g, 4.48 mmol) was added dropwise 2-bromo-2-methylpropane (9.18 ml, 81.76 mmol). The mixture is left stirring at 0°C for 60 minutes. After this time the reaction mixture is brought to reflux for 3 h. The reaction progress was monitored by TLC (hexane/EtOAc = 7:3 as phase mobile). Having observed the formation of the product, the reaction mixture is filtered. The filtrate is washed with a solution of 2.5 M NaOH and the organic layer was dried on Na₂SO₄ anhydrous and the solvent was evaporated under reduced pressure. The residual solid was purified through column chromatography (silica gel, hexane/ethyl acetate = 7:3) giving 0.118 g of yellow solid. 55% yield. M.p. 98-100 °C. ¹H NMR (500 MHz, CDCl₃, δ): 7.32 (d, 2H, J = 8.7 Hz, aromatic protons); 7.06 (d, 2H, J = 8.6 Hz, aromatic protons); 6.98 (d, 2H, J = 8.6 Hz, aromatic protons); 6.90 (d, 2H, J=8.7 Hz, aromatic protons); 2.43 (s, 3H, isoxazole-CH₃); 1.37 (s, 9H, C(CH₃)₃); 1.34 (s, 9H, C(CH₃)₃). ¹³C NMR (500 MHz, CDCl₃, δ): 166.10, 160.58, 156.58, 154.97, 130.39, 130.11, 129.84, 129.08, 125.17, 124.23, 124.09, 123.90, 123.60, 122.21, 115.27, 78.89, 78.72, 28.86, 28.83, 11.56. GC-MS (70 Ev): *m/z* (%): 379 (M⁺, 11), 267 (100), 120 (88), 104(5), 56(37). HPLC Rt = 32.872 min (mobile phase: CH₃CN/H₂O 70:30; stationary phase: ZORBAX ECLIPSE Plus C18, analytical 4.6x250 mm, 5 μm); rate = 1 mL/min.

4-(4-t-Butyloxyphenyl)-3-(4-methoxyphenyl)-5-methylisoxazole (16e). To a solid mixture of 3,4-bis(4-hydroxyphenyl)-5-methylisoxazole (**14**, 0.150 g, 0.53 mmol) and basic lead (II) carbonate (1.64 g, 2.12 mmol) was added dropwise 2-bromo-2-methylpropane (4.34 ml, 38.69 mmol). The mixture is left stirring at 0°C for 60 minutes. After this time the reaction mixture is brought to reflux for 3 h. The reaction progress was monitored by TLC (hexane/EtOAc = 7:3 as phase mobile). Having observed the formation of the product, the reaction mixture is filtered. The filtrate is washed with a solution of 2.5 M NaOH, and the organic layer was dried on anhydrous Na₂SO₄, and the solvent was evaporated under reduced pressure. The residual solid was purified through column chromatography (silica gel, hexane/ethyl acetate = 7:3) giving 0.042 g of yellow oil. 33% yield. ¹H NMR (500 MHz, CDCl₃, δ): 7.36 (d, 2H, J = 8.9 Hz, aromatic protons); 7.06 (d, 2H, J=8.7 Hz, aromatic protons); 6.99 (d, 2H, J=8.7 Hz, aromatic protons); 6.81 (d, 2H, J=8.9 Hz, aromatic protons); 3.80 (s, 3H, OCH₃); 2.42 (s, 3H, isoxazole-CH₃); 1.38 (s, 9H, C(CH₃)₃). ¹³C NMR (500 MHz, CDCl₃, δ): 166.06, 160.74, 160.37, 154.99, 130.97, 130.42, 129.69, 129.06, 125.27, 124.09, 123.63, 121.58, 115.19, 114.11, 113.80, 78.70, 55.20, 28.87, 11.54. GC-MS (70 Ev): *m/z* (%): 337 (M⁺, 29), 322 (30), 281 (100), 266 (91). HPLC Rt =15.201 min (mobile phase: CH₃CN/H₂O 70:30; stationary phase: ZORBAX ECLIPSE Plus C18, analytical 4.6x250mm, 5 μm); rate = 1 mL/min.

General synthesis of of the carboxylic acid 17a-l (Scheme 2 and Table1).

2.5 M *n*BuLi (0.548 mL in dry hexane) was dropwise added to a stirred solution of 3,4-diaryl-5-methylisoxazole (0.140 g, 0.39 mmol) solubilized in anhydrous THF (40 mL) kept at -78°C and under an argon atmosphere. After 1h, anhydrous gaseous CO₂ was bubbled into the stirred red colored reaction mixture, till the color disappearance. Then, the yellow stirred reaction mixture was allowed to warm to room temperature, to be concentrated under reduced pressure, after the addition of 3N HCl (5 mL). The aqueous solution was extracted twice with EtOAc, and the combined organic extracts were dried over anhydrous Na₂SO₄, filtered and the solvent distilled under reduced pressure. The residual solid underwent column chromatography (silica gel, hexane/ethyl acetate = 7:3; 6:4, 1:1; 4:6; 3:7, 2:8; 1:9; only EtOAc and MeOH/ethyl acetate = 1:9; 2:9).

2-(3,4-Bis(4-ethoxyphenyl)isoxazole-5-yl)acetic acid (17a). 41% yield. Brown solid. M.p. 81-85 °C. ¹H-NMR (500 MHz, CDCl₃/CD₃OD = 1:1, δ): 7.29 (d, 2H, *J* = 8.9 Hz, aromatic protons); 7.10 (d, 2H, *J* = 8.7 Hz, aromatic protons); 6.85 (d, 2H, *J* = 8.7 Hz, aromatic protons); 6.79 (d, 2H, *J* = 8.9 Hz, aromatic protons); 4.03-3.97 (m, 4H, OCH₂CH₃); 3.67 (s, 2H, CH₂COOH); 1.39-1.34 (m, 6H, aromatic protons). ¹³C-NMR (500MHz, CDCl₃, δ): 172.45, 163.85, 160.85, 159.93, 158.67, 130.90, 129.57, 121.57, 120.82, 116.93, 114.64, 114.36, 63.40, 32.94, 14.36. HRMS (ESI) *m/z* calcd for ([C₂₁H₂₀NNaO₅] + Na)⁺: 412.1140; found: 412.1131. ESI-MS-MS: 412.1131, 297.0741, 193.0596, 141.0299. HPLC Rt = 1.936 min (mobile phase: CH₃CN/H₂O 70:30; stationary phase: ZORBAX ECLIPSE Plus C18, analytical 4.6x250mm, 5 μm); rate = 1 mL/min.

2-(3,4-Bis(4-propoxyphenyl)isoxazole-5-yl)acetic acid (17b). 44% yield. White solid. M.p. 135-138 °C. ¹H-NMR (500 MHz, CDCl₃/CD₃OD=1:1, δ): 7.26 (d, 2H, *J* = 8.8 Hz, aromatic protons); 7.11 (d, 2H, *J* = 8.7 Hz, aromatic protons); 6.82 (d, 2H, *J* = 8.7 Hz, aromatic protons); 6.79 (d, 2H, *J* = 8.8 Hz, aromatic protons); 3.89-3.85 (m, 4H, OCH₂CH₂CH₃); 3.62 (s, 2H, CH₂COOH); 1.79-1.72 (m, 4H, OCH₂CH₂CH₃); 1.01-0.98 (m, 6H, OCH₂CH₂CH₃). ¹³C-NMR (500 MHz, CDCl₃/CD₃OD=1:1, δ): 165.46, 160.76, 160.16, 158.83, 130.86, 129.45, 121.82, 120.92, 116.30, 114.46, 114.24, 69.28, 22.34, 22.26, 9.84, 9.79. HRMS (ESI) *m/z* calcd for ([C₂₃H₂₄NNaO₅] + Na)⁺: 440.1450; found: 440.1444. ESI-MS-MS: 440.1444, 354.1422, 311.0880, 207.0752. HPLC Rt = 3.872 min (mobile phase: CH₃CN/H₂O 45:55; stationary phase: ZORBAX ECLIPSE Plus C18, analytical 4.6x250mm, 5 μm); rate = 1 mL/min.

2-(3,4-Bis(4-*n*-butoxyphenyl)isoxazole-5-yl)acetic acid (17c). 64% yield. Yellow solid. M.p. = 67-69. ¹H-NMR (500 MHz, CDCl₃/CD₃OD=1:1, δ): 7.27 (d, 2H, *J* = 8.8 Hz, aromatic protos); 7.12 (d, 2H, *J* = 8.6 Hz, aromatic protons); 6.84 (d, 2H, *J* = 8.7 Hz, aromatic protons); 6.80 (d, 2H, *J* = 8.9 Hz, aromatic protons); 3.94-3.91 (m, 4H, OCH₂CH₂CH₂CH₃); 2,63 (s, 2H, CH₂COOH); 1.76-1.69

(m, 4H, OCH₂CH₂CH₂CH₃); 1.50-1.42 (m, 4H, OCH₂CH₂CH₂CH₃); 0.97-0.93 (m, 6H, OCH₂CH₂CH₂CH₃). ¹³C-NMR (500MHz, CDCl₃/CD₃OD=1:1, δ): 165.13, 160.79, 160.14, 158.82, 130.87, 129.49, 121.74, 120.89, 116.44, 114.52, 114.29, 67.57, 67.53, 31.16, 31.07, 19.04, 19.00, 13.31, 13.26. HRMS (ESI) m/z calcd for ([C₂₅H₂₈NNaO₅] + Na)⁺: 468.1757; found: 468.1768. ESI-MS-MS: 468.1768, 424.1861, 382.1758, 325.1056, 221.0914. HPLC Rt = 3.532 min (mobile phase: CH₃CN/H₂O 50:50; stationary phase: ZORBAX ECLIPSE Plus C18, analytical 4.6x250mm, 5 μm); rate = 1 mL/min.

2-(3,4-Bis(4-benzyloxyphenyl)isoxazole-5-yl)acetic acid (17d). 58% yield. White solid. M.p. = 220-221 °C. ¹H NMR (500 MHz, CDCl₃/CD₃OD=1:1, δ): 7.36-7.25 (m, 12H, aromatic protons); 7.11 (d, 2H, *J* = 8.7 Hz, aromatic protons); 6.88 (d, 2H, *J* = 8.7 Hz, aromatic protons); 6.85 (d, 2H, *J* = 8.9 Hz, aromatic protons); 4.98 (s, 2H, OCH₂C₆H₅); 4.97 (s, 2H, OCH₂C₆H₅); 3.60 (s, 2H, CH₂COOH). ¹³C NMR (500 MHz, CDCl₃/CD₃OD=1:1, δ): 175.82, 165.41, 160.67, 159.69, 158.40, 136.66, 136.49, 130.95, 129.61, 128.46, 128.44, 127.95, 127.91, 127.44, 127.39, 122.27, 121.41, 116.24, 114.98, 114.78, 69.95, 69.93, 34.44. HRMS (ESI) m/z calcd for ([C₃₁H₂₄NNaO₅] + Na)⁺: 536.1444; found: 536.1454. ESI-MS-MS: 536.1454, 401.1011, 310.0560, 255.0741, 185.0136, 141.0311. HPLC Rt = 4.062 min (mobile phase: H₂O/CH₃CN 55:45; stationary phase: ZORBAX ECLIPSE Plus C18, analytical 4.6x250mm, 5 μm); rate = 1 mL/min.

2-(3,4-Bis(4-*tert*-butoxyphenyl)isoxazole-5-yl)acetic acid (17e). 60% yield. White solid. M.p. = 158-160 °C. ¹H NMR (500 MHz, CDCl₃/CD₃OD=1:1, δ): 7.26 (d, 2H, *J* = 8.7 Hz, aromatic protons); 7.12 (d, 2H, *J* = 8.5 Hz, aromatic protons); 6.93 (d, 2H, *J* = 8.5 Hz, aromatic protons); 6.89 (d, 2H, *J* = 8.6 Hz, aromatic protons); 3.66 (s, 2H, CH₂COOH); 1.32 (s, 9H, OC(CH₃)₃); 1.31 (s, 9H, OC(CH₃)₃). ¹³C NMR (500 MHz, CDCl₃/CD₃OD=1:1, δ): 174.87, 165.36, 160.79, 156.50, 154.94, 130.42, 129.03, 124.77, 124.02, 123.68, 123.56, 116.41, 79.20, 78.95, 34.28, 29.97, 29.50, 28.45. HRMS (ESI) m/z calcd for ([C₂₅H₂₈NNaO₅] + Na)⁺: 468.1757; found: 468.1771. ESI-MS-MS: 468.1771, 368.1227, 311.0520, 221.0909, 164.0201, 141.0311. HPLC Rt = 3.400 min (mobile phase: H₂O/CH₃CN 55:45; stationary phase: ZORBAX ECLIPSE Plus C18, analytical 4.6x250mm, 5 μm); rate = 1 mL/min.

2-(3,4-Bis(4-phenoxyphenyl)isoxazole-5-yl)acetic acid (17f). 54% yield. White solid. M.p. = 155-157 °C. ¹H NMR (500 MHz, CDCl₃/CD₃OD=1:1, δ): 7.39-7.30 (m, 6H, aromatic protons); 7.24 (d, 2H, *J* = 8.7 Hz, aromatic protons); 7.14-7.08 (m, 2H, aromatic protons); 7.01-6.99 (m, 4H, aromatic protons); 6.94 (d, 2H, *J* = 8.7 Hz, aromatic protons); 6.91 (d, 2H, *J* = 8.8 Hz, aromatic protons); 3.66 (s, 2H, CH₂COOH). ¹³C NMR (500 MHz, CDCl₃/CD₃OD=1:1, δ): 166.23, 160.47, 158.82, 157.31, 156.54, 156.16, 131.22, 129.80, 129.68, 129.60, 124.52, 123.80, 123.51, 119.38, 119.11, 118.25, 117.79, 115.99, 34.44. HRMS (ESI) m/z calcd for (C₂₉H₂₀NNaO₅] + Na)⁺: 508.1131; found:

508.1142. ESI-MS-MS: 508.1142, 464.1286, 241.0595, 139.0119. HPLC Rt = 3.354 min (mobile phase: H₂O/CH₃CN 50:50; stationary phase: ZORBAX ECLIPSE Plus C18, analytical 4.6x250mm, 5 μm); rate = 1 mL/min.

2-(4-(4-Ethoxyphenyl)-3-(4-methoxyphenyl)isoxazole-5-yl)acetic acid (17g). 40% yield. Yellow solid. M.p. 126-128 °C. ¹H NMR (500 MHz, CDCl₃/CD₃OD=1:1, δ): 7.30 (d, 2H, *J* = 8.9 Hz, aromatic protons); 7.13 (d, 2H, *J* = 8.7 Hz, aromatic protons); 6.85-6.81 (m, 4H, aromatic protons); 4.01 (q, 2H, *J* = 7.0 Hz, OCH₂CH₃); 3.77 (s, 3H, OCH₃); 3.63 (s, 2H, CH₂COOH); 1.38 (t, 3H, *J* = 7.0 Hz, OCH₂CH₃). ¹³C NMR (500 MHz, CDCl₃/CD₃OD=1:1, δ): 165.22, 160.76, 160.54, 158.59, 130.90, 129.55, 121.83, 121.14, 116.42, 114.53, 113.81, 63.34, 54.87, 14.33. HRMS (ESI) *m/z* calcd for ([C₂₀H₁₈NNaO₅] + Na)⁺: 398.0974; found: 398.0974. ESI-MS-MS: 398.0974, 312.0984, 193.0597, 76.9972. HPLC Rt = 1.994 min (mobile phase: H₂O/CH₃CN 45:55; stationary phase: ZORBAX ECLIPSE Plus C18, analytical 4.6x250mm, 5 μm); rate = 1 mL/min.

2-(4-(4-Propoxyphenyl)-3-(4-methoxyphenyl)isoxazole-5-yl)acetic acid (17h). 27% yield. White solid. M.p. 133-135 °C. ¹H NMR (500 MHz, CDCl₃/CD₃OD=1:1, δ): 7.29 (d, 2H, *J* = 8.9 Hz, aromatic protons); 7.11 (d, 2H, *J* = 8.8 Hz, aromatic protons); 6.84-6.80 (m, 4H, aromatic protons); 3.88 (t, 2H, *J* = 6.5 Hz, OCH₂CH₂CH₃); 3.77 (s, 3H, OCH₃); 3.62 (s, 2H, CH₂COOH); 1.81-1.73 (m, 2H, OCH₂CH₂CH₃); 1.0 (t, 3H, *J* = 7.5 Hz, OCH₂CH₂CH₃). ¹³C NMR (500 MHz, CDCl₃/CD₃OD=1:1, δ): 165.26, 160.75, 160.52, 158.78, 130.88, 129.55, 121.76, 121.12, 116.38, 114.58, 113.86, 69.44, 54.97, 34.28, 22.41, 10.14. HRMS (ESI) *m/z* calcd for ([C₂₁H₂₀NNaO₅] + Na)⁺: 412.1131; found: 412.1133. ESI-MS-MS: 412.1133, 326.1126, 207.0752, 141.0296. HPLC Rt = 2.529 min (mobile phase: H₂O/CH₃CN 50:50; stationary phase: ZORBAX ECLIPSE Plus C18, analytical 4.6x250mm, 5 μm); rate = 1 mL/min.

2-(4-(4-*n*-Butoxyphenyl)-3-(4-methoxyphenyl)isoxazole-5-yl)acetic acid (17i). 34% yield. White solid. M.p. 123-125 °C. ¹H NMR (500 MHz, CDCl₃/CD₃OD=1:1, δ): 7.29 (d, 2H, *J* = 8.7 Hz, aromatic protons); 7.09 (d, 2H, *J* = 8.4 Hz, aromatic protons); 6.83-6.79 (m, 4 H, aromatic protons); 3.91 (t, 2H, *J* = 6.5 Hz, OCH₂C₂H₂CH₂CH₃); 3.76 (s, 3H, OCH₃); 3.62 (s, 2H, CH₂COOH); 1.75-1.69 (m, 2H, OCH₂C₂H₂CH₂CH₃); 1.47-1.43 (m, 2H, OCH₂C₂H₂CH₂CH₃); 0.94 (t, 3H, *J* = 7.4 Hz, OCH₂C₂H₂CH₂CH₃). ¹³C NMR (500 MHz, CDCl₃/CD₃OD=1:1, δ): 164.83, 160.75, 160.49, 158.80, 130.88, 129.57, 121.66, 121.10, 116.54, 114.61, 113.88, 67.64, 55.04, 31.19, 29.54, 19.11, 13.56. HRMS (ESI) *m/z* calcd for ([C₂₂H₂₂NNaO₅] + Na)⁺: 426.1288; found: 426.1289. ESI-MS-MS: 426.1289, 340.1284, 221.0905, 141.0302, 76.9984. HPLC Rt = 2.937 min (mobile phase: H₂O/CH₃CN 55:45; stationary phase: ZORBAX ECLIPSE Plus C18, analytical 4.6x250mm, 5 μm); rate = 1 mL/min.

2-(4-(4-Benzoyloxyphenyl)-3-(4-methoxyphenyl)isoxazole-5-yl)acetic acid (17j). 46% yield. White solid. M.p. = 151-153°C. ¹H NMR (500 MHz, CDCl₃/CD₃OD=1:1, δ): 7.35-7.24 (m, 7 H, aromatic protons); 7.09 (d, 2H, *J* = 8.6 Hz, aromatic protons); 6.87 (d, 2H, *J* = 8.6 Hz, aromatic protons); 6.75 (d, 2H, *J* = 8.8 Hz, aromatic protons); 3.88 (s, 2H, OCH₂C₆H₅); 3.73 (s, 3H, OCH₃); 3.60 (s, 2H, CH₂COOH). ¹³C NMR (500 MHz, CDCl₃/CD₃OD=1:1, δ): 175.26, 165.18, 160.69, 160.41, 158.37, 136.66, 130.95, 129.61, 128.48, 127.93, 127.46, 124.58, 122.27, 121.17, 116.27, 114.96, 113.87, 69.94, 55.08, 30.11, 29.57, 22.56, 13.90. HRMS (ESI) *m/z* calcd for ([C₂₅H₂₀NNaO₅] + Na)⁺: 460.1131; found: 460.1139. ESI-MS-MS: 460.1139, 325.0681, 283.0573, 255.0748, 164.0208, 141.0306. HPLC *R*_t = 2.685 min (mobile phase: H₂O/CH₃CN 50:50; stationary phase: ZORBAX ECLIPSE Plus C18, analytical 4.6x250mm, 5 μm); rate = 1 mL/min.

2-(4-(4-*tert*-Butoxyphenyl)-3-(4-methoxyphenyl)isoxazole-5-yl)acetic acid (17k). 86% yield. White solid. M.p. = 108-110°C. ¹H NMR (500 MHz, CDCl₃/CD₃OD=1:1, δ): 7.29 (d, 2H, *J* = 8.8 Hz, aromatic protons); 7.14 (d, 2H, *J* = 8.4 Hz, aromatic protons); 6.97 (d, 2H, *J* = 8.5 Hz, aromatic protons); 6.82 (d, 2H, *J* = 8.9 Hz, aromatic protons); 3.77 (s, 3H, OCH₃); 3.69 (s, 2H, CH₂COOH); 1.34 (s, 9H, C(CH₃)₃). ¹³C NMR (500 MHz, CDCl₃/CD₃OD=1:1, δ): 164.41, 160.83, 160.64, 155.03, 130.41, 129.56, 124.67, 124.42, 124.02, 120.92, 116.68, 113.79, 78.93, 54.85, 31.75, 30.97, 29.89, 29.47, 28.38, 22.46, 13.59. HRMS (ESI) *m/z* calcd for ([C₂₂H₂₂NNaO₅] + Na)⁺: 426.1288; found: 426.1294. ESI-MS-MS: 426.1294, 326.0768, 283.0584, 221.0918, 164.0206, 141.0309. HPLC *R*_t = 2.761 min (mobile phase: H₂O/CH₃CN 55:45; stationary phase: ZORBAX ECLIPSE Plus C18, analytical 4.6x250mm, 5 μm); rate = 1 mL/min.

2-(4-(4-Phenoxyphenyl)-3-(4-methoxyphenyl)isoxazole-5-yl)acetic acid (17l). 52% yield. White solid. M.p. = 195-197°C. ¹H NMR (500 MHz, CDCl₃/CD₃OD=1:1, δ): 7.33-7.29 (m, 4H, aromatic protons); 7.18 (d, 2H, *J* = 8.4 Hz, aromatic protons); 7.09 (t, 1H, *J* = 7.2 Hz, aromatic protons); 6.98 (d, 2H, *J* = 7.9 Hz, aromatic protons); 6.91 (d, 2H, *J* = 8.4 Hz, aromatic protons); 6.83 (d, 2H, *J* = 8.6 Hz, aromatic protons); 3.77 (s, 3H, OCH₃); 3.63 (s, 2H, OCH₂COOH). ¹³C NMR (500 MHz, CDCl₃/CD₃OD=1:1, δ): 175.44, 165.56, 160.76, 160.63, 157.31, 156.40, 131.16, 129.69, 129.57, 124.43, 123.66, 120.95, 119.22, 118.28, 116.07, 113.90, 54.91, 34.37. HRMS (ESI) *m/z* calcd for ([C₂₄H₁₈NNaO₅] + Na)⁺: 446.0975; found: 446.0981. ESI-MS-MS: 446.0981, 360.0898, 241.0615, 139.0149, 76.9983. HPLC *R*_t = 2.615 min (mobile phase: H₂O/CH₃CN 50:50; stationary phase: ZORBAX ECLIPSE Plus C18, analytical 4.6x250mm, 5 μm); rate = 1 mL/min.

4.3. Biology

4.3.1. Cyclooxygenase activity inhibition determination

The target compounds **12**, **15a-f**, **16a-f**, **5** (mofezolac), and **17a-l** were evaluated for their ability to inhibit ovine COX-1/COX-2 enzyme (percent inhibition at 50 mM). Inhibition of the enzyme was determined using a colorimetric COX (ovine) inhibitor screening assay kit (Catalog No. 760111, Cayman Chemicals, Ann Arbor, MI, USA) following the procedure described in the catalog according to the manufacturer's instructions.

COX is a bifunctional enzyme exhibiting both cyclooxygenase and peroxidase activity. The COX component converts arachidonic acid to a hydroperoxide (PGG₂), and the peroxidase component reduces the endoperoxide to the corresponding alcohol (PGH₂), the precursor of PGs, thromboxanes, and prostacyclins. The Colorimetric COX Inhibitor Screening Assay measures the peroxidase component of overall cyclooxygenases activity. The peroxidase activity is assayed colorimetrically by monitoring the appearance of oxidized *N,N,N,N'*-tetramethyl-*p*-phenylenediamine (TMPD) at 590 nm. 6e23 were dissolved in a minimum volume of DMSO to prepare to stock solutions.

4.3.3 Inhibition of AA-induced Platelet aggregation

Platelet rich (PRP) and poor (PPP) plasma were prepared by differential centrifugation and the maximum platelet aggregation was monitored by turbidimetric method using Chrono-log 560VS Aggregometer (Chrono-Log, Havertown, PA, USA). The compounds (0 -100 μM) were pre-incubated in PRP for 2 min before addition of arachidonic acid (AA - 500 μM) (Cayman Chemical Company, Ann Arbor, MI, USA). The platelet aggregation tests were performed in triplicate and the positive and negative controls were acetylsalicylic acid (ASA - 100 μM) (Sigma Aldrich) and dimethyl sulfoxide (DMSO 1%) (Sigma Aldrich), respectively [43].

4.3.4 *In vitro* anticoagulant assays

Platelet poor (PPP) plasma were prepared by differential centrifugation and the assays were performed in coagulation analyzer CoagLab® IV (Beijing Shining Sun Technology Co. Ltd., China) [44]. In the APTT assay, plasma samples were first incubated with the compounds (100 μM) for 15 minutes at room temperature and then for 2 minutes at 37 °C. Next, cephalin (100 μl) was added and incubated for 2 minutes. The reaction was triggered with 100 μl of 0.025 M CaCl₂ in a final volume of 300μL. In the PT test, similarly, 97 μL of plasma were first incubated with the compounds for 15 minutes at room temperature and then 2 minutes at 37 °C. Then 100 μL of PBS were added and incubated for 3 minutes. The reaction was triggered with 100 μL of calcium thromboplastin, in a final volume of 300 μL. The plasma clotting time was monitored in seconds at 37 °C.

4.3.5 Hemolytic activity and platelet viability

The hemolytic activity of compounds was investigated according to Parnham and Wetzig [45–46]. The citrated blood was centrifuged at 2500 rpm for 15 minutes and the erythrocyte pellet was washed 3 times with PBS (pH 7.4) and resuspended in same buffer. Then, the compounds were incubated with the suspension of erythrocytes for 3h at 37 °C in accord to ASTM F756-00 (Standard Practice for Assessment of Hemolytic Properties of Materials) [47]. The release of hemoglobin was measured after centrifugation of samples (2500 rpm for 15 min) and checked in a spectrophotometer at 540 nm. The complete hemolysis was obtained using 1% Triton X-100 as positive control. Less than 10% hemolysis was considered non-hemolytic [11]. In the assessment of platelet viability, the PRP was incubated with the compounds (100 µM) for 60 minutes at 37°C. After centrifugation at 4000rpm for 10 min, the quantification of lactate dehydrogenase (LDH) present in the supernatant was measured in a microplate reader (490nm) and expressed in percentage referring to platelet lysis. For this evaluation a commercial enzymatic kit from Cayman Chemical (Cayman Chemical Co, Ann Arbor, Mich) [48].

4.3.6 Cytotoxicity Assay

Vero cell line was purchased from the Rio de Janeiro Cell Bank (BCRJ, RJ, Brazil) and grown in Dulbecco's Modified Eagle's Medium (DMEM) supplemented with 10% fetal bovine serum and 10 µg/mL gentamicin at 37°C with 5% CO₂. Cells were seeded in 96-well plates until 70-90% confluency and treated with compounds at 100 µM. After 24 h of exposure, the MTT viability assay was performed with MTT at 0.5 mg/mL in PBS and incubation for 2 h. Next, DMSO was added, and the plates were analyzed using SpectraMax Paradigm multi-mode microplate reader (Molecular Devices) at 570 and 650 nm. Cytotoxicity was expressed as the percentage of cell viability after the treatment compared to untreated cells [49]

4.3.7 Statistical analysis

The results of in vitro assays were expressed as mean ± SD or SEM from three separate experiments. Differences between the mean values of the control and experimental groups were assessed using one-way analysis of variance (ANOVA), followed by Tukey's test. Statistical analyses were performed using Prism program (GraphPad Software Inc., CA, USA), and a p-value of ≤ 0.05 was considered statistically significant. The IC₅₀ values of the compounds reported in Table 1 and Table 2 were determined by nonlinear curve fitting using the same statistical program.

4.4 Computational methods

4.4.1 Volsurf+ QSAR

The VolSurf+ software (Molecular Discovery Ltd, UK, version 1.1.1) is a software that allows to convert the structural information embedded in GRID MIFs into 128 descriptors. 3D structures of the compounds in Table 1 were used as input data and were subjected to molecular interaction fields (MIFs) to generate descriptors using the following probes: N1 (amide nitrogen), O (carbonyl oxygen), H2O (water probe) and DRY (hydrophobic probe) [35]. Additional non-MIF-derived descriptors were generated to create a total of 128 descriptors, including descriptors that quantify molecular size, shape, hydrophilic and hydrophobic regions, interaction energy moments, capacity factors, amphiphilic moments, hydrophobic–lipophilic balance and other descriptors. These descriptors are simple to use and make it easy to interpret and understand the mechanism of action and/or physical meaning.

The QSAR model was developed using Partial Least Squares (PLS) included in the VolSurf+ software. PLS is a statistical procedure based on linear regression that allows extracting and rationalizing the multivariate information, to explain the maximum correlation between the descriptors matrix X and response matrix Y by calculating a new set of orthogonal variables, therefore uncorrelated, called latent variables (LVs). The autoscaling pre-process, for all independent variables was applied. The performance of regression-based models was estimated by the explained variance in the coefficient of determination (R^2) and coefficient of determination in cross-validation by leave-one-out (Q^2). The optimal number of LVs, which are orthogonal linear combinations of the original variables, and the model were determined using the highest value of the Q^2 .

4.4.2 FLAP ligand-based virtual screening

Ligand based virtual screening (LBVS) was performed using the FLAP software (Molecular Discovery Ltd, UK, version 2.2.2). We employed the structure of the Mofezolac co-crystallized into the COX-1 enzyme as template for LBVS, PDB ID codes 5wbe (Mofezolac, 63X); the 25 newly synthesized compounds, reported in Table 1, were used as database for the LBVS approaches. Compounds to be screened were modelled in their most abundant protomer at pH = 7.4 and considering up to 50 conformers with RMSD >0.2 for each compound.

The screening, conducted at the normal accuracy level, allowed us to generate the molecular interaction fields and evaluate the similarity between our dataset and the template by means of the GRID probes defining shape (H), hydrophobic interactions (DRY), H-bond donor (N1) and H-bond (O) acceptor interactions [50].

4.4.3 FLAP structure-based virtual screening

Selected compounds from LBVS were further screened in a structure-based approach (SBVS), using the catalytic site of *o*COX-1 (PDB ID: 5WBE) as a template. The FlapSite algorithm (implemented in FLAP)[6] was used for the identification of cavities in the *o*Cox-1 3D protein structures, which were described in terms of GRID MIFs.[10] Thirteen pockets were detected on the enzyme structure, that is as a dimer. The top-ranked pockets are perfectly overlaid with the X-ray ligand, corresponding to the catalytic sites, and were selected for the Structure based virtual screening. Compounds to be screened were modelled in their most abundant protomer at pH = 7.4 and considering up to 50 conformers with RMSD >0.2 for each compound. The same GRID probes used in LBVS were used to describe templates and compounds to be screened. Virtual screening was performed using the normal accuracy level and by using 100 minima point for quadruplets generation.

4.5 Ethics and Compliance

All human blood samples were obtained from adult volunteers, healthy, 18 e 40 years, without use of drugs or other substances that could interfere with the experiment for at least 15 days (Ethics Committee ID number 5.218.874).

Author Contributions

RS, DA, AC, SF and PV performed the synthesis and structural characterization of all the compounds MM and MGP - conducting *in vitro* assays (COXs inhibition assays) and data analysis. CB and CGF performed *in silico* investigations. PR - conducting *in vitro* assays (antiplatelet, anticoagulant and hemolysis assays) and data analysis. RG - conducting *in vitro* assays (platelet viability) and data analysis. AdO - formal analysis and data curation. MdP - conducting *in vitro* assays (cytotoxicity assay) and data analysis. LR -supervision of the cytotoxicity assays, funding acquisition. PS - general supervision of *in vitro* assays, data curation, funding acquisition. AA performed the crystallographic part of the work. AS supervised and coordinated all the research activities and funding acquisition. All the co-authors contributed to write - original draft, review & editing.

Declaration of competing interest

The authors declare that they have no known competing financial interests or personal relationships that could have appeared to influence the work reported in this paper.

Acknowledgments

This work was funded by (a) the project financed by the Italian Ministero dello Sviluppo Economico (MISE, Ministry of Economic Development) “GENESI” code 092- Sviluppo di radiofarmaci e biomarker innovativi per la diagnosi dei tumori dell’apparato riproduttivo maschile e femminile (Development of innovative radiopharmaceuticals and biomarkers for the diagnosis of tumors of male and female reproductive system) (2021-2023); (b) NEXTGENERATIONEU (NGEU) funded by the Ministry of University and Research (MUR), National Recovery and Resilience Plan (NRRP), project MNESYS (PE0000006) – A Multiscale integrated approach to the study of the nervous system in health and disease (DN. 1553 11.10.2022); (c) AD thanks NEXTGENERATIONEU (NGEU), funded by the Ministry of University and Research (MUR), National Recovery and Resilience Plan (NRRP), project HPC – “National Centre for HPC, Big Data and Quantum Computing – HPC” “Simulazioni, calcolo e analisi dei dati ad alte prestazioni” code CN000000013 (DD MUR N. 3138 del 16/12/2021) for a grant; (d) First AIRC Grant-MFAG2015 (Project Id. 17566). We also thank the financial support of Fundação Carlos Chagas Filho de Amparo à Pesquisa do Estado do Rio de Janeiro (FAPERJ), Conselho Nacional de Desenvolvimento Científico e Tecnológico (CNPq) and Coordenação de Aperfeiçoamento de Pessoal de Nível Superior (CAPES).

Abbreviations

AA	Arachidonic Acid
ANOVA	One-Way Analysis of Variance
APTT	activated Partial Thromboplastin Time
ASA	Acetylsalicylic Acid
AUC	Area Under the Curve
COX	Cyclooxygenase
DIFF	Diffusivity
DMEM	Dulbecco’s Modified Eagle’s Medium
DRDRAC	Dry-Dry-Acceptor 3D Triplets Pharmacophoric Areas
ESI	Electrospray Ion Source
GI	Gastrointestinal

<i>h</i> COX-1	Human Cyclooxygenase 1
HRMS	High-Resolution Mass Spectrometry
HSA	Hydrophobic Surface Areas
HWBA	Human Whole Blood Assay
IC ₅₀	50% Inhibitory Concentration
IW4	Integy Moment 4
LBVS	Ligand Based Virtual Screening
LDH	Lactate Dehydrogenase
LOO	Leave One Out
LV	Latent-Variable
MIFs	Molecular Interaction Fields
na	not applicable
<i>o</i> COX-1	Ovine Cyclooxygenase 1
PET	Positron Emission Tomography
PGE ₂	Prostaglandin E2
PGG ₂	Prostaglandin G2
PGH ₂	Prostaglandin H2
PGI ₂	Prostacyclin/Prostaglandin I2
PGs	Prostaglandins
PLS	Partial Least Squares
POL	Polarizability
PPP	Platelet Poor Plasma
PRP	Platelet Rich Plasma
PT	Prothrombin Time
Q ⁴	Coefficient of Determination in cross-validation by Leave-One-Out

QSAR	Quantitative Structure Activity Relationship
R	Rugosity
R ⁴	Coefficient of Determination
ROC	Receiver Operating Characteristic
SBVS	Structure Based Virtual Screening
SD	Standard Deviation
SI	Selective Index
Soly	Solubility
T	Test
Tc	control Time
TLC	Thin-Layer Chromatography
tNSAIDs	traditional Non-Steroidal Anti-Inflammatory Drugs
TXA ₂	Thromboxane A2
V	Volume
VS+	Volt Surf+

REFERENCES

- [1] M. Miciaccia, B.D. Belviso, M. Iaselli, G. Cingolani, S. Ferorelli, M. Cappellari, P. Loguercio Polosa, M.G. Perrone, R. Caliendo, A. Scilimati. Three-dimensional structure of human cyclooxygenase (hCOX)-1. *Sci Rep.* 11 (2021) 4312. <https://doi.org/10.1038/s41598-021-83438-z>.
- [2] M.J. Lucido, B.J. Orlando, A.J. Vecchio, M.G. Malkowski. Crystal Structure of Aspirin-Acetylated Human Cyclooxygenase-2: Insight into the Formation of Products with Reversed Stereochemistry. *Biochemistry.* 55 (2016) 1226–1238. <https://doi.org/10.1021/acs.biochem.5b01378>.
- [3] G. Cingolani, A. Panella, M.G. Perrone, P. Vitale, G. Di Mauro, C.G. Fortuna, R.S. Armen, S. Ferorelli, W.L. Smith, A. Scilimati. Structural basis for selective inhibition of Cyclooxygenase-1 (COX-1) by diarylisoxazoles mofezolac and 3-(5-chlorofuran-2-yl)-5-methyl-4-phenylisoxazole (P6). *Eur J Med Chem.* 138 (2017) 661–668. <https://doi.org/10.1016/j.ejmech.2017.06.045>.
- [4] A.J. Vecchio, M.G. Malkowski. The structural basis of endocannabinoid oxygenation by cyclooxygenase-2. *J Biol Chem.* 286 (2011) 20736–20745. <https://doi.org/10.1074/jbc.M111.230367>.
- [5] L. Friedrich, G. Cingolani, Y.H. Ko, M. Iaselli, M. Miciaccia, M.G. Perrone, K. Neukirch, V. Bobinger, D. Merk, R.K. Hofstetter, O. Werz, A. Koeberle, A. Scilimati, G. Schneider. Learning from Nature: From a Marine Natural Product to Synthetic Cyclooxygenase-1 Inhibitors by Automated De Novo Design. *Adv Sci.* 8 (2021) e2100832. <https://doi.org/10.1002/advs.202100832>.

- [6] M.P. Perrone, M. Miciaccia, P. Vitale, S. Ferorelli, C.D.C.B. Araújo, G.S. de Almeida, T.F. Souza Domingos, L.C.R.P. da Silva, M. de Pádula, L.M. Cabral, P.C. Sathler, C. Bonaccorso, C.G. Fortuna, A. Scilimati. An attempt to chemically state the cross-talk between monomers of COX homodimers by double/hybrid inhibitors mofezolac-spacer-mofezolac and mofezolac-spacer-arachidonic acid. *Eur J Med Chem.* 209 (2021) 112919. <https://doi.org/10.1016/j.ejmech.2020.112919>.
- [7] M.G. Perrone, O. Luisi, A. De Grassi, S. Ferorelli, G. Cormio, A. Scilimati. Translational Theragnosis of Ovarian Cancer: where do we stand?. *Curr Med Chem.* 27 (2020) 5675–5715. <https://doi.org/10.2174/0929867326666190816232330>.
- [8] A. Scilimati, S. Ferorelli, M.C. Iaselli, M. Miciaccia, M.L. Pati, C.G. Fortuna, A.M. Aleem, L.J. Marnett, M.G. Perrone. Targeting COX-1 by mofezolac-based fluorescent probes for ovarian cancer detection. *Eur J Med Chem.* 179 (2019) 16–25. <https://doi.org/10.1016/j.ejmech.2019.06.039>.
- [9] M.G. Perrone, P. Vitale, M. Miciaccia, S. Ferorelli, A. Centonze, R. Solidoro, C. Munzone, C. Bonaccorso, C.G. Fortuna, K. Kleinmanns, L. Bjørge, A. Scilimati. Fluorochrome Selection for Imaging Intraoperative Ovarian Cancer Probes. *Pharmaceuticals (Basel)*, 15 (2022) 668. <https://doi.org/10.3390/ph15060668>.
- [10] M.G. Perrone, D.D. Lofrumento, P. Vitale, F. De Nuccio, V. La Pesa, A. Panella, R. Calvello, A. Cianciulli, M.A. Panaro, A. Scilimati. Selective cyclooxygenase-1 inhibition by p6 and gastrotoxicity: preliminary investigation. *Pharmacology.* 95 (2015) 22–28. <https://doi.org/10.1159/000369826>.
- [11] A. Majithia, D.L. Bhatt. Novel Antiplatelet Therapies for Atherothrombotic Diseases. *Arterioscler Thromb Vasc Biol.* 39 (2019) 546–557. <https://doi.org/10.1161/ATVBAHA.118.310955>.
- [12] S.P. Grover, W. Bergmeier, N. Mackman. Platelet Signaling Pathways and New Inhibitors. *Arterioscler Thromb Vasc Biol.* 38 (2018) e28–e35. <https://doi.org/10.1161/ATVBAHA.118.310224>.
- [13] Q. Xiang, X. Pang, Z. Liu, G. Yang, W. Tao, Q. Pei, Y. Cui. Progress in the development of antiplatelet agents: Focus on the targeted molecular pathway from bench to clinic. *Pharmacol Ther.* 203 (2019) 107393. <https://doi.org/10.1016/j.pharmthera.2019.107393>.
- [14] F. Franchi, F. Rollini, Y. Park, D.J. Angiolillo. Platelet thrombin receptor antagonism with vorapaxar: pharmacology and clinical trial development. *Future Cardiol.* 11 (2015) 547–564. <https://doi.org/10.2217/fca.15.50>.
- [15] Y.X. Zhang, T.T. Yang, L. Xia, W.F. Zhang, J.F. Wang, Y.P. Wu. Inhibitory Effect of Propolis on Platelet Aggregation In Vitro. *J Healthc Eng.* (2017) 3050895. <https://doi.org/10.1155/2017/3050895>.
- [16] E.M. Antman, D. DeMets, J. Loscalzo. Cyclooxygenase inhibition and cardiovascular risk. *Circ.* 112 (2005) 759–770. <https://doi.org/10.1161/CIRCULATIONAHA.105.568451>.
- [17] E.N. Liberopoulos, M.S. Elisaf, A.D. Tselepis, A. Archimandritis, D. Kiskinis, D. Cokkinos, D. P. Mikhailidis. Upper gastrointestinal haemorrhage complicating antiplatelet treatment with aspirin and/or clopidogrel: where we are now? *Platelets.* 17 (2006) 1–6. <https://doi.org/10.1080/09537100500237004>.
- [18] P. Vitale, S. Tacconelli, M.G. Perrone, P. Malerba, L. Simone, A. Scilimati, A. Lavecchia, M. Dovizio, E. Marcantoni, A. Bruno, P. Patrignani. Synthesis, pharmacological characterization, and docking analysis of a novel family of diarylisoxazoles as highly selective cyclooxygenase-1 (COX-1) inhibitors. *J Med Chem.* 56 (2013) 4277–4299. <https://doi.org/10.1021/jm301905a>.
- [19] D. Rocchi, J.F. González, O. Martín-Cámara, M.G. Perrone, M. Miciaccia, A. Scilimati, C. Decouty-Pérez, E. Parada, J. Egea, J.C. Menéndez. m-Terphenylamines, Acting as Selective COX-1 Inhibitors, Block Microglia Inflammatory Response and Exert Neuroprotective Activity. *Molecules (Basel)*. 28 (2023) 5374. <https://doi.org/10.3390/molecules28145374>.
- [20] M.G. Perrone, P. Vitale, S. Ferorelli, A. Boccarelli, M. Coluccia, A. Pannunzio, F. Campanella, G. Di Mauro, C. Bonaccorso, C.G. Fortuna, A. Scilimati. Effect of mofezolac-galactose distance in conjugates

targeting cyclooxygenase (COX)-1 and CNS GLUT-1 carrier. *Eur J Med Chem.* 141 (2017) 404–416. <https://doi.org/10.1016/j.ejmech.2017.09.066>.

[21] M. G. Perrone, P. Vitale, A. Panella, S. Ferorelli, M. Contino, A. Lavecchia, A. Scilimati, A. Isoxazole-Based-Scaffold Inhibitors Targeting Cyclooxygenases (COXs). *ChemMedChem.* 11 (2016) 1172–1187. <https://doi.org/10.1002/cmdc.201500439>.

[22] M.L. Pati, P. Vitale, S. Ferorelli, M. Iaselli, M. Miciaccia, A. Boccarelli, G.D. Di Mauro, C.G. Fortuna, T.F. Souza Domingos, L.C. Rodrigues Pereira da Silva, M. de Pádula, L.M. Cabral, P.C. Sathler, A. Vacca, A. Scilimati, M.G. Perrone. Translational impact of novel widely pharmacological characterized mofezolac-derived COX-1 inhibitors combined with bortezomib on human multiple myeloma cell lines viability. *Eur J Med Chem.* 164 (2019) 59–76. <https://doi.org/10.1016/j.ejmech.2018.12.029>.

[23] M. Miciaccia, M. Iaselli, S. Ferorelli, P. Loguercio Polosa, M.G. Perrone, A. Scilimati. Ovine COX-1 Isoenzyme Bio-production. *Curr Enzym Inhib.* 18 (2022) 2–9. <https://dx.doi.org/10.2174/1573408017666211108104731>.

[24] M.G. Perrone, M. Miciaccia, S. Ferorelli, A. Scilimati. A Simplified Direct O₂ Consumption-Based Assay to Test COX Inhibition. *Curr Enzym Inhib.* 18 (2022) 10–18. <https://dx.doi.org/10.2174/1573408018666220204104612>.

[25] A. Scilimati, M.G. Perrone, P. Vitale. Heterocycles and their radiolabeled analogs useful as COX-1 selective inhibitors. Patent WO2014115020A1, 2014.

[26] X-ray Crystallographic Information file MSA 17.cif contains the supplementary crystallographic data for this paper, and is supplied as independent Supporting Information files for this article. This file can also be obtained free of charge from the Cambridge Crystallographic Data Centre via www.ccdc.cam.ac.uk/data_request/cif (CCDC 2281317).

[27] N.P. Rai, P.N. Arunachalam. Efficient Synthesis of tert Butyl Ethers under Solvent Free Conditions. *Synth Commun.* 37 (2007) 2891–2896. <https://doi.org/10.1080/00397910701470578>.

[28] Z. Liu, R.C. Larock. Facile O-arylation of phenols and carboxylic acids. *Org Lett.* 6 (2004) 99–102. <https://doi.org/10.1021/ol0361406>.

[29] P. Vitale, M.G. Perrone, P. Malerba, A. Lavecchia, A. Scilimati. Selective COX-1 inhibition as a target of theranostic novel diarylisoxazoles. *Eur J Med Chem.* 74 (2014) 606–618. <https://doi.org/10.1016/j.ejmech.2013.12.023>.

[30] M.G. Perrone, P. Malerba, J. Uddin, P. Vitale, A. Panella, B.C. Crews, C.K. Daniel, K. Ghebreselasie, M. Nickels, M.N. Tantawy, H.C. Manning, L.J. Marnett, A. Scilimati. PET radiotracer [¹⁸F]-P6 selectively targeting COX-1 as a novel biomarker in ovarian cancer: preliminary investigation. *Eur J Med Chem.* 80 (2014) 562–568. <https://doi.org/10.1016/j.ejmech.2014.04.074>.

[31] M.E. Machado, P. de Souza Furtado, C. da Costa Bernardes Araújo, A. Simon, M.C. de Moraes, L.C. Rodrigues Pereira da Silva, F.A. do Carmo, L.M. Cabral, P.C. Sathler. Novel rivaroxaban-loaded poly(lactic-co-glycolic acid)/poloxamer nanoparticles: preparation, physicochemical characterization, in vitro evaluation of time-dependent anticoagulant activity and toxicological profile. *Nanotechnology.* 32 (2021) 135101. <https://doi.org/10.1088/1361-6528/abd0b5>.

[32] D. Fischer, Y. Li, B. Ahlemeyer, J. Krieglstein, T. Kissel. In vitro cytotoxicity testing of polycations: influence of polymer structure on cell viability and hemolysis. *Biomaterials.* 24 (2003) 1121–1131. [https://doi.org/10.1016/s0142-9612\(02\)00445-3](https://doi.org/10.1016/s0142-9612(02)00445-3).

[33] F. Tellería, S. Mansilla, D. Méndez, M. Sepúlveda, R. Araya-Maturana, L. Castro, A. Trostchansky, E. Fuentes. The Use of Triphenyl Phosphonium Cation Enhances the Mitochondrial Antiplatelet Effect of the Compound Magnolol. *Pharmaceuticals.* 16 (2023) 210. <https://doi.org/10.3390/ph16020210>.

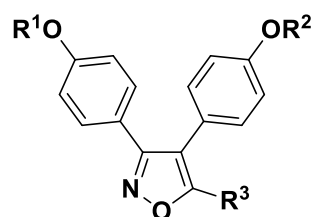
- [34] International Organization for Standardization Biological Evaluation of Medical Devices - Part 5: Tests for in vitro cytotoxicity. ISO 10993-5. 2009.
- [35] G. Cruciani, P. Crivori, P.A. Carrupt, B. Testa, Molecular fields in quantitative structure–permeation relationships: the VolSurf approach, *Journal of Molecular Structure: THEOCHEM*. 503 (2000) 17–30. [https://doi.org/10.1016/S0166-1280\(99\)00360-7](https://doi.org/10.1016/S0166-1280(99)00360-7).
- [36] C.G. Fortuna, V. Barresi, C. Bonaccorso, G. Consiglio, S. Failla, A. Trovato-Salinaro, G. Musumarra, Design, synthesis and in vitro antitumour activity of new heteroaryl ethylenes, *Eur J Med Chem*. 47 (2012) 221–227. <https://doi.org/10.1016/J.EJMECH.2011.10.060>.
- [37] C. Bonaccorso, I. Naletova, C. Satriano, G. Spampinato, V. Barresi, C.G. Fortuna, New Di(heteroaryl)ethenes as Apoptotic Anti-proliferative Agents Towards Breast Cancer: Design, One-Pot Synthesis and In Vitro Evaluation, *ChemistrySelect*. 5 (2020) 2581–2587. <https://doi.org/10.1002/SLCT.201903502>.
- [38] S. Cross, M. Baroni, L. Goracci, G. Cruciani, GRID-based three-dimensional pharmacophores I: FLAPpharm, a novel approach for pharmacophore elucidation, *J Chem Inf Model*. 52 (2012) 2587–2598. <https://doi.org/10.1021/ci300153d>.
- [39] M. Baroni, G. Cruciani, S. Sciabola, F. Perruccio, J.S. Mason, A common reference framework for analyzing/comparing proteins and ligands. Fingerprints for Ligands and Proteins (FLAP): Theory and application, *J Chem Inf Model*. 47 (2007) 279–294. <https://doi.org/10.1021/CI600253E>.
- [40] C.G. Fortuna, C. Bonaccorso, A. Bulbarelli, G. Caltabiano, L. Rizzi, L. Goracci, G. Musumarra, A. Pace, A.P. Piccionello, A. Guarcello, P. Pierro, C.E.A. Cocuzza, R. Musumeci, New linezolid-like 1,2,4-oxadiazoles active against Gram-positive multiresistant pathogens, *Eur J Med Chem*. 65 (2013) 533–545. <https://doi.org/10.1016/J.EJMECH.2013.03.069>.
- [41] C.J. Smith, Y. Zhang, C.M. Koboldt, J. Muhammad, B.S. Zweifel, A. Shaffer, J.J. Talley, J.L. Masferrer, K. Seibert, P.C. Isakson, Pharmacological analysis of cyclooxygenase-1 in inflammation, *Proc Natl Acad Sci U S A*. 95 (1998) 13313–13318. <https://doi.org/10.1073/PNAS.95.22.13313/ASSET/894C7E40-932E-4EF2-B3B1-61718A960DA7/ASSETS/GRAPHIC/PQ2183243007.JPEG>.
- [42] T. Ochi, Y. Motoyama, T. Goto, The analgesic effect profile of FR122047, a selective cyclooxygenase-1 inhibitor, in chemical nociceptive models, *Eur J Pharmacol*. 391 (2000) 49–54. [https://doi.org/10.1016/S0014-2999\(00\)00051-0](https://doi.org/10.1016/S0014-2999(00)00051-0).
- [43] A.L. Lourenço, R.R.S. Salvador, L.A. Silva, M.S. Saito, J.F.R. Mello, L.M. Cabral, C.R. Rodrigues, M.A.F. Vera, E.M.F. Muri, A.M.T. de Souza, C.S. Craik, L.R.S. Dias, H.C. Castro, P.C. Sathler. Synthesis and mechanistic evaluation of novel N'-benzylidene-carbohydrazide-1H-pyrazolo[3,4-b]pyridine derivatives as non-anionic antiplatelet agents. *Eur. J. Med. Chem*. 135 (2017) 213–229. <https://doi.org/10.1016/j.ejmech.2017.04.023>.
- [44] M.S. Saito, K.C. Zatta, P.C. Sathler, P.S. Furtado, N. C O Miguel, F.S. Frattani, M. Berger, V. Lavayen, A.R. Pohlmann, S.S. Guterres. Therapeutic implementation in arterial thrombosis with pulmonary administration of fucoidan microparticles containing acetylsalicylic acid. *Int. J. Pharm*. 622 (2022) 121841. <https://doi.org/10.1016/j.ijpharm.2022.121841>.
- [45] M.J. Parnham, H. Wetzig. Toxicity screening of liposomes. *Chem. Phys. Lipids*. 64 (1993) 263–274. [https://doi.org/10.1016/0009-3084\(93\)90070-j](https://doi.org/10.1016/0009-3084(93)90070-j).
- [46] M. Bauer, C. Lautenschlaeger, K. Kempe, L. Tauhardt, U.S. Schubert, D. Fischer. Poly(2-ethyl-2-oxazoline) as alternative for the stealth polymer poly(ethylene glycol): comparison of in vitro cytotoxicity and hemocompatibility. *Macromol Biosci*. 12 (2012) 986–998. <https://doi.org/10.1002/mabi.201200017>.
- [47] F04 Committee. Practice for Assessment of Hemolytic Properties of Materials; ASTM International, 2013.

[48] D. Méndez, F.A. Urra, J.P. Millas-Vargas, M. Alarcón, J. Rodríguez-Lavado, I. Palomo, A. Trostchansky, R. Araya-Maturana, E. Fuentes. Synthesis of antiplatelet ortho-carbonyl hydroquinones with differential action on platelet aggregation stimulated by collagen or TRAP-6. *Eur. J. Med. Chem.* 192 (2020) 112187. <https://doi.org/10.1016/j.ejmech.2020.112187>.

[49] T. Mosmann. Rapid colorimetric assay for cellular growth and survival: application to proliferation and cytotoxicity assays. *J. Immunol.* 65 (1983) 55–63. [https://doi.org/10.1016/0022-1759\(83\)90303-4](https://doi.org/10.1016/0022-1759(83)90303-4).

[50] E. Carosati, S. Sciabola, G. Cruciani, Hydrogen bonding interactions of covalently bonded fluorine atoms: From crystallographic data to a new angular function in the GRID force field, *J Med Chem.* 47 (2004) 5114–5125. <https://doi.org/10.1021/jm0498349>.

Table 1. COX inhibitory activity of **12**, **15a-f** and **16a-f** and of the corresponding acetic acids **5**, **17a-i** and their Selectivity Index (SI).



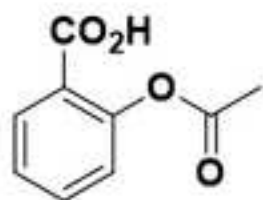
Compound	R ¹	R ²	R ³	oCOX-1 IC ₅₀ (μM) ^a (percentage inhibition, %) ^b	hCOX-2 IC ₅₀ (μM) ^a (percentage inhibition, %) ^b	SI ^c
12	Me	Me	Me	0.076 (100)	0.35 (71)	5
15a (MSA19)	Et	Et	Me	0.23 (79)	>50	>217
15b (MSA27)	n-Pro	n-Pro	Me	>50 (40)	>50 (27)	na ^d
15c (MSA32)	n-Bu	n-Bu	Me	>50 (18)	>50 (7)	na
15d (MSA20)	Benzyl	Benzyl	Me	>50 (37)	>50 (13)	na
15e (MSA38)	t-Bu	t-Bu	Me	>50 (32)	>50 (31)	na
15f (MSA30)	Phenyl	Phenyl	Me	>50 (6)	>50 (8)	na
16a (MSA33)	Me	Et	Me	0.046 (76)	>50 (18)	>1087
16b (MSA34)	Me	n-Pro	Me	1.3 (61)	>50 (18)	>38
16c (MSA35)	Me	n-Bu	Me	>50 (42)	>50 (26)	na
16d (MSA37)	Me	Benzyl	Me	>50 (47)	>50 (12)	na
16e (MSA51)	Me	t-Bu	Me	>50 (0)	>50 (0)	na
16f (MSA36)	Me	Phenyl	Me	>50 (29)	>50 (8)	na
5 (mofezolac)	Me	Me	CH ₂ COOH	0.0079 (100)	>50 (45)	>6329
17a (MSA42)	Et	Et	CH ₂ COOH	0.12 (85)	>50 (12)	>417
17b (MSA55)	n-Pro	n-Pro	CH ₂ COOH	>50 (0)	3.6 (57)	<0.072
17c (MSA39)	n-Bu	n-Bu	CH ₂ COOH	0.053 (61)	>50 (16)	>943

17d (MSA57)	Benzyl	Benzyl	CH ₂ COOH	>50 (15)	>50 (4)	na
17e (MSA60)	Phenyl	Phenyl	CH ₂ COOH	>50 (0)	>50 /24)	na
17f (MSA56)	t-Bu	t-Bu	CH ₂ COOH	>50 (0)	>50 (16)	na
17g (MSA45)	Me	Et	CH ₂ COOH	0.12 (87)	>50 (7)	>417
17h (MSA53)	Me	n-Pro	CH ₂ COOH	0.079 (72)	6.9 (79)	87
17i (MSA54)	Me	n-Bu	CH ₂ COOH	0.32 (64)	0.45 (76)	1.4
17j (MSA59)	Me	Benzyl	CH ₂ COOH	0.45 (60)	>50 (35)	>111
17k (MSA61)	Me	Phenyl	CH ₂ COOH	>50 (0)	>50 (23)	na
17l (MSA58)	Me	t-Bu	CH ₂ COOH	>50 (0)	>50 (24)	na

^aIC₅₀ values are the means of at least three independent measurements. ^bInhibition percentage (%) determined at the highest final inhibitor concentration used (50 μM). ^cSelectivity Index (SI) = COX-2 IC₅₀/COX-1 IC₅₀. ^dnot applicable.

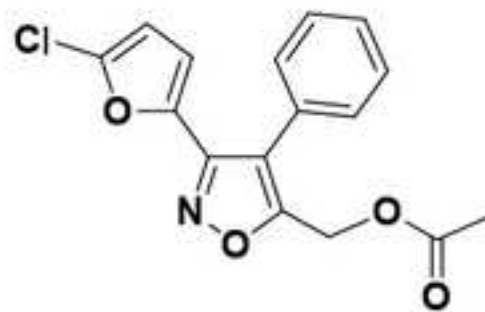
Table 2. Concentration required to inhibit 50% of arachidonic acid (AA)-induced platelet aggregation (IC_{50}) for the compounds. Results are expressed as mean \pm standard deviation (SD).

Compound	IC_{50} (μ M)
ASA	36.2 \pm 3.4
15a	1.0 \pm 0.1
16a	2.5 \pm 0.8
17c	>100
17a	0.7 \pm 0.3
17g	29.5 \pm 0.4
17h	72.1 \pm 3.4
17j	>100

**1 (aspirin)**

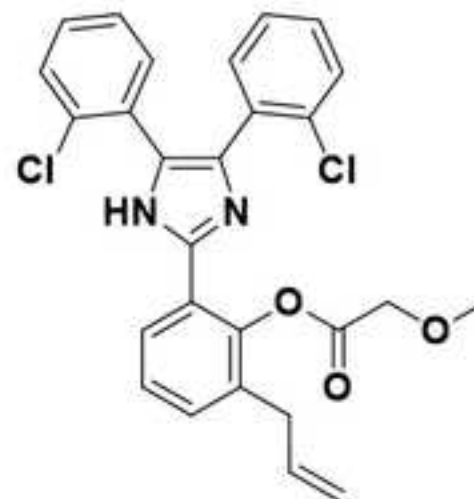
COX-1 $\text{IC}_{50} = 1.7 \mu\text{M}$
COX-2 $\text{IC}_{50} > 100 \mu\text{M}$

SI > 58.82

**2**

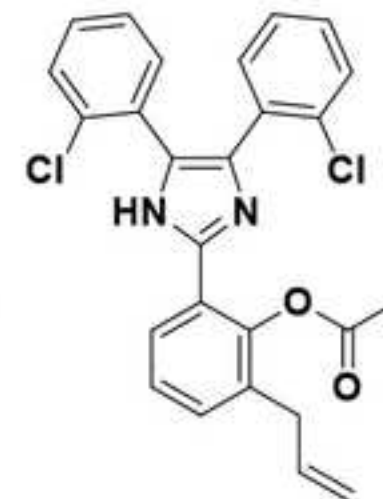
COX-1 $\text{IC}_{50} = 5.0 \mu\text{M}$
COX-2 $\text{IC}_{50} > 100 \mu\text{M}$

SI > 20

**3**

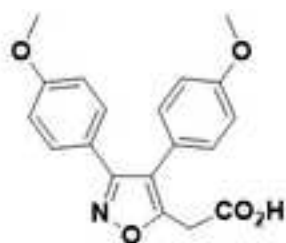
COX-1 $\text{IC}_{50} = 0.16 \mu\text{M}$
COX-2 $\text{IC}_{50} > 100 \mu\text{M}$

SI > 625

**4**

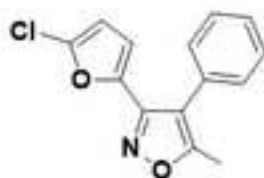
COX-1 $\text{IC}_{50} > 100 \mu\text{M}$
COX-2 $\text{IC}_{50} > 100 \mu\text{M}$

SI = inactive

**5 (mofezolac)**

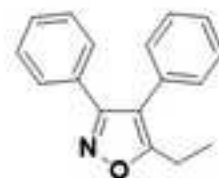
COX-1 IC_{50} = 0.0079 μ M
COX-2 IC_{50} > 100 μ M

SI > 12,658

**6 (P6)**

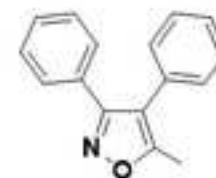
COX-1 IC_{50} = 0.5 μ M
COX-2 IC_{50} > 100 μ M

SI > 200

**7 (P9)**

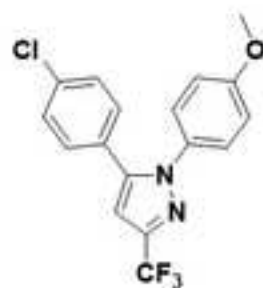
COX-1 IC_{50} = 0.05 μ M
COX-2 IC_{50} > 1.49 μ M

SI = 2.98

**8 (P10)**

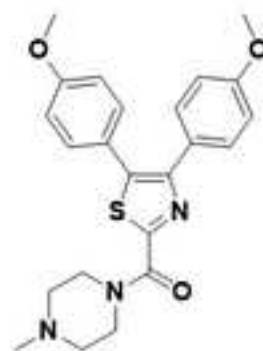
COX-1 IC_{50} = 0.09 μ M
COX-2 IC_{50} = 2.49 μ M

SI = 27.67

**9 (SC560)**

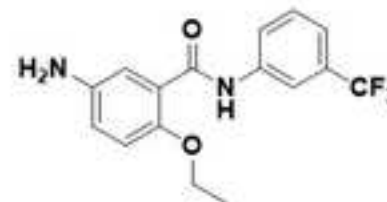
COX-1 IC_{50} = 0.07 μ M
COX-2 IC_{50} = 74.9 μ M

SI = 1,070

**10 (FR122047)**

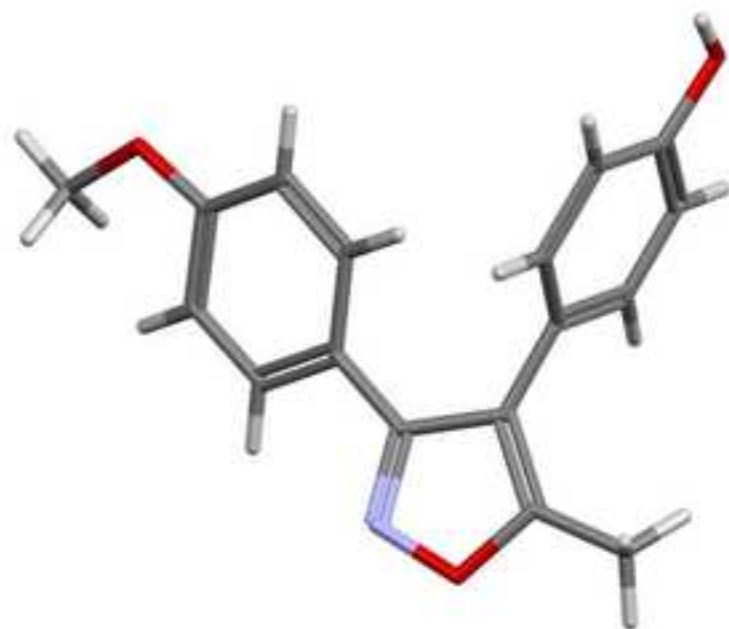
COX-1 IC_{50} = 0.028 μ M
COX-2 IC_{50} = 65 μ M

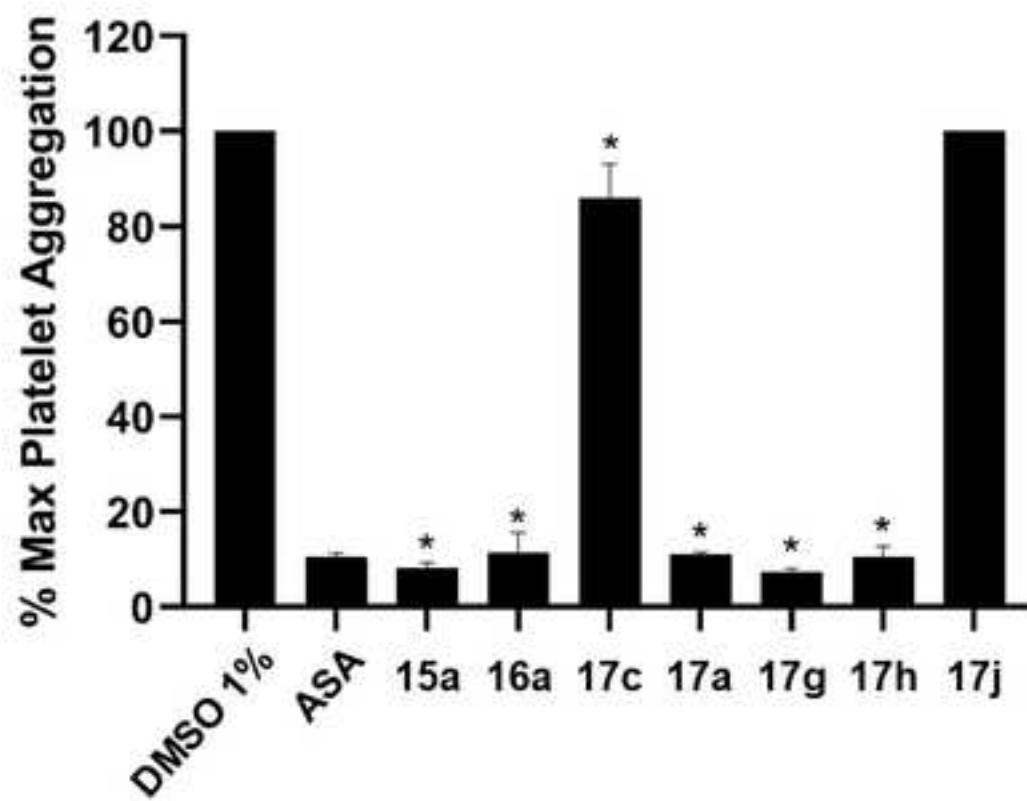
SI = 2,321

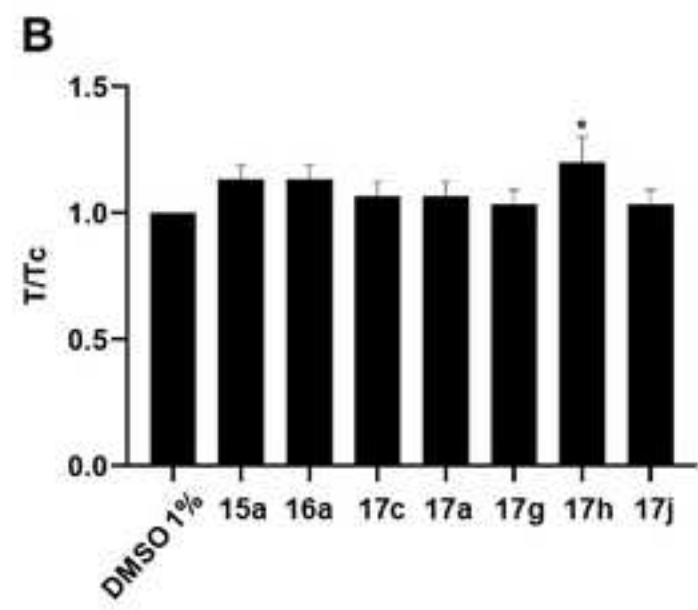
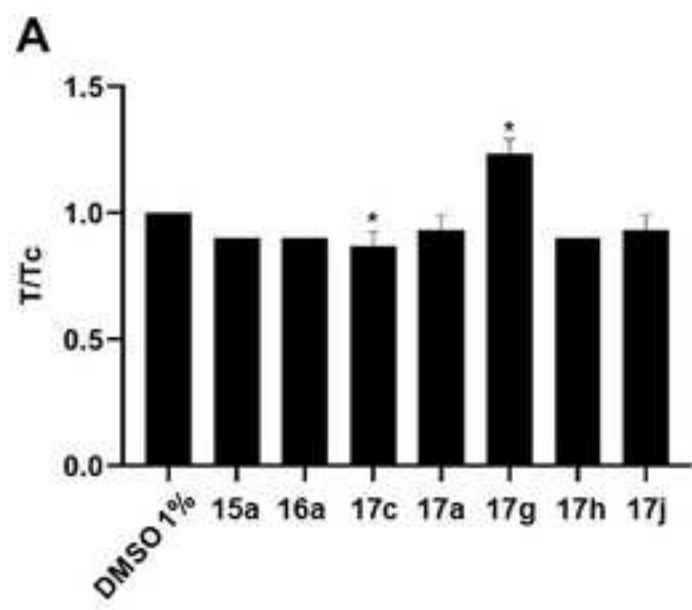
**11 (ABEX-3TF)**

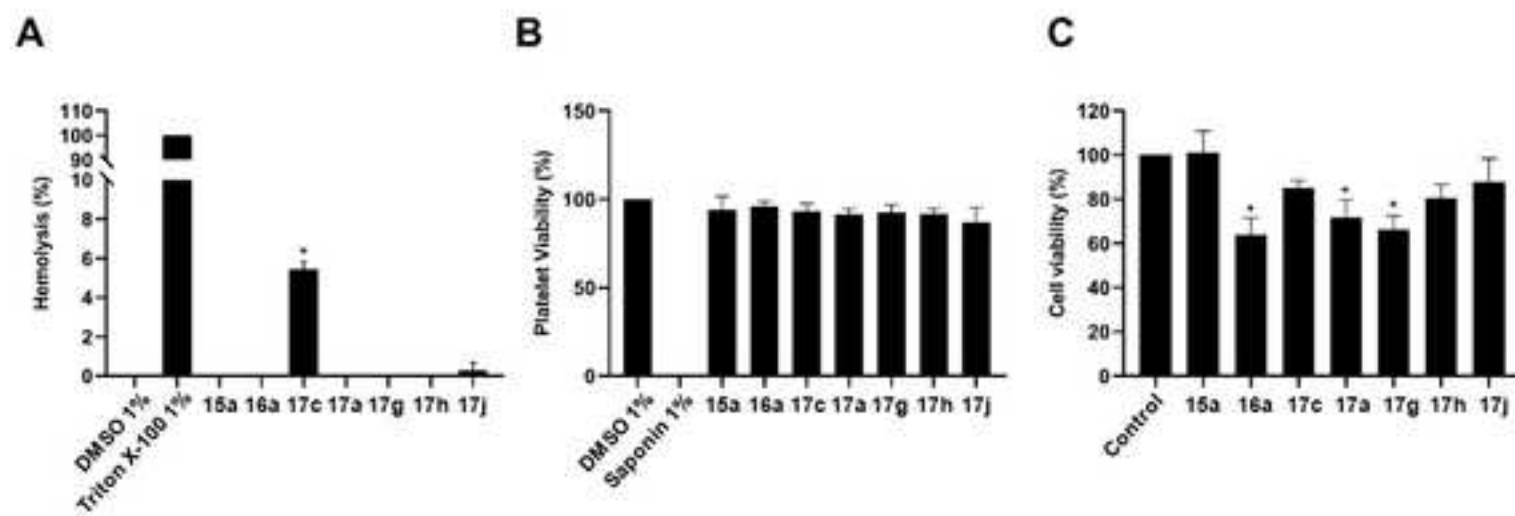
COX-1 IC_{50} = 3.2 μ M
COX-2 IC_{50} > 100 μ M

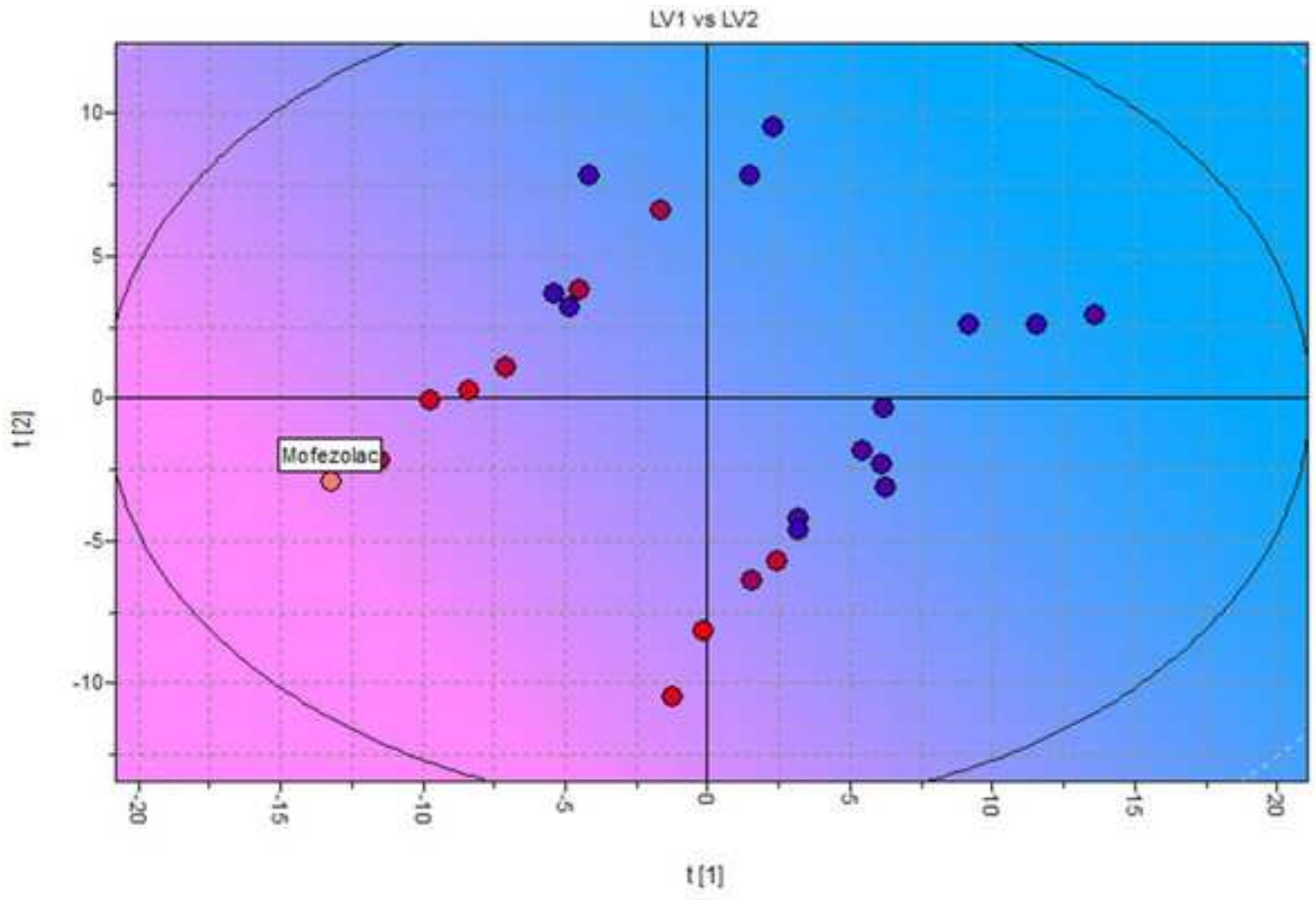
SI > 31.25

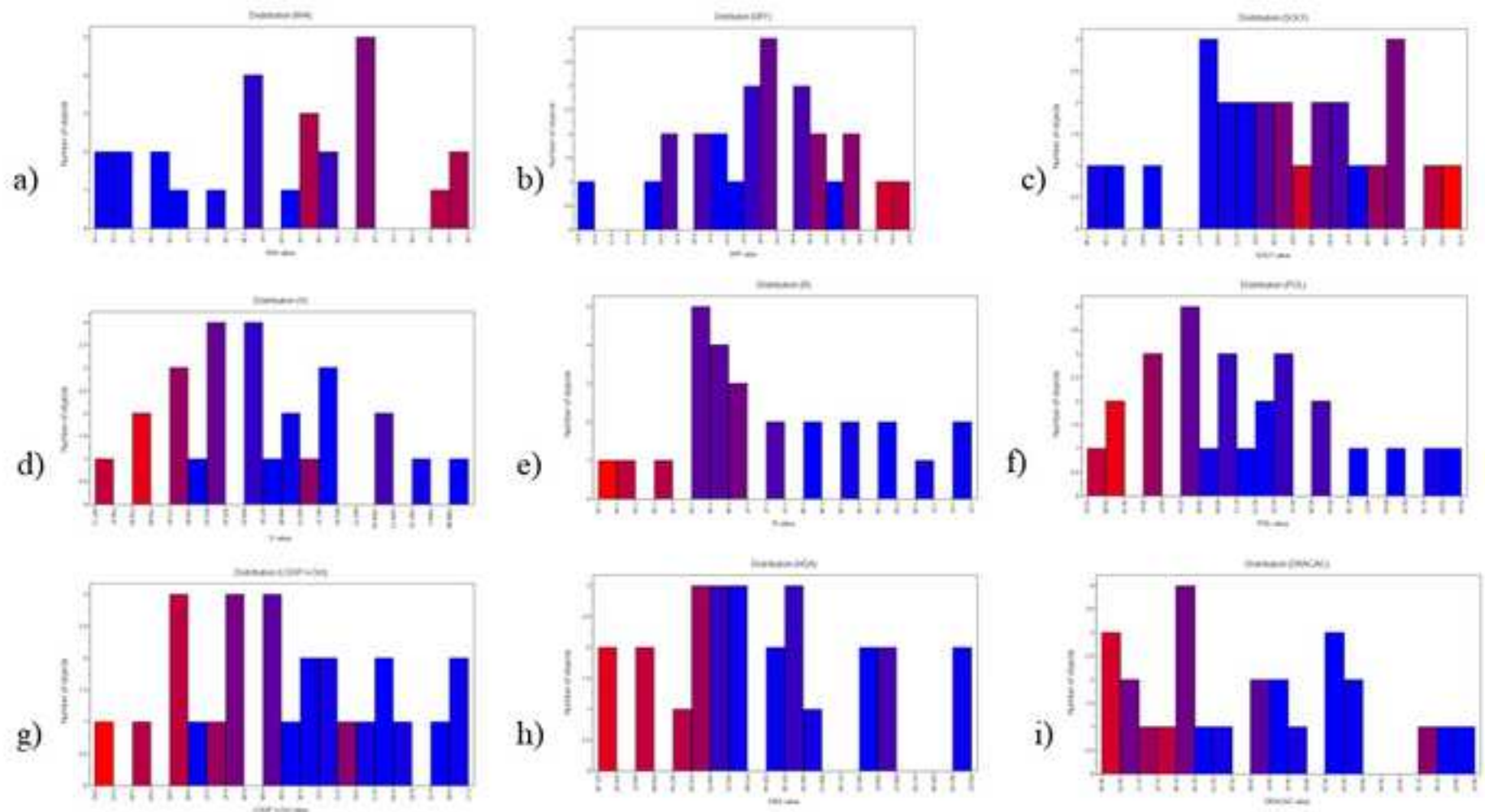


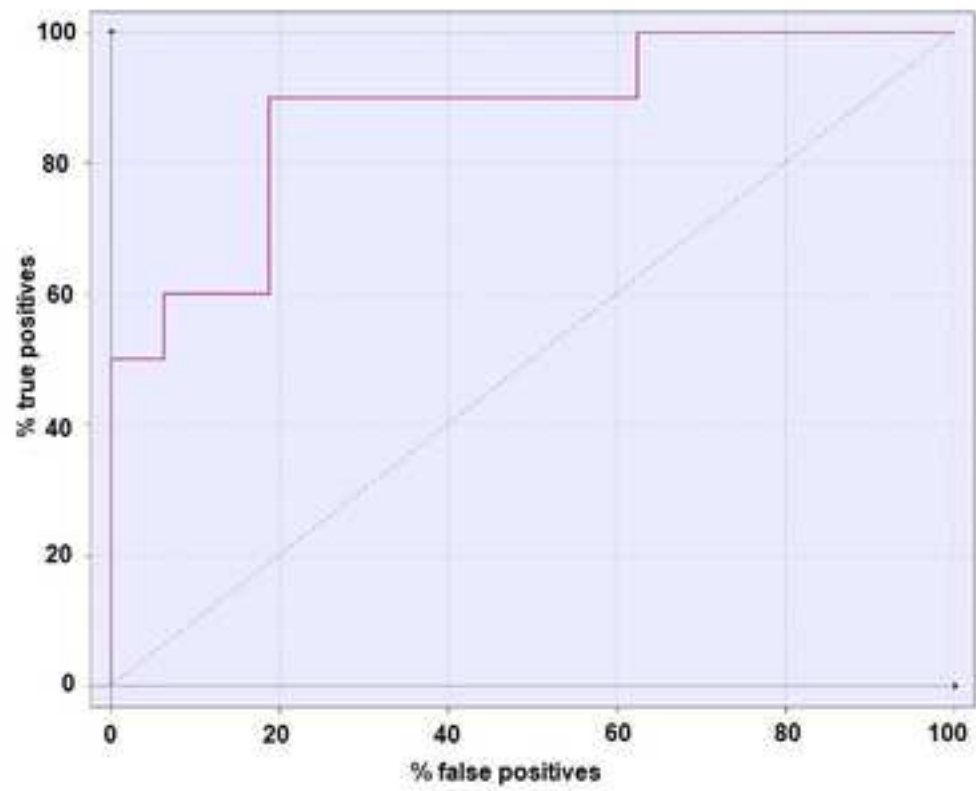


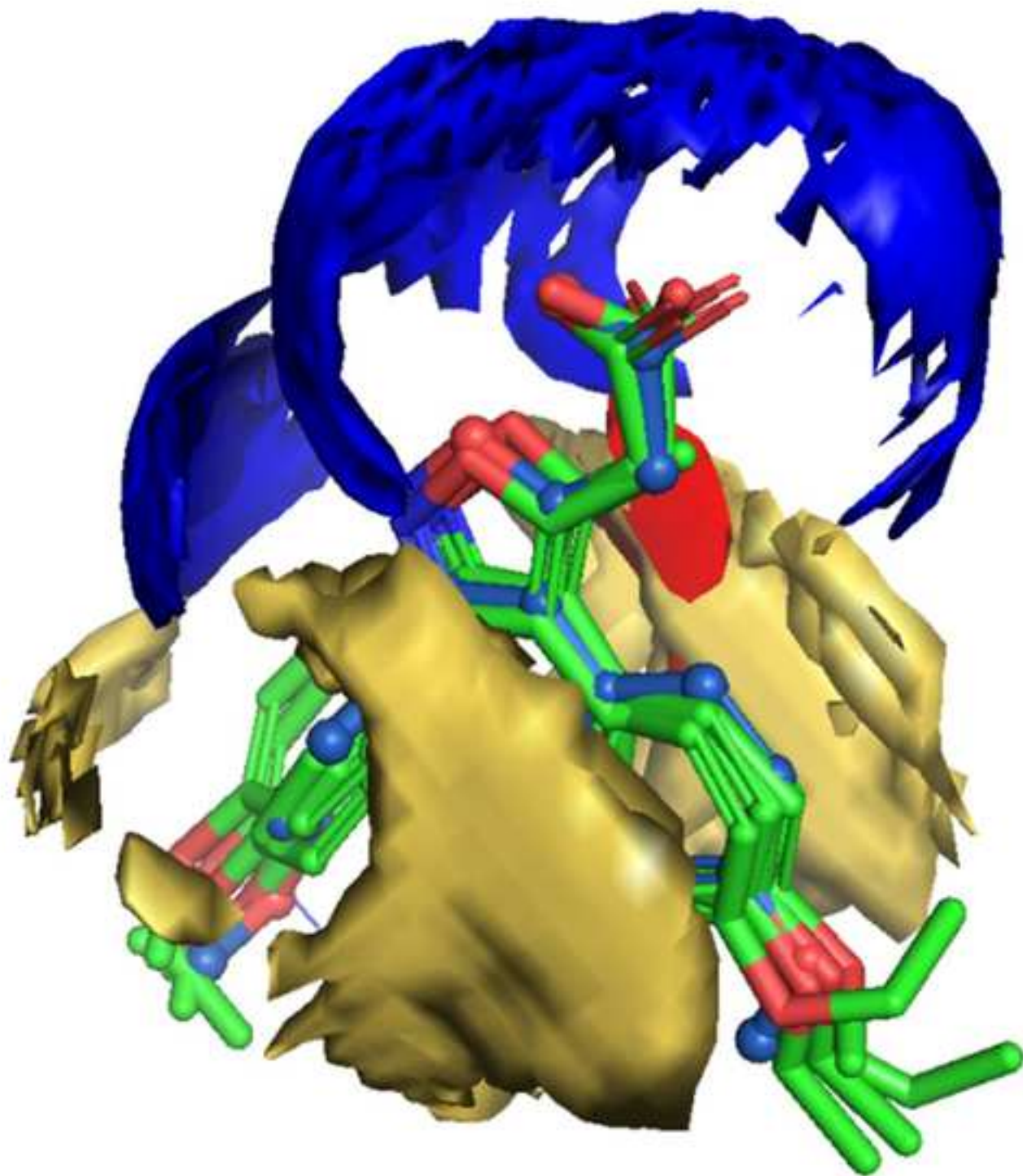


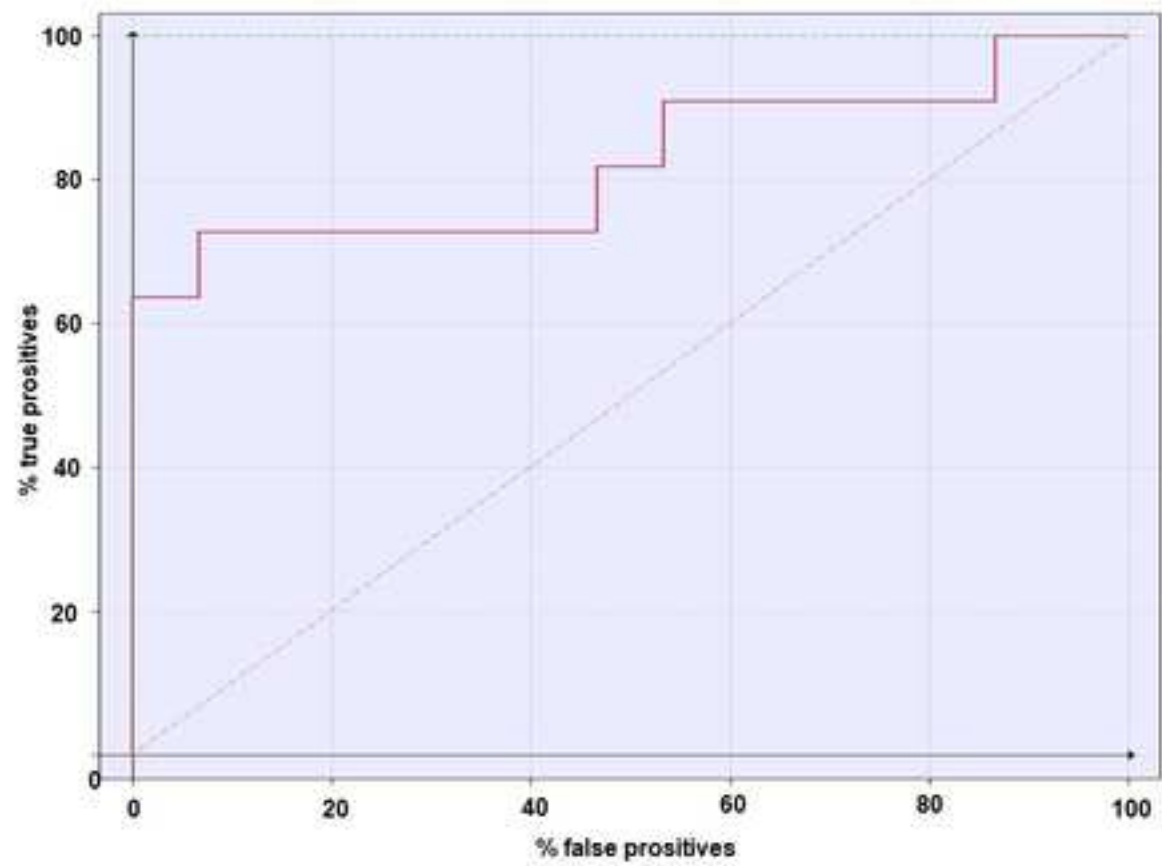


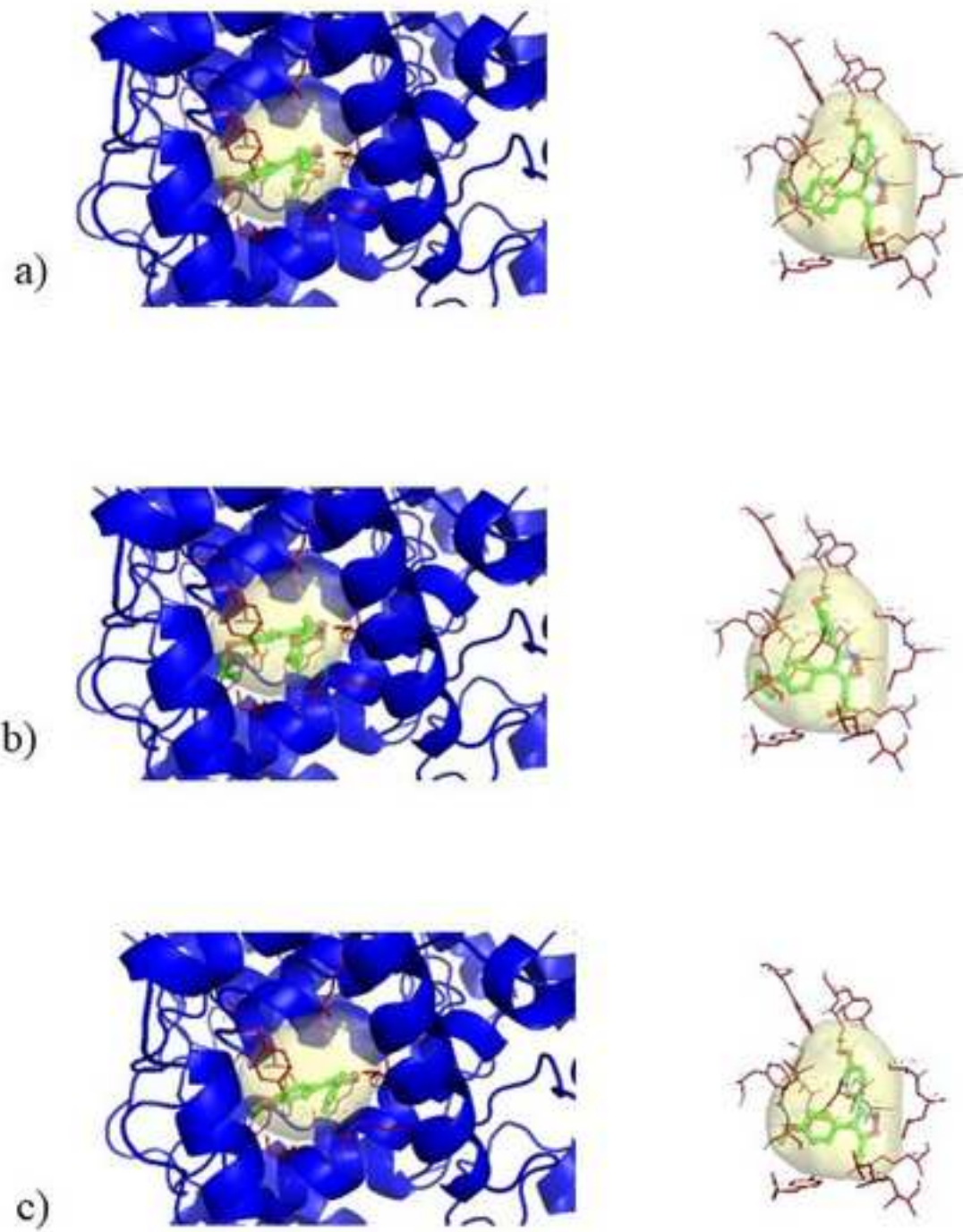


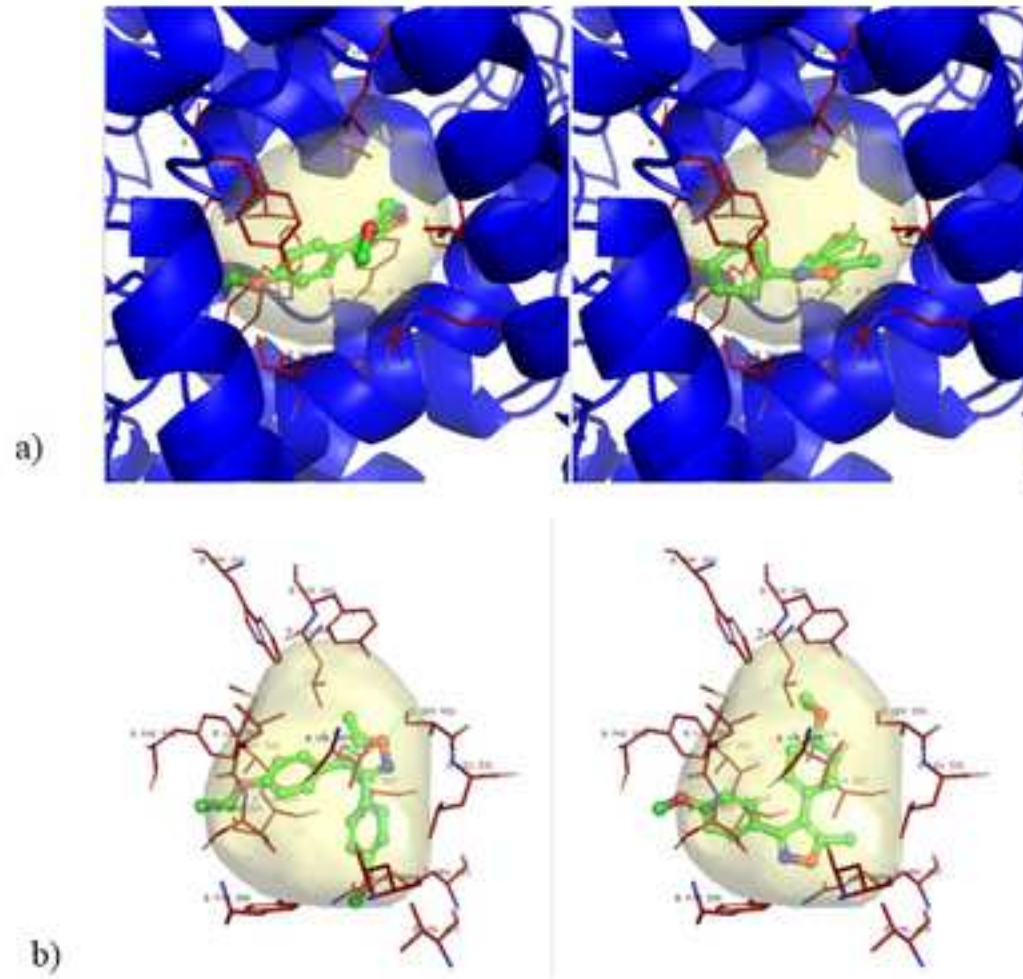


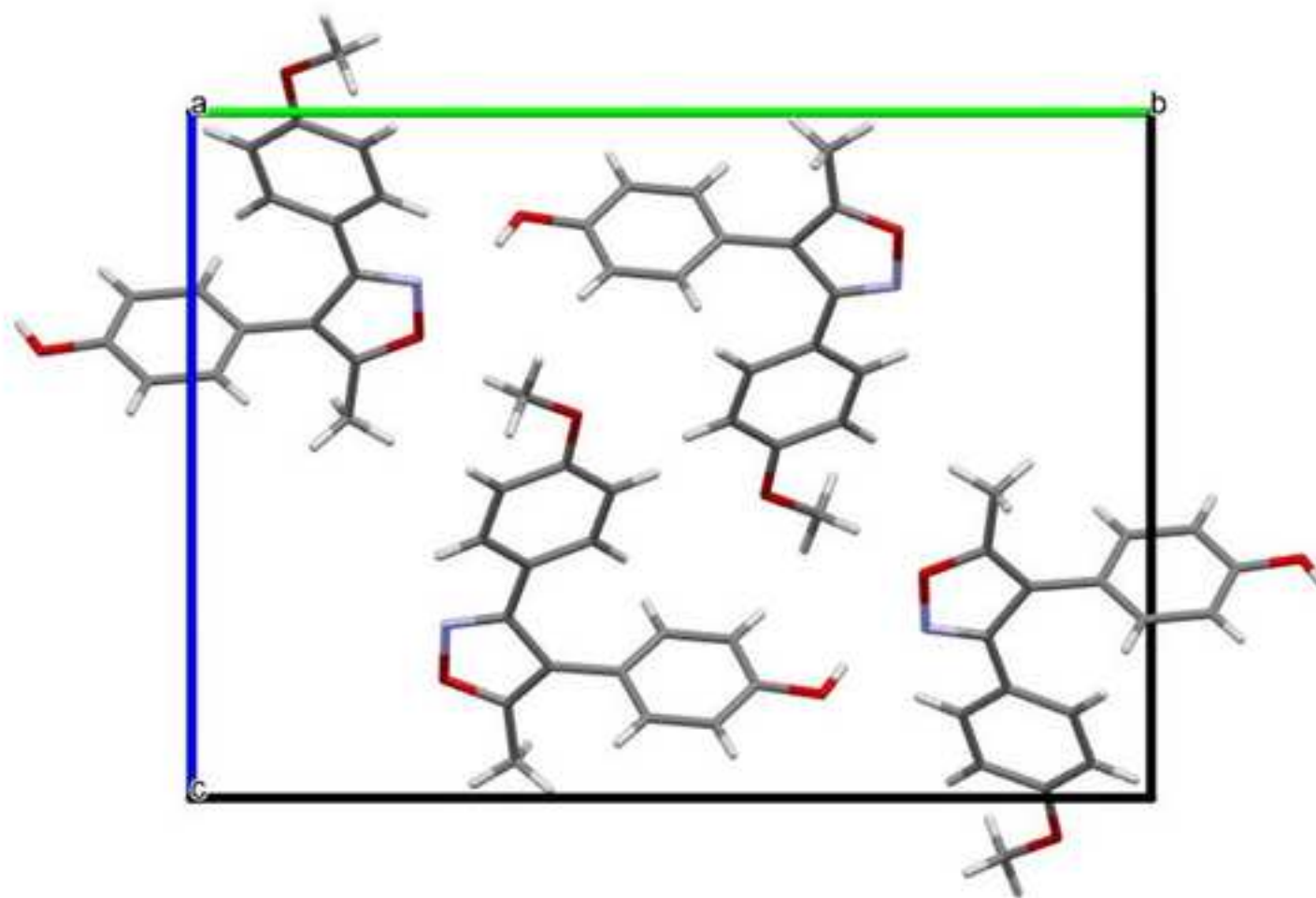


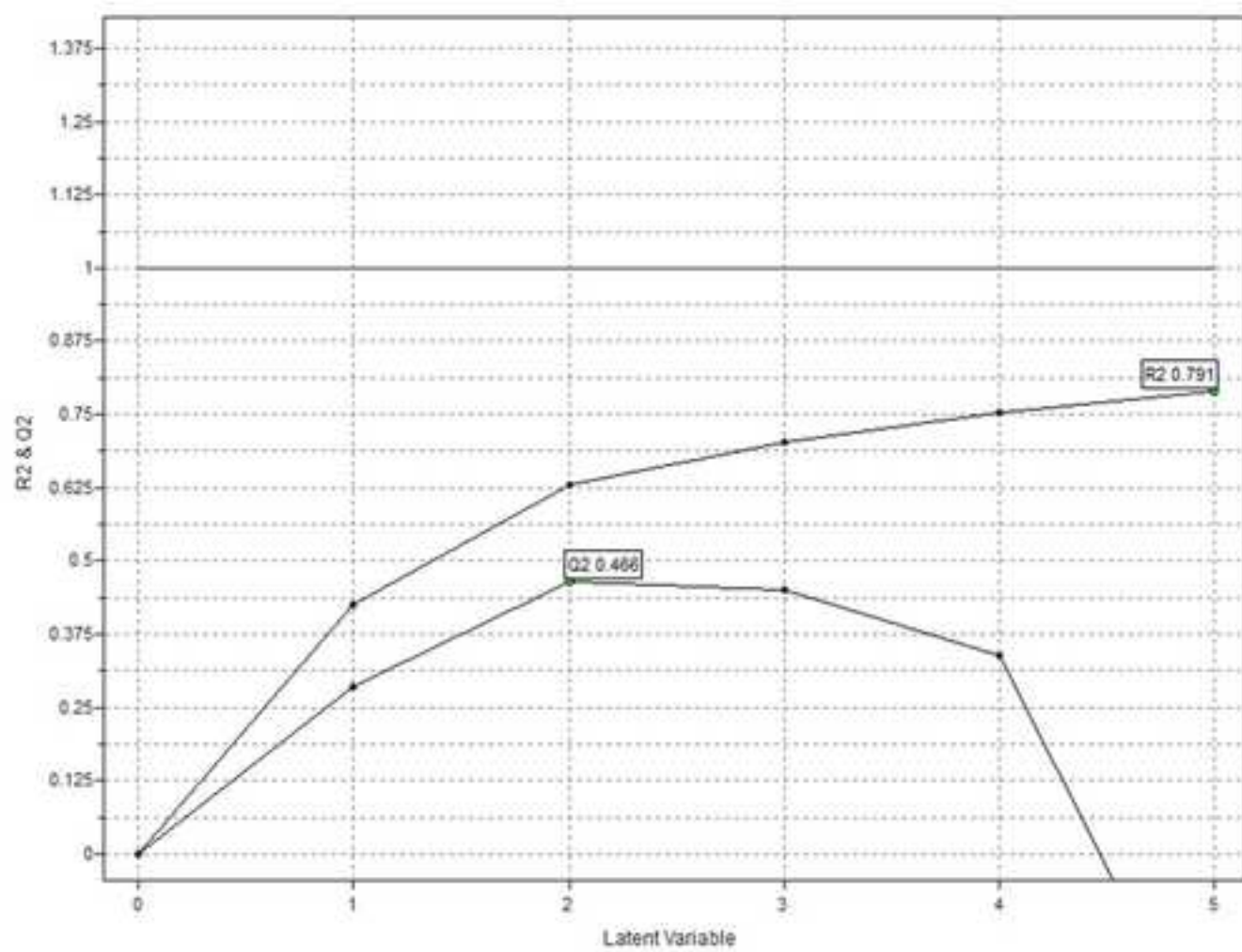


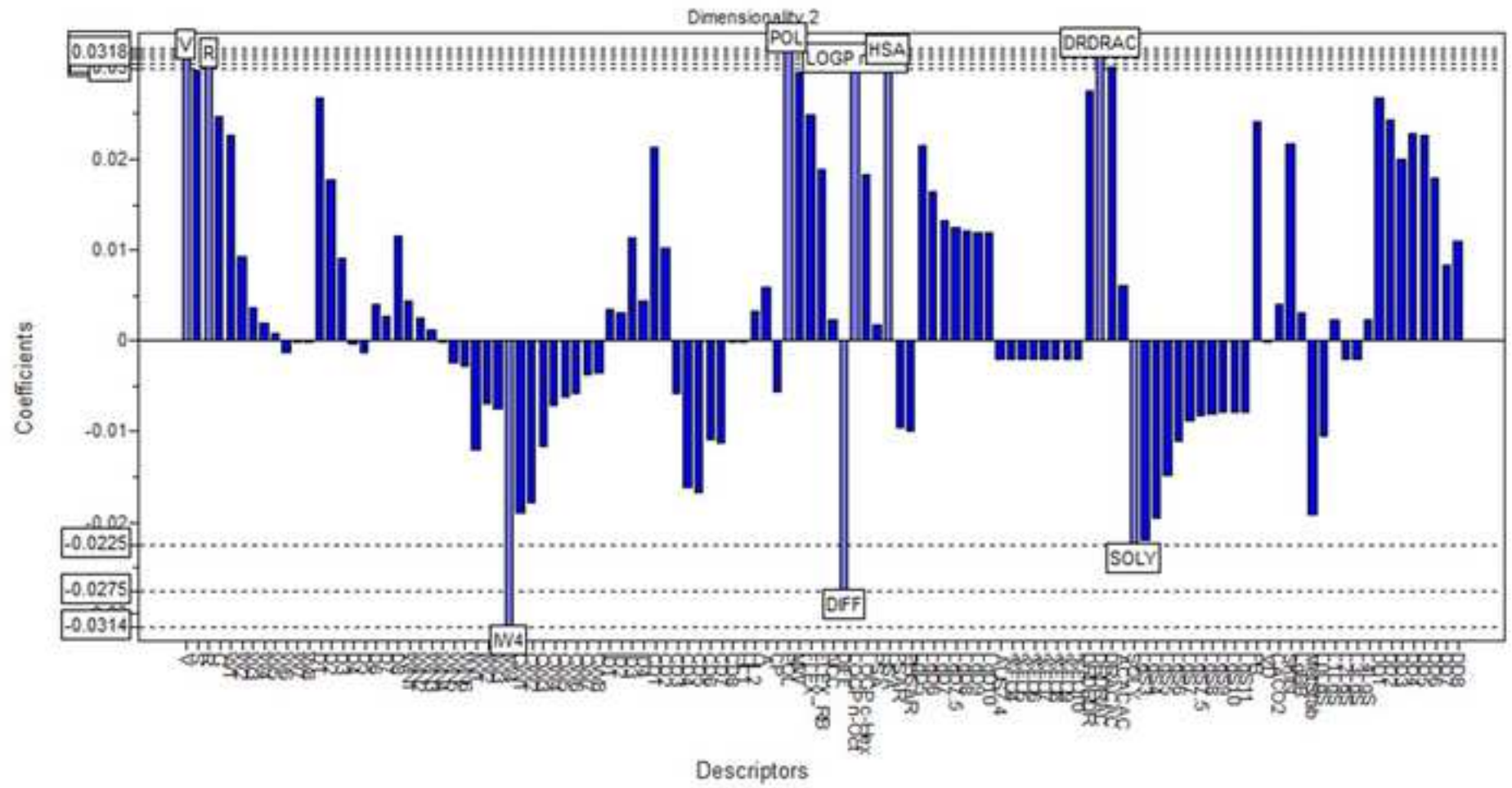


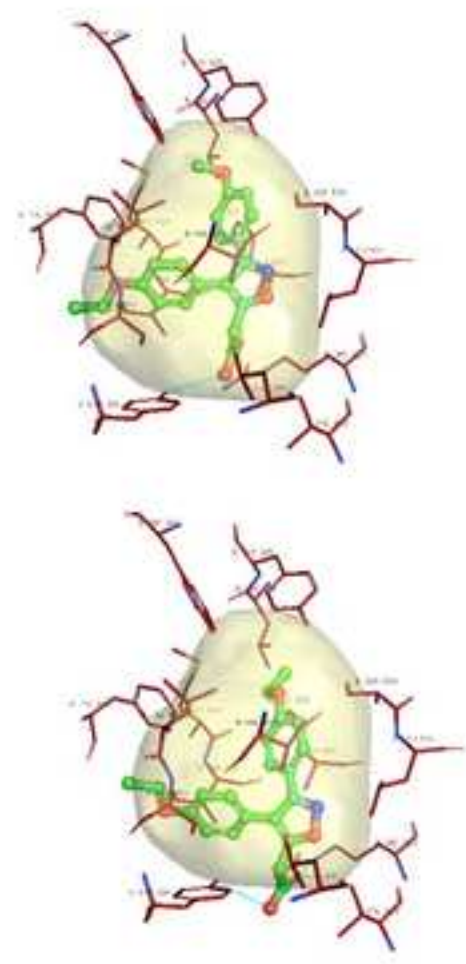
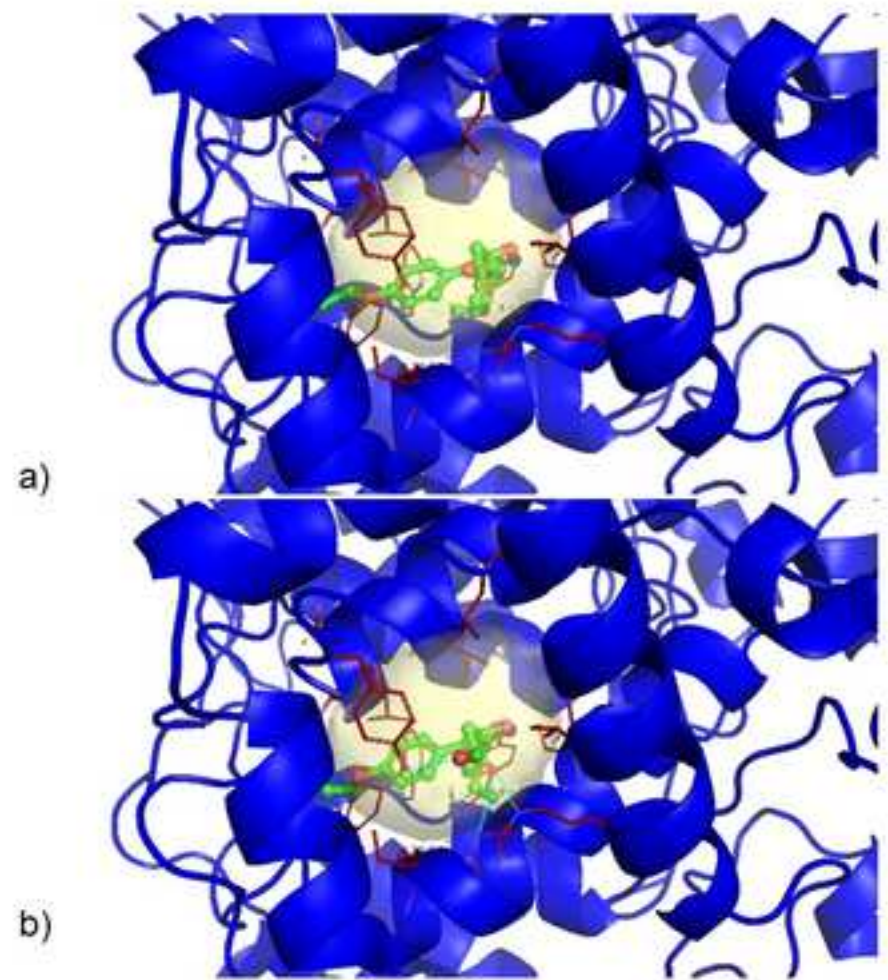














[Click here to access/download](#)

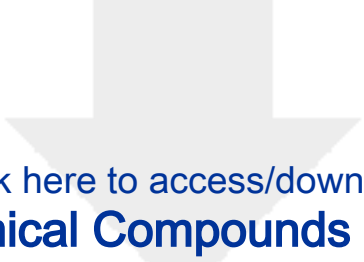
Supplementary Material - For Publication Online
Supplementary material.docx





Click here to access/download
Chemical Compounds (.mol)
Scheme 1.cdx





Click here to access/download
Chemical Compounds (.mol)
Scheme 2.cdx



Declaration of interests

The authors declare that they have no known competing financial interests or personal relationships that could have appeared to influence the work reported in this paper.

The authors declare the following financial interests/personal relationships which may be considered as potential competing interests: